# MASTER THESIS

Course code: BIO5011 Hidehiko Kato / Candidate no.: 3

# Effect of temperature on growth and gene expression of *Tetradesmus* sp. for application in wastewater treatment

Date: 16/MAY/2022 Total number of pages: 81

NORD University

www.nord.no

# Acknowledgment

Firstly, my great thanks to my supervisor, Dr. Christopher Jonathan Hulatt who has supported me throughout this thesis and given me the freedom to make my own path at every step of the project. I am grateful for him letting me pursue this work. I am also grateful to Dr. Peter S. C. Schulze for letting me take a part in the ALGACYCLE project and to a Ph.D. student (at the time of writing) Hirono Suzuki for assisting me throughout the project. I have thoroughly enjoyed being a part of the AMBiome team at Nord University. Also, I would like to express my gratitude toward Martina Elisabeth Luise Kopp who helped me countless times by checking the quality of the extracted RNA and improving the yield, Anjana Mahesh Palihawadana for his kindness in letting me use the freeze-dryer and GC-FID, and everyone in the ALGACYCLE project especially those who are from the Necton and the GreenCoLab located in Portugal. I would also like to thank Anne Margrete Leiros Nilsen for sharing her laughter and always letting me know that I'm not alone in this journey and walked through tough times together. Because of these outstanding people, I am confidently able to tell others that the knowledge and experience I've gained regarding microalgae and genomics are much more than the MSc level. I am unable to fully articulate my gratitude toward those people by using adjectives that currently exist.

**IndexTable of contents**

List of figures

List of tables

# Abstract

Microalgae have been studied for more efficient and environment-friendly means of wastewater treatment due to their ability to uptake dissolved organic and inorganic materials to produce cellular carbohydrates, proteins, and lipids, whilst yielding oxygen and ultimately clean water as byproducts. When cultivated in large-scale outdoor pond or bioreactor systems, the growth and metabolism of microalgae will be altered by fluctuating temperature depending on geographic location, seasonal weather patterns, and climate change. In addition, the thermal responses can be varied depending on species or strains. Optimizing the growth of microalgae will be one of the most critical aspects of utilizing algal biomass for wastewater treatment.

A well-known strain of *Tetradesmus obliquus* (UTEX393) and a commercially grown strain (SNS0120) were pre-cultivated at 10 °C and then inoculated into lab-scale flat-panel photobioreactors with a turbidostat mode with continuous light with warm white LED lamps. The growth rate was measured from 10 °C to 40 °C with 3 °C increments and the data was fitted to a total of 24 thermal performance models to determine accurate thermal optima for both strains. The effects of temperature on fatty acids, photosynthesis, and gene expression were also discussed.

The optimal growth temperatures for the UTEX393 and SNS0120 were determined as 27.3 °C and 26.8 °C respectively. The main effect of temperature was the increased growth rate for both strains. The UTEX393 showed higher growth performance at all temperatures compared to the SNS0120 as well as the thermal tolerances. Interestingly, the accumulation of total fatty acids was not significantly influenced by temperature, yet the omega-3/omega-6 ratio was reduced as the temperature increased. The overall results suggest that the UTEX393 is practicable to cultivate in the outdoor PBR or wastewater treatment throughout the year in the regions where the temperature of the culture fluctuates between 10 to 37 °C while the SNS0120 requires the temperature to be closely monitored and controlled below 31 °C.

Temperature also influenced the gene expression of the UTEX393. The changed gene expressions represented the cells managing metabolic fluxes under the higher growth rate at 25 °C vs 10 °C. At 34 °C, thermal inactivation of growth was associated with the expression of genes associated with thermal stress responses.

# 1 Introduction

## 1.1 Background

Unicellular photosynthetic organisms such as microalgae have been studied for more efficient and environment-friendly means of wastewater treatment due to their ability to uptake nitrate, nitrite, ammonium, phosphorous, and other trace elements from wastewater. Microalgae utilize those dissolved organic and inorganic materials and $CO_2$ to produce cellular carbohydrates, proteins, and lipids, whilst yielding oxygen and ultimately clean water (water without harmful pollutants) as byproducts (Muñoz & Guieysse, 2006; Ramanan et al., 2016).

When cultivated in large-scale outdoor pond or bioreactor systems, the growth and metabolism of microalgae will be altered by fluctuating environmental factors such as temperature, light, salinity, pH, and nutrients surrounding the algal ponds or photobioreactors (Aussant et al., 2018; Robertson et al., 2013; Stengel et al., 2011). Cultivating specific microalgal species under non-optimized growth conditions may lead to significant loss of biomass. Among those environmental factors, the temperature cannot be controlled in an energy-efficient way, yet represents one of the most significant variables influencing the growth of microalgae. The temperature experienced by microalgae cell cultures varies based on geographic location, seasonal and daily weather patterns, bioreactor/pond system design, and long-term climate change. Examining the effects of temperature on the growth performance of the algal strains is needed to achieve maximum bioremediation performance in terms of nutrient uptake and biomass production (Lage et al., 2021; C. Zhang et al., 2014).

## 1.2 Advantages of algae in wastewater bioremediation

Bioremediation of polluted water (i.e. wastewater treatment) is considered one of the most influential measures to improve the environment globally (Coelho et al., 2015). Along with the exponentially growing population, agricultural intensification, and expanding industries, aquifers, waterways, and other aquatic environments will be polluted with more organic wastes, pathogens, toxic materials, and heavy metals that, without proper treatment, cause detrimental effects on ecosystems (Jackson, 2021; Olvera et al., 2017; Tortajada & Biswas, 2018; United Nations, 2019; Xiaoming et al., 2018; L. Zhang et al., 2018). In order to maintain a healthy

environment with increased demands for wastewater treatment together with the limitation on available land for expanding treatment facilities and landfill sites, the treatment processes must be done more efficiently than current methods (UN SDG, 2022).

Current conventional wastewater treatment processes consist of a combination of physical, chemical, and biological processes, of which the biological process is carried out by groups of aerobic microorganisms that consume organic matter as their nutrition and turn them into metabolic end products (e.g. biomass, $CO_2$, $NH_3$, and $CH_4$) under reduction of dissolved oxygen, leading anoxic environment in the wastewater and sludge (Anjum et al., 2016; Grobbelaar, 2013; Karia & Christian, 2006; Khiewwijit et al., 2015; Soomaree, 2015). This may cause an issue with nitrifying bacteria which transform ammonia into nitrate under an oxygen-rich environment (Schulze et al., 2017). Thus, the traditional wastewater treatment methods will be unsustainable if the demands are increased (Kamali et al., 2019).

In opposition to the oxygen depletion from the wastewater and sludges caused by the aerobic respiration, photosynthesis by a microalgal consortium is possibly able to generate a sufficient quantity of dissolved $O_2$ to support other microorganisms in the wastewater (Figure 1) (Wang et al., 2015). In addition, Microalgae have shown their effective removals of $NH_4^+$, $PO_4^{3-}$ and heavy metals (Cr, Cu, Zn, Pb, and Cd) (Grobbelaar, 2013; Marinova et al., 2018; Mohammed & Markert, 2006; Monteiro et al., 2009; Salah El Din et al., 2009), as well as the biosorption of persistent organic pollutants in the wastewater (Michalak et al., 2013; Plöhn et al., 2021; O. Spain et al., 2021). Another example is their responses to the other microorganisms. Some microalgal species (e.g. *Isochrysis galbana*, *Scenedesmus sp.*, and *Chlorella sp.*) have been reported to be capable of excreting bactericides or fungicides preferentially against the gram-positive bacterium present in the wastewater causing strong inhibitory activities ultimately reducing the human and plant pathogens in the wastewater (Alsenani et al., 2020; DellaGreca et al., 2010; Ghasemi et al., 2007; Lee et al., 2006; Najdenski et al., 2013; Niveshika et al., 2016).

In addition to their extraordinary oxygen production and ability to uptake nutrients and $CO_2$ from the wastewater, microalgae display high growth rates and are capable of producing large quantities of biomass by utilizing the pollutants in the water. There are studies regarding their biomasses to be incorporated into varieties of technologies due to their capabilities of producing value-added biomaterials while treating the wastewater. For instance, microalgal biomasses can

be used as biofuels, animal feed, bio-stimulants (e.g. auxins, cytokinins, gibberellins, abscisic acid, and ethylene), and other biochemicals (Algacycle, 2021; AlgaePARC, 2022; Chisti, 2007; Colla & Rouphael, 2020; National Ocean Service, 2022; Navarro-López et al., 2020; Wijffels & Barbosa, 2010; Yap et al., 2021). Therefore, the efficient cultivation of microalgal biomass is considered one of the most promising methods to enhance the efficiency of wastewater treatment (Plöhn et al., 2021; Yap et al., 2021).

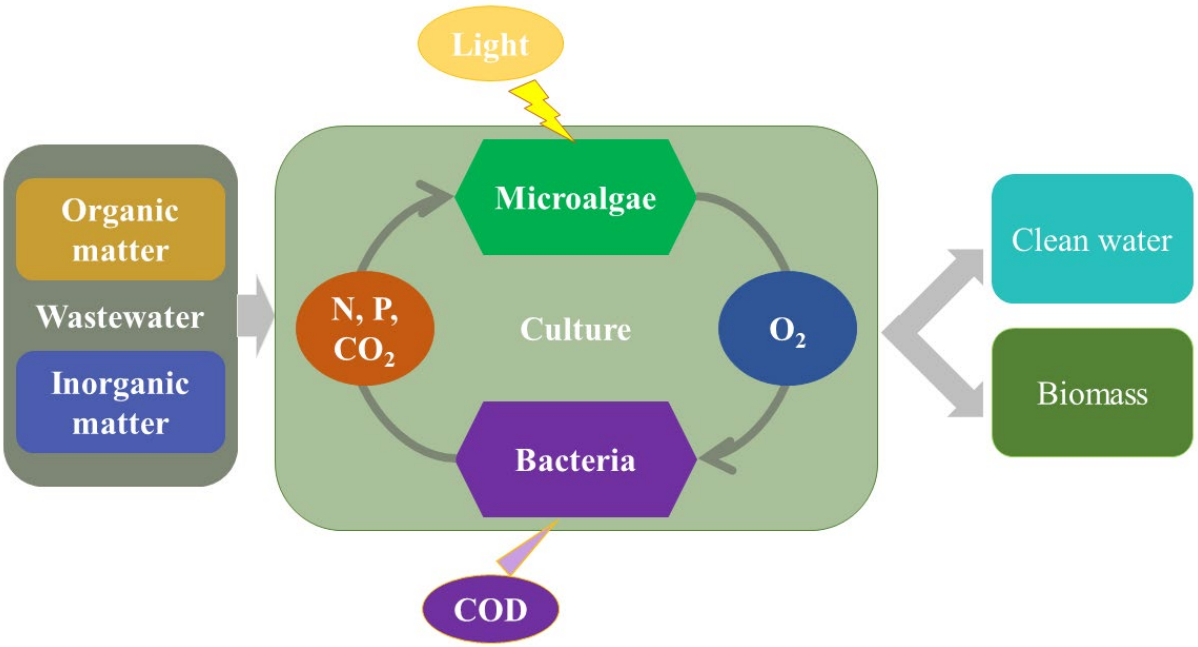


*Figure 1. Diagram of the main biological phenomena using microalgae/bacteria consortia for nutrient recovery from wastewaters (Acién Fernández et al., 2018). This microbial consortium will ultimately produce clean water and algal biomass as by-products. COD: Chemical Oxygen Demands.*

### 1.3 Large-scale cultivation of microalgae in ponds and bioreactors

Microalgae cultivation methods can be categorized into either enclosed photobioreactors (PBRs) or open ponds systems (Campbell et al., 2011). Open pond systems include natural, circular, raceway, or High-Rate Algal Pond (HRAP) systems. The major advantages of these systems are relatively low cost and low energy demands compared to the PBRs. However, these open culture systems face issues such as temperature fluctuation, water evaporation, dilution (nutrition or biomass caused by rain, etc.), and contamination by predators and other fast-growing heterotrophs (Tredici, 2010). The open pond systems are also used for the algal-based wastewater treatment processes which are termed oxidization (or stabilization) ponds. The HRAP system is a particularly cost-effective approach as the pond-based wastewater treatment

system uses very shallow pond depth with high algal density (R. J. Craggs et al., 2011). This system can utilize already existing ponds which will be environmentally and economically beneficial (R. Craggs et al., 2014). For instance, those ponds eliminate sludge disposal, produce less odor, and are capable of consistently providing a higher degree of nutrient removal and disinfection compared to the conventional biological wastewater treatment systems (Craggs RJ., 2005; McGrath & Mason, 2004; Oruganti et al., 2022). Despite these advantages of the algal wastewater treatment systems, the growth of microalgae will still face the same issues as the open algal cultivation ponds (Brenner & Abeliovich, 2013).

The PBRs are closed systems that protect cultures from evaporation, dilution, and contamination from the surrounding environment. Various PBR designs have been developed including flat, tubular, manifold, helical, flexible films, hybrid, floating, and biofilms (Zittelli et al., 2013). Tubular PBRs are the most common design and preferred by many commercial algae productions, and they can be subdivided into three main shapes which are serpentine, manifold, and helical. Serpentine PBRs consist of straight tubes connected by U-bends to form a flat loop that may be arranged either vertically or horizontally for achieving sufficient mixing by the air bubbling. Manifold PBRs are made of parallel tubes connected at the ends by two manifolds which reduce the head losses and lower oxygen concentrations. (Rodolfi et al., 2010; Tredici, 2010; Zittelli et al., 2013). Flat panels allow them to be closely packed together and achieve high photosynthetic efficiency, and a high rate of air bubbling for giving the culture adequate turbulence and scouring of the reactor walls (Bassi et al., 2011; Hu, 2013; Tredici, 2010; Wijffels & Barbosa, 2010). Flat plate photobioreactors with short optical path lengths can achieve higher areal production rates and culture densities than conventional reactors, and provide better temperature control over other conventional designs which makes it a useful tool to simulate the temperature effects on growth by isolating the temperature from other environmental factors (Polycarpou, 2019; Richmond, 2013). Due to the nature of the closed system, most of PBRs are relatively easier to control temperature, lighting, and gas exchange compared to the open systems (Skjånes et al., 2016).

It is important to investigate the effects of temperature on the growth performance of each microalgae species or strain intended for treating wastewater. This information is applicable for designing cultivation strategies for both outdoor PBRs and open ponds which experience wide ranges of temperature fluctuations throughout a day (Béchet et al., 2010; Slegers et al., 2013). In this study, conducting lab-scale simulations on the growth of two strains of *Tetradesmus*

*obliquus* by using the flat plate photobioreactors, will provide some critical knowledge for scaling up to the larger open pond cultivation systems.

### 1.4 Temperature effects on growth of microalgae

The majority of microalgae species are capable of carrying out photosynthesis and cellular division over a wide range of temperatures generally between 5 and 30°C, and the optimal temperature for growth for cultivated species is often between 20 and 30 °C (Breuer et al., 2013; Guedes et al., 2011; Hodaifa et al., 2010; Li, 1980). Lethal temperatures for mesophilic microalgae have been stated in the literature from 30 to 35 °C onwards (Butterwick et al., 2005; Kudo et al., 2000).

Growth and metabolic rate increase with temperature until a thermal optimum, above which further increases in temperature cause inactivation of cell metabolism (Falkowski, 1980; Fawley, 1984; D. P. Maxwell et al., 1994). The growth rate will start to decrease when the temperature exceeds the optimal temperature and sharply decrease beyond the threshold. This is generally explained by heat stress which can inactivate/denature enzymes or modify proteins that are involved in photosynthetic and respiration processes and cause an imbalance between energy demand and ATP production (Raven & Geider, 1988; Salvucci & Crafts-Brandner, 2004a). The temperature range between optimal and lethal varies depending on species, strains, or even generations (Figure 2) (Kessler, 2006; Suzuki & Takahashi, 2008). A narrow range between the thermal optimum and the threshold temperature may indicate that the species/strains are sensitive to temperature fluctuation, while a wide range may indicate that the species or strains are able to survive by acclimation or adaptation strategies against the temperature shift (Ras et al., 2013).

Besides the differences in thermal tolerances among species/strains, the optimal growth temperature may also vary with the environment thermal history (Cheregi et al., 2021; Kremp et al., 2012). Microalgae strains are predisposed to adaptation depending on previous constraints experienced in their initial environment (Huertas et al., 2011). The plasticity of microalgae to genetically adapt to unfavorably warm conditions can offer a long-term solution for future outdoor cultures liable to experience elevated temperatures in the long run. Seasonal temperature variations could give enough time for generational adaptation and might ensure a stable growth rate.

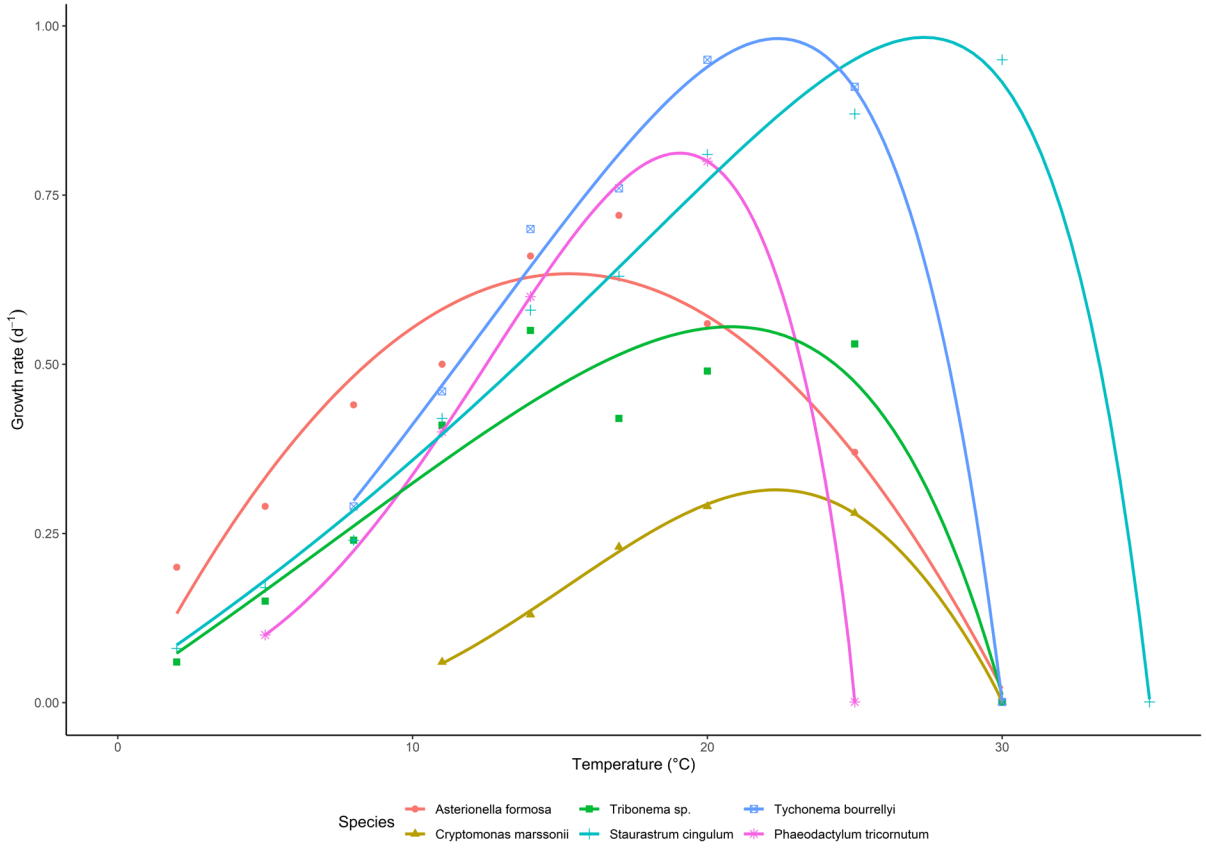


*Figure 2. The effects of temperature on growth rates in various microalgal species. Optimum and lethal temperature varies depending on the species. Differences in growth rate and biomass production amongst strains will directly influence the efficiency of nutrient uptake (Butterwick et al., 2005). Growth data for above six species were obtained from Butterwick et al. (2005), then the best-fit models for each species were determined among 24 different temperature curve models.*

### 1.5 *Tetradesmus obliquus*

*Tetradesmus obliquus,* also known as *Scenedesmus obliquus*, is a mesophilic freshwater microalgal species in the class *Chlorophyceae* and has been studied for various applications including biofuels (biodiesel, hydrogen), fish feed ingredients, and wastewater treatment (Anisha & John, 2014; Barbosa & Wijffels, 2013; Breuer et al., 2013; Hodaifa et al., 2009, 2010; Patnaik et al., 2019; Wijffels & Barbosa, 2010). For this genus, there is still not enough data to understand its thermal performance including its high-temperature survivability, low-temperature performance, and what its thermal optimum is. To estimate and explore the growth behaviours of cells under different temperature conditions, accurate mathematical modeling of the growth rate is essential. Different models can be used to estimate optimized growth

conditions including the optimal growth temperature, and this causes variation in the results (Bozkurt & Erkmen, 2001; Ras et al., 2013; Vieira Costa et al., 2002). As a consequence, how the thermal performance of a novel isolate (i.e. SNS0120) can be compared to the well-known isolate remains unclear.

In the literature, the effect of temperature combined with pH and nutrient deprivation was reported to increase the accumulation of the lipids in the *T. obliquus* (Breuer et al., 2012). *T. obliquus* can accumulate around 20 % in non-stressed culture and around 30 to 40 % under nitrogen starved conditions (Calhoun et al., 2021; Shao et al., 2017). However, the sole effect of the temperature on lipid accumulation and lipid profile has not been tested for this species. In addition, the photosynthetic machinery of *T. obliquus* may alter its pigment composition, enzymatic activity, and membrane fluidity in response to temperature (Chalifour & Juneau, 2011; Huner et al., 2003; Necchi Jnr, 2004). In order to detect the changes in photosynthetic performance and stress response caused by the temperature variation, chlorophyll fluorescence can be measured by using pulse amplitude modulation (PAM) fluorometry (Masojídek et al., 2001; K. Maxwell & Johnson, 2000). The maximum quantum yield of photosystem II ($F_v/F_m$) of green algae at the optimal condition is about 0.7 to 0.8 (de Marchin et al., 2015; G. N. Johnson et al., 1993). The $F_v/F_m$ can be an indicator of the functional performance of the cells exposed to the temperature fluctuation, yet some species of microalgae are able to maintain high $F_v/F_m$ under the thermal stress conditions (Akimov & Solomonova, 2019; Yong et al., 2019). The photosynthetic performance at low, near thermal optimum, and high temperatures have not been studied for the *T. obliquus*.

The genome of *T. obliquus* UTEX393 has been recently sequenced and is publicly available for genomic approaches. Transcriptomics is a widely-adopted comprehensive analysis of whole sets of transcripts and their expression levels in a particular cell, tissue, organ, or whole organism corresponding to a particular time, developmental stages, or under some specific physiological conditions (Hulatt et al., 2020; Milward et al., 2016; Yadav et al., 2018). Only a few *Scenedesmus/Tetradesmus* species were previously investigated for their gene expressions under conditions that trigger carbon partitioning to lipid and starch accumulation (Msanne et al., 2020). However, thermal effects with transcriptomics haven't been studied in *Tetradesmus*.

### 1.6 Aim of the study

**The overall objective of this work was to test the effects of temperature on the performance of *Tetradesmus* from the perspective of outdoor mass cultivation.** In our work, a well-known strain UTEX393 and a commercially grown strain (later referred to as the SNS0120) of *T. obliquus* will be investigated for their growth performance and temperature responses since the optimizing the growth of microalgae will be one of the most critical aspects of maximizing the efficiency of bioremediation and utilizing algal biomasses. In order to generate a better estimation of the growth performance and thermal responses, determining a more appropriate mathematical model is essential (Padfield et al., 2021). In addition, the sole effects of temperature on photosynthetic performance and the lipid accumulation of both strains will be investigated and discussed. Furthermore, the effect of temperature on cell-wide gene expression in *Tetradesmus* UTEX393 could represent a powerful method to describe the effects of temperature on key metabolic pathways, including respiration, lipid biosynthesis, and photosynthesis.

**The specific aims were**

1. Compare the growth rates of two strains of *T. obliquus* over a wide range of temperatures to establish the most suitable strains for wastewater treatment in outdoor bioreactors
2. Determine the effects of temperature on the fatty acid composition and photosynthetic performance of *T. obliquus*
3. Compare the effects of low, optimal, and high temperature on the gene expression of *T. obliquus*

These results will allow us to foresee the growth of the *T. obliquus* UTEX393 and SNS0120 at the geographic locations where the cultures will be established and will be beneficial for establishing large-scale algal cultures for wastewater treatment.

# 2 Materials and Methods

## 2.1 Cultivation

### 2.1.1 *Tetradesmus* strains

A strain of *Tetradesmus obliquus* UTEX393 originally obtained from the UTEX Culture Collection of Algae (USA, *https://utex.org*) by Wageningen University & Research (Wageningen, The Netherlands) and kindly provided to us from cryopreserved stock. Another strain (SNS0120) of the same genus was obtained from the NECTON Companhia Portuguesa de Culturas Marinhas SA. The SNS0120 was isolated from freshwater in Pataias, Portugal (39.6832°N, 9.0018°W).

### 2.1.2 Experimental growth medium selection

The growth of Tetradesmus in two cultivation media, Nutribloom™ (NB) and Bold's basal medium (BBM) were initially compared to decide which medium was most suitable for the temperature experiments. The NB was obtained from NECTON S.A. (Olhão, Portugal) and 4.5 mL of the NB was added to 995.5 mL of Milli-Q water to prepare a total volume of 1 L medium consisting of $NaNO_3$ 9mM, $K_2HPO_4$ 0.5 mM, $Cl_3Fe$ 0.1mM, $Na_2EDTA$ 0.1 mM, $ZnCl_2$ 4.5 µM, $ZnSO_4 \cdot 7H_2O$ 4.5 µM, $MnCl_2 \cdot 4H_2O$ 4.5µM, $MgSO_4 \cdot 7H_2O$ 9µM, Na2MoO4·$2H_2O$ 0.45µM, $CuSO_4 \cdot 5H_2O$ 0.45 µM, $CoCl_2 \cdot 6H_2O$ 0.45 µM, Thiamine (vitamin $B_1$) 46.8 nM, Biotin (vitamin H) 9 nM, and Cyanocobalamin (vitamin $B_{12}$) 9 nM. The initial medium was pH 4.2, so it was adjusted to pH 6.2 by adding 1.2 g/L of TrisBase to make an alkaline buffer, then adjusted with HCl. All of the media used in this thesis were filtered by using the glass microfiber filters (47 mm diameter x 0.7 mm thickness, pore size 1 µm, VWR) and autoclaved (121 °C for 20 min) prior to use. Preparation of the BBM medium followed the recipe described by the Culture Collection of Cryophilic Algae (H. W. Bischoff and H. C. Bold, 1963). The BBM was modified with triple nitrate concentration (3N-BBM) matched the concentration of nitrate in the NB medium (Starr & Zeikus, 1993). The 3N-BBM was consisted of $NaNO_3$ 9mM, $MgSO_4 \cdot 7H_2O$ 0.3mM, 0.4 mM NaCl, $K_2HPO_4$ 0.4 mM, $KH_2PO_4$ 1.3 mM, $CaCl_2 \cdot 2H_2O$ 0.17 mM, $ZnSO_4 \cdot 7H_2O$ 031 µM, $MnCl_2 \cdot 4H_2O$ 7 µM, $MoO_3$ 5 µM, $CuSO_4 \cdot 5H_2O$ 6 µM, $Co(NO_3)_2 \cdot 6H_2O$ 2 µM, $H_3BO_3$ 0.2 mM, $Na_2EDTA \cdot 2H_2O$ (Titriplex III) 0.1 mM, KOH 0.6 mM, $FeSO_4 \cdot 7H_2O$

18 µM, soil extract 50 mL, Thiamine (vitamin $B_1$) 3 µM, Biotine (vitamin H) 1.02 nM, and Cyanocobalamin (vitamin $B_{12}$) 0.1 nM. The medium was adjusted to pH 6.5.

Twenty mL of each algal strain was inoculated into 400 mL glass tubes filled with either NB (natural pH 4.2), NB (adjusted pH 6.2), or 3N-BBM medium ($n$=3 each). The top of the tubes was sealed with silicone caps with three ports for air supply, air vent, and sampling. The 400 mL tube photobioreactors were placed in the environmental chamber (Series 6000, Termaks AS, Bergen Norway) at 20°C, 70 µmol $m^{-2}s^{-1}$ incident light intensity in a 24h:0h light/dark cycle for 14 days. A spectrophotometer DR3900 (HACH) was used to measure optical density at 540 nm ($OD_{540}$) and 680 nm ($OD_{680}$) for each tube daily.

### 2.1.3 Inoculum preparation for temperature experiments

Temperature experiments were conducted in very intensive flat plate photobioreactors, so both the inoculum and experiments used a 3N-BBM medium at triple concentration (3 × 3N-BBM) to ensure that nutrient deprivation could not occur. The pH was adjusted to 6.5. Cultures of UTEX393 and the SNS0120 were maintained in 400 mL tube photobioreactors filled with the medium at 10 ℃ under constant light at 70 µmol $m^{-2}s^{-1}$ in a Series 6000 incubator (Termaks AS, Bergen Norway) for approximately one week. Atmospheric air was used for maintaining the culture without additional $CO_2$ enrichment.

## 2.2 Temperature experiment

### 2.2.1 Photobioreactor setup and inoculation

Approximately 100 mL of the UTEX393 or SNS0120 was inoculated to the heat-sterilized flat-panel photobioreactor (Algaemist-S, Wageningen UR, The Netherlands) (Figure 3) with approximately 300 mL of medium. The flat panel was built with an airlift loop and temperature-controlled cultivation vessel supplied with water from a recirculating heater/cooler (Julabo F250). The total liquid volume in the reactor was 400 mL with a 14 mm light path. Aeration and mixing were provided by a mixture of filtered air at 200 ±4 mL/min and $CO_2$ at 4±1 mL/min (2% $CO_2$ in air). The initial temperature was set to 10 ℃. All cultures were initially illuminated at 80 µmol $m^{-2}s^{-1}$ continuous light with warm white LED lamps (Bridgelux, BXRA W1200). The incident light intensity was determined as the average over the entire surface of the inside

of the front glass panel of the reactor by using the LI-250A Light Meter (LI-COR Biosciences, USA). The external medium tank was prepared and connected to the medium intake port through the peristaltic pump. The turbidity of the culture was measured by the light sensors. Turbidity was calculated according to equation 1:

$$\text{Turbidity} = \frac{I_{in} - I_{out}}{I_{in}} \times 100\% \qquad [1]$$

Once the light sensor reading (arbitrary units) reached around 70 to 60, around 3 to 4 days after inoculation, the incident light intensity was increased to 140 µmol PAR $m^{-2}$ $s^{-1}$ and then maintained throughout the experiments. Using turbidostat control, the medium was automatically added whenever the light sensor reached 20 units or lower to keep the optical density constant. The volume of the out-flow was measured every 24 hours. The temperature experiment was initiated after the volume of the out-flow became constant. Temperatures tested for the experiment was 10, 13, 16, 19, 22, 25, 28, 31, 34, 37, and 40 ℃.

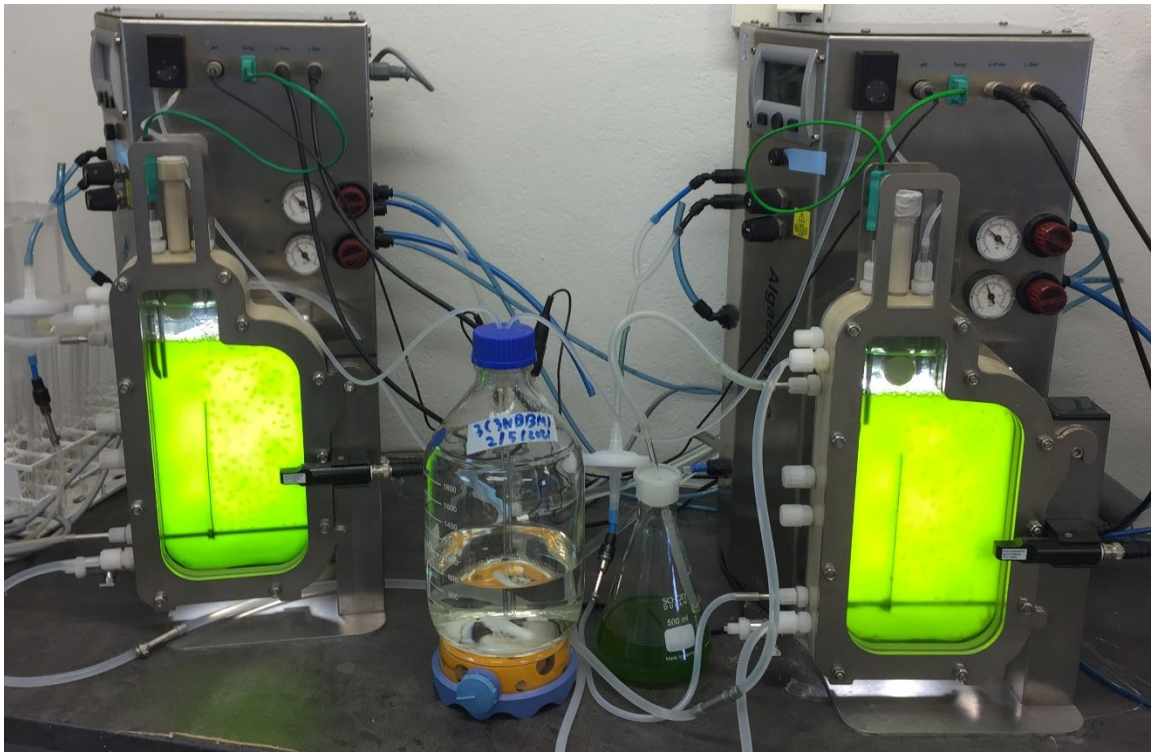

*Figure 3. The assembled Algaemist-S flat-panel photobioreactor. 2L bottle in the middle holds the medium. Erlenmeyer flask collects the out-flow from the reactor. Light-blocking covers were temporarily removed in this picture.*

### 2.2.2 Out-flow measurement

Both UTEX393 and SNS0120 were exposed to each set temperature for 3 days, starting at 10 ℃. The volume of the out-flow was measured for the second and the third days at the set temperature. The temperature was increased by 3 ℃ after each third day of measurement until the cultures collapsed at high temperatures. The growth rate per day was determined according to equation 2:

$$\text{Growth rate } (\text{day}^{-1}) = \frac{\frac{(V_1 + V_2)}{2}}{V_t} \quad [2]$$

$V_1$: out-flow volume (mL $d^{-1}$) measured on day 2, $V_2$: out-flow volume (mL $d^{-1}$) measured on day 3, $V_t$: volume of the photobioreactor (400 mL).

### 2.2.3 Sampling

At the end of each temperature treatment, approximately 55 mL of culture was sampled using sterile needles and syringes for lipid analysis, transcriptomics analysis, photosynthesis measurement, optical density measurement, and dry weight measurements.

For the lipid analysis, 10 mL of culture was added to a 15 mL centrifuge tube and then spun for 3 minutes at 2500 rpm. The supernatant was discarded, and the biomass was transferred into a 1.5 mL Eppendorf tube with 1 mL of Milli-Q water and then centrifuged for 1 minute. The supernatant was removed by using a pipette. The 1.5 mL tube containing the biomass was immediately dipped into liquid nitrogen and then stored at -80 ℃.

For the transcriptomics analysis, 1.5 mL of sample was collected into 1.5 mL Eppendorf tubes. The samples were pelleted by centrifugation (5,000 rpm for 2 mins), the supernatants were discarded, then the cell pellets were immediately quenched in liquid nitrogen. The samples were stored at −80 ℃ until RNA extraction.

The temperature experiment was duplicated for the SNS0120 and quadruplicated for the UTEX393. Alternate photobioreactors were swapped for each strain whenever starting a new replicate in order to avoid statistical biases arising from e.g. instrument-specific effects.

### 2.2.4 Optical density measurement

150 µl of the sample was added to a 1 cm path length cuvette and diluted 6-fold by adding 750 µl of Milli-Q water. The optical density at 540 nm and 680 nm was measured by using a Spectrophotometer DR3900 (HACH, Manchester, UK).

### 2.2.5 Dry weight measurement

Glass microfiber filters (47 mm diameter x 0.7 mm thickness, pore size 1.0 µm, VWR) were dried in an oven DRY-Line (VWR) at 97 °C overnight and then weighed. Five mL of sample was filtrated under a mild vacuum. The wet filters containing the samples were dried at 97 °C overnight and then weighed. The dry weight was then calculated from the difference in weight between the dry filters with and without biomass as shown in equation 3.

$$\text{Dry weight (mg/mL)} = \frac{(\text{final weight (mg)} - \text{initial weight (mg)})}{\text{volume (mL)}} \qquad [3]$$

### 2.2.6 Maximum photochemical efficiency of PSII and electron transport rate

10 µl of the sample was taken directly from the bioreactor by using a sterilized needle and syringe. The sample was diluted with 1250 µl of Mill-Q water in a cuvette (1 cm path length), which was placed in a Multi-Color PAM chlorophyll fluorometer (Heinz Walz GmbH, Germany) and dark-adapted for 5 mins prior to the measurement. Following dark-adaptation, a saturation pulse measurement using blue (440 nm) light was applied to measure the maximum quantum yield of photosystem II ($F_v/F_m$) (Kitajima & Butler, 1975) described in equation 4:

$$\frac{F_m - F_0}{F_m} = \frac{F_v}{F_m} \qquad [4]$$

Where $F_0$ is the minimal fluorescence under modulated measuring light and $F_m$ is the maximum fluorescence under saturating light. The difference between these two extreme values was calculated as the variable fluorescence ($F_v$).

The saturation pulse measurement was extended to a full rapid light curve protocol where the sample was sequentially exposed to increasing actinic illumination of 440 nm light with 20 seconds intervals between the steps, and the relative electron transport rate (ETR) was calculated after each of the illumination steps.

The relative ETR (rETR) was calculated according to the equation 5 (Heinz Walz GmbH, 2013):

$$\mathrm{rETR} = \mathrm{PAR} \times \mathrm{ETR\_Factor} \times \mathrm{Y(II)} \quad [5]$$

Where ETR_Factor was the default setting for the relative absorbance of photosystem II (0.42) and PAR was the photosynthetically active radiation irradiance (µmol $e^-$ $m^{-2}$ $s^{-1}$). The effective photochemical yield of photosystem II (Y(II)) (Genty et al., 1989) was calculated according to equation 6:

$$\mathrm{Y(II)} = \frac{F_m' - F}{F_m'} \quad [6]$$

Where $F_m'$ is the maximum fluorescence of the illuminated sample during the saturation pulse and F is the fluorescence level immediately before the saturation pulse. The light curve was fit with the Platt et al model to estimate the maximum ETR ($ETR_{max}$) (Platt et al., 1980).

### 2.2.7 Fatty acid extraction and gas chromatography

Fatty acid extraction and quantification were performed as described by Breuer et al. (2013). Samples stored in the -80 ℃ were lyophilized in a FreeZone 18 liter -50°C freeze dryer (Labconco Corporation, USA) for approximately 48 hours. Approximately 6 mg of lyophilized samples were weighed with a precision balance (Mettler Toledo MX-5, USA) and transferred into 2 mL bead-beating tubes containing 400 µl of 0.1 mm glass beads. 1 mL of chloroform: methanol (4:5) mixture was added to each tube, and then cell disruption was performed by Precellys evolution homogenizer (Bertin Instruments, France) at 6,000 rpm for 60 sec for 3 cycles with 30-second intervals between. The homogenate was transferred to a 10 mL glass tube with the addition of another 3 mL chloroform: methanol. Phase separation was done by adding 2.5 mL of the tris-base mixture (2-Amino-2-(hydroxymethyl)-1,3-propanediol including

1M NaCl and HCl (for adjusting pH to 7.5) to the glass tubes followed by vortex mixing (5 sec) and centrifugation (1,000 rpm, 5 min). The chloroform fraction (bottom phase) was transferred to the fresh 10 mL glass tubes. In order to recover as much chloroform fraction as possible, the phase separation process was repeated 2 more times by adding 1 mL of chloroform to the old tubes instead of adding the Tris-base mixture. The chloroform fraction was completely evaporated under a stream of $N_2$ gas to recover total fatty acids by using the Reacti-Therm Heating and Stirring Modules TS-18820 (Thermo Scientific). The fatty acids were derivatized to fatty acid methyl esters (FAMEs) by adding 3 mL of methanol containing 5 % $H_2SO_4$ followed by 3 h of incubation at 70 ℃ in the oven DRY-Line (VWR). 3 mL of $H_2O$ followed by 3 mL of hexane were added to the FAMEs, and then 15 min of vortex-mixing followed by centrifugation (1000 rpm for 5 min) were done to separate the FAMEs. 2 mL of the hexane phase (top phase) were collected in the fresh glass tubes, and 2 mL of H2O was added to wash the hexane phase. Hexane phases were collected in 1.5 mL vials after centrifuging (1000 rpm for 5 min). Quantification of the FAMEs was conducted by Gas Chromatograph and Flame Ionization Detector (GC-FID, SCION 436-GC, SCION Instruments) fitted with a splitless injector and a 30 m CP-WAX column (Agilent Technologies, USA). Supelco 37-component standards (Sigma-Aldrich, Oslo, Norway) were used for the identification and quantitation of the FAMEs with five-point calibrations. Blanks were included throughout extraction and derivatization, to eliminate trace background peaks.

### 2.3 Transcriptomics analysis

#### 2.3.1 RNA extraction

The samples were placed on ice and 500 µl of Trizol (Sigma-Aldrich, Oslo, Norway) was added to each sample, then transferred to 2 mL tubes containing 0.3 mL of glass beads (0.1 mm). Cells were homogenized with a Precellys evolution homogenizer (Bertin Instruments, France) at 6000 rpm for 60 sec for 2 cycles with 10-second intervals between. The homogenized samples were incubated for 5 minutes at room temperature, then 200 µl of chloroform was added followed by 5 seconds of vortex-mixing and 3 mins incubation at room temperature. Samples were centrifuged (12000 G/rcf, 15 min, 4 ℃). 100 µl of the supernatant containing RNA was transferred to a 1.5 mL Eppendorf tube followed by 100 µl of 100% ethanol. The mixture was transferred to the spin column included in the RNA clean-up kit (RNA clean & concentrator, Zymo Research, USA) and followed the kit's instruction with a modification to exclude usage

of the RNA Binding Buffer. A total of 50 µl flow-through (extracted RNA samples) were collected. 40 µl of each sample was transferred to a new 1.5 Eppendorf tube and immediately stored in -80 ℃. 10 µl of the extracted RNA samples were used for RNA quality check.

### 2.3.2 RNA quantity and quality check

NanoDrop One® (ThermoFisher Scientific, USA) and TapeStation 2200 with the RNA ScreenTape (Agilent Technologies, Germany) were used to confirm that the sample RNA quantity and quality were sufficient for sequencing. The samples with an RNA Integrity Number (RIN) less than 6.3 were excluded from the Illumina sequencing.

### 2.3.3 RNA sequencing

The mRNAs were purified from total RNA by using poly-T oligo-attached magnetic beads. The first strands of cDNA were synthesized by using random hexamer primers followed by the second strands of cDNA synthesis. The library was constructed after end-repair, A-tailing, adapter ligation, size selection, amplification, and purification (Figure 4). The library was checked with Qubit and real-time PCR for quantification and a bioanalyzer for size distribution detection. Sequencing was done using the Illumina platform, and the sequenced reads (raw reads) which were low quality (undetermined base > 10% or Q score <= 5) or contain adapters, were removed.

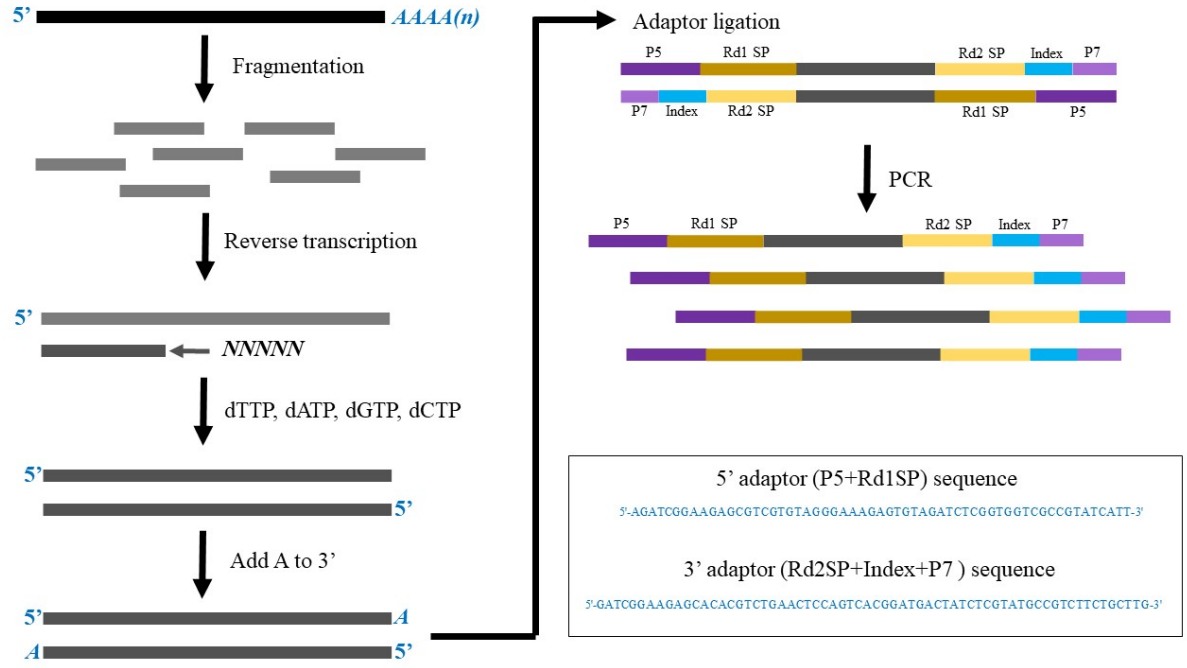


*Figure 4. The steps for library preparation. Each fragment size was 150 bp long.*

### 2.3.4 Bioinformatics tools

The *T. obliquus* UTEX393 genome reference sequence (GCA_900108755.1_sob1_genomic.fna) was obtained from the NCBI. We were unable to obtain a gene annotation file, therefore the genome sequence was annotated *de novo* using the transcript sequences generated in this study as described in (Hulatt et al., 2021). First, a *de novo* library of repetitive elements was constructed using RepeatModeler, which was used to annotate and mask repeat elements in the genome sequence. Genes were then annotated using Braker2 and RNA-seq evidence from three sample libraries (one each from 10, 25, and 34 °C treatments). In total 16432 protein-coding genes were annotated and a summary of the genomic repetitive elements is shown in Table 1. Annotation of gene function was conducted using BlastP against the SwissProt database, plus InterProScan and EggNog mapping tools to provide support for protein function.

*Table 1. Summary of the annotation of repeats, different types of repeat elements in the genome, and the % of the genome of each element.*

| | | | |
|---|---|---|---|
| Sequences: | 1368 | | |
| Total length: | 107715903 bp | | |
| GC level: | 56.89% | | |
| Bases masked: | 26006773 bp ( 24.14 %) | | |
| | Number of elements | Length occupied (bp) | Percentage of sequence (%) |
| **Retroelements** | 141019 | 16199881 | 15.04 |
| SINEs: | 0 | 0 | 0 |
| Penelope: | 0 | 0 | 0 |
| LINEs: | 22534 | 2568410 | 2.38 |
| CRE/SLACS: | 0 | 0 | 0 |
| L2/CR1/Rex: | 0 | 0 | 0 |
| R1/LOA/Jockey: | 25 | 3513 | 0 |
| R2/R4/NeSL: | 0 | 0 | 0 |
| RTE/Bov-B: | 274 | 62005 | 0.06 |
| L1/CIN4: | 65 | 27579 | 0.03 |
| LTR elements: | 118485 | 13631471 | 12.66 |
| BEL/Pao: | 93681 | 11053454 | 10.26 |
| Ty1/Copia: | 0 | 0 | 0 |
| Gypsy/DIRS1: | 3073 | 337034 | 0.31 |
| Retroviral: | 0 | 0 | 0 |
| **DNA transposons** | 2184 | 173206 | 0.16 |
| hobo-Activator | 2184 | 173206 | 0.16 |
| Tc1-IS630-Pogo | 0 | 0 | 0 |
| En-Spm | 0 | 0 | 0 |
| MuDR-IS905 | 0 | 0 | 0 |
| PiggyBac | 0 | 0 | 0 |
| Tourist/Harbinger | 0 | 0 | 0 |
| Other (Mirage, P-element, Transib) | 0 | 0 | 0 |
| **Rolling-circles:** | 0 | 0 | 0 |
| **Unclassified:** | 78182 | 9623259 | 8.93 |
| **Total interspersed repeats:** | | 25996346 | 24.13 |
| **Small RNA:** | 105 | 10427 | 0.01 |
| **Satellites:** | 0 | 0 | 0 |
| **Simple repeats:** | 0 | 0 | 0 |
| **Low complexity:** | 0 | 0 | 0 |

Mapping of RNA-seq read to the reference genome was conducted with HISAT2 with the paired reads option. The .sam alignment files were converted to the binary-alignment-map (.bam) format and sorted with SAMTOOLS. Aligned reads were assigned to the genomic features and counted those quantities by using the “featureCounts” function in the SUBREAD program.

The counted features for all 12 samples were added to a data frame using R version 4.1.2. Differentially expressed genes were estimated by using "edgeR", "limma", and "variancePartition" R packages (Hoffman & Roussos, 2021; Hoffman & Schadt, 2016; Law et al., 2014). R function *cpm()* was used to filter genes with greater than 1 counts-per-million (CPM) in all the samples. Subsequently, R-function *calcNormFactors()* with the Trimmed Mean of M-values normalization (TMM) method was used to calculate normalization factors to scale the raw library sizes (Robinson et al., 2010). Due to the repeated measurements at increasing temperatures, we included a random effect to the design matrix. The *voomWithDreamWeights()* R-function was applied to calculate log2-counts per million (logCPM), to estimate the mean-variance relationship, and to use this to compute appropriate observation-level weights. The *dream()* R-function was used to fit the linear mixed model (restricted maximum likelihood, REML) for each gene for calculating the log2-Fold Change. The p-value was estimated by applying the empirical Bayes statistics for differential expression "eBayes()". The Kenward-Roger approximation and the Satterthwaite approximation were used in the REML to estimate the p-values and control the false positive rate (Gabriel Hoffman, 2020). Finally, the *topTable()* function was used for summarizing the genes from the fitted mixed model. Volcano plots were generated to visualize significantly differentially expressed genes as well as upregulated or downregulated genes by using the "ggplot2" R package. GO enrichment analysis was performed separately for up- and downregulated genes using classic Fisher's exact test in R-package topGO v2.46 (Alexa & Rahnenfuhrer, 2021).

### 2.4 Statistical analysis

#### 2.4.1 Medium selection

The unpaired t-test was used to compare the $OD_{540}$ and $OD_{680}$ for both NB (pH4.2) and 3N-BBM at the end of the experiment. The same statistical test was used for comparing NB (pH6.2) and 3N-BBM.

#### 2.4.2 Specific growth rate, $F_v/F_m$, ETR, and GC-FID

The pairwise t-test for paired samples was performed to determine whether there were any significant differences in growth rate, photosynthesis, and lipid contents between low (10 °C), optimal (25 °C), and high (34 °C) temperatures.

### 2.4.3 Thermal performance curve model determination

The thermal performance curve was fitted by using R version 4.1.2 and the rTPC R package (Padfield et al., 2021). The package contained 24 thermal performance models (Appendix 1): Beta, Boatman, Briere2, Delong, Flinn, Gaussian, Hinshelwood, Joehnk, Johnson_Lewin, Kamykowski, Lactin2, Modified gaussian, O'neill, Pawar, Quadratic, Ratkowsky, Rezende, Sharpe-Schoolfield high, Spain, Thomas1 &2, Weibull temperature performance models were compared (Angilletta, 2006; Boatman et al., 2017, 2017; Briere et al., 1999; C. N. Hinshelwood, 1947; DeLong et al., 2017; Flinn, 1991; Jöhnk et al., 2008; F. H. Johnson & Lewin, 1946; Kamykowski, 1985; Kontopoulos et al., 2018; Lactin et al., 1995; Lynch & Gabriel, 1987; Montagnes et al., 2008; Niehaus et al., 2012; O'Neill, R.V. et al., 1972; Ratkowsky et al., 1983a; Rezende & Bozinovic, 2019; Schoolfield et al., 1981; J. D. Spain, 1982; M. K. Thomas et al., 2017; Weibull, 1995). R function *nls_multstart()* in the nls.multstart R package was used to fit the curves with multiple sets of random start-parameter values picked from a uniform distribution between "start_lower" and "start_upper" for each parameter. The function returned the model fit after 100 new start parameter combinations (Padfield et al., 2021). All the models were fitted to the growth rate and calculated the corrected Akaike's information criterion (AICc) (Akaike, 1974; Hurvich et al., 1998). The best fit model was determined based on the lowest AICc value among the 24 models.

After the best-fit model was determined, the areas under the curves were calculated by using the function *auc()* in the Flux R-package in order to compare the differences between the two strains. All the statistical analyses in this thesis were performed by using the R version 4.1.2.

# 3 Results

## 3.1 Medium selection

Cultures with Bold's Basal Medium (3N-BBM) showed typical rapid growth and vivid green culture color soon after the beginning of the experiment. However, limited growth was observed initially in the NB at low pH (pH 4.2) (Figure 5, Figure 6). Eventually, after a long period of lag phase, growth in the NB was observed approximately 6 days after the start of the experiment, but the algae grown with NB remained unusually pale yellow. Significant differences were found ($p < 0.01$) for both $OD_{540}$ and $OD_{680}$ between the two media (Figure 6), and overall showed that the NB medium at naturally low pH was unsuitable for cultivation.

Using NB medium with corrected pH (pH 6.2), growth was much improved and comparable to the control 3N-BBM medium (Figure 7). The green coloration in both media was also very similar (Figure 5). Statistically, significant differences were not found ($p > 0.05$) for both $OD_{540}$ and $OD_{680}$ between the two media, indicating that the NB medium could be a suitable replacement for conventional media, but requires additional buffering of the pH (Figure 7).

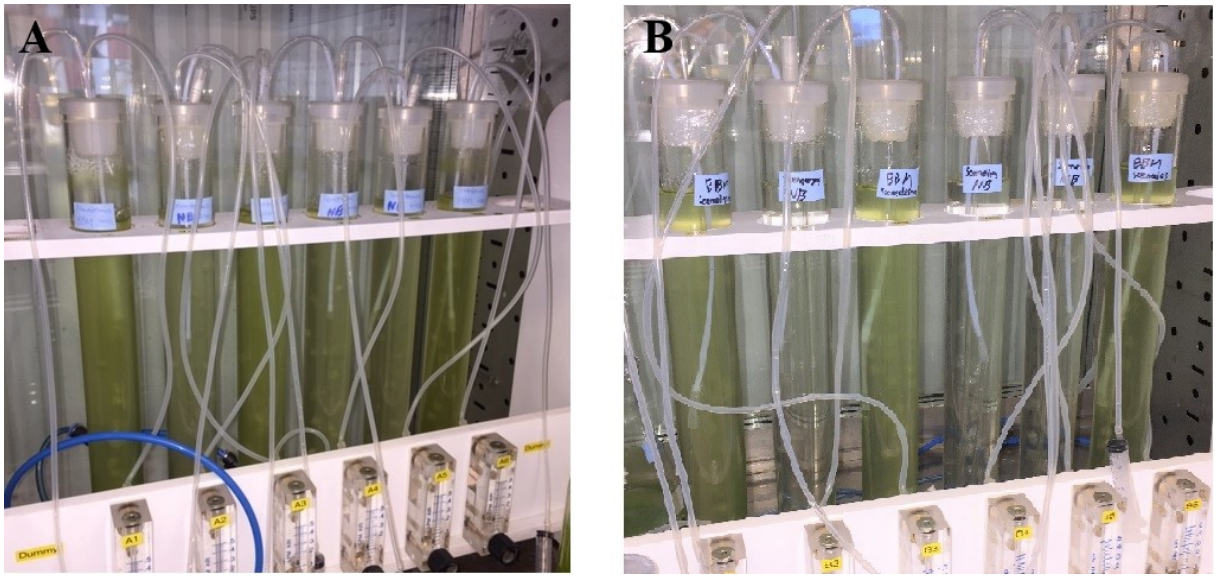


*Figure 5. The color of cultures in the medium with different pH. (A): comparison between NB (pH6.2) and BBM (pH 6.5). Both NB and BBM indicated similarities in the color of cultures simultaneously. (B): comparison between NB (pH 4.2) and BBM (pH 6.5). Cultures grown in the NB were transparent in color on day 2 while cultures with the BBM already showed vivid green color.*

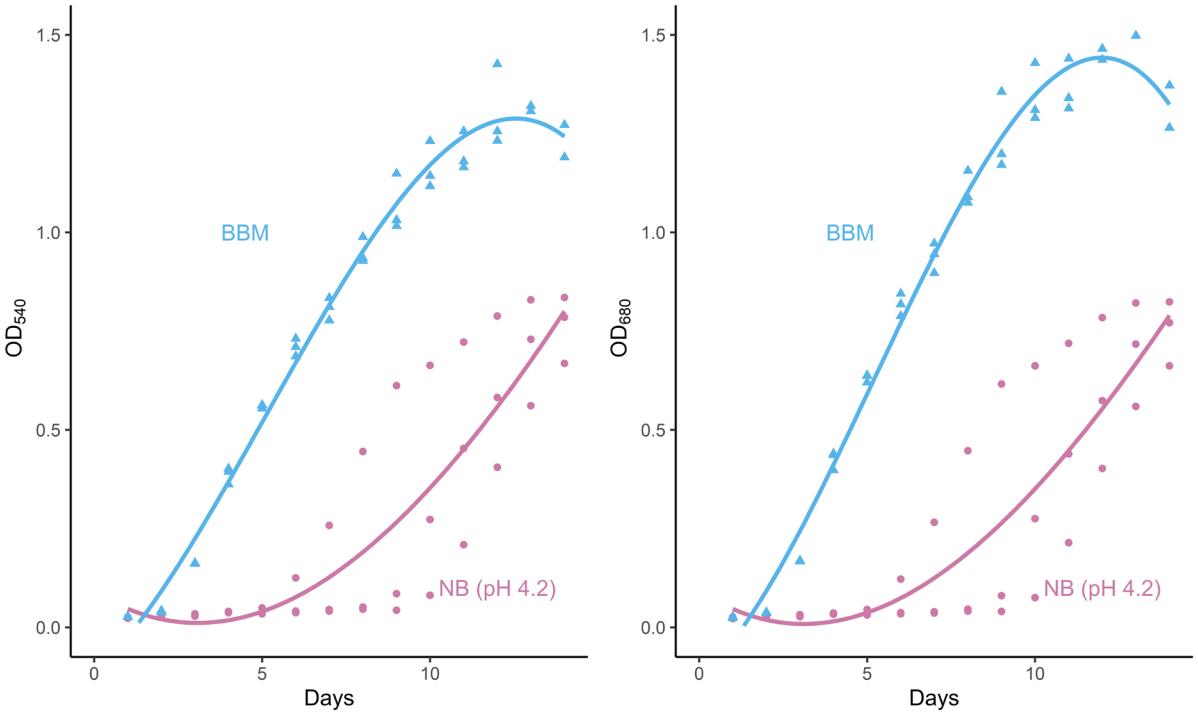


*Figure 6. Comparison of $OD_{540}$ and $OD_{680}$ of the culture grown in the NB (pH 4.2) and BBM (pH 6.5). BBM indicated rapid growth, and the NB showed no growth until day 5. These curves were fitted by using the locally weighted least squares regression (loess) method.*

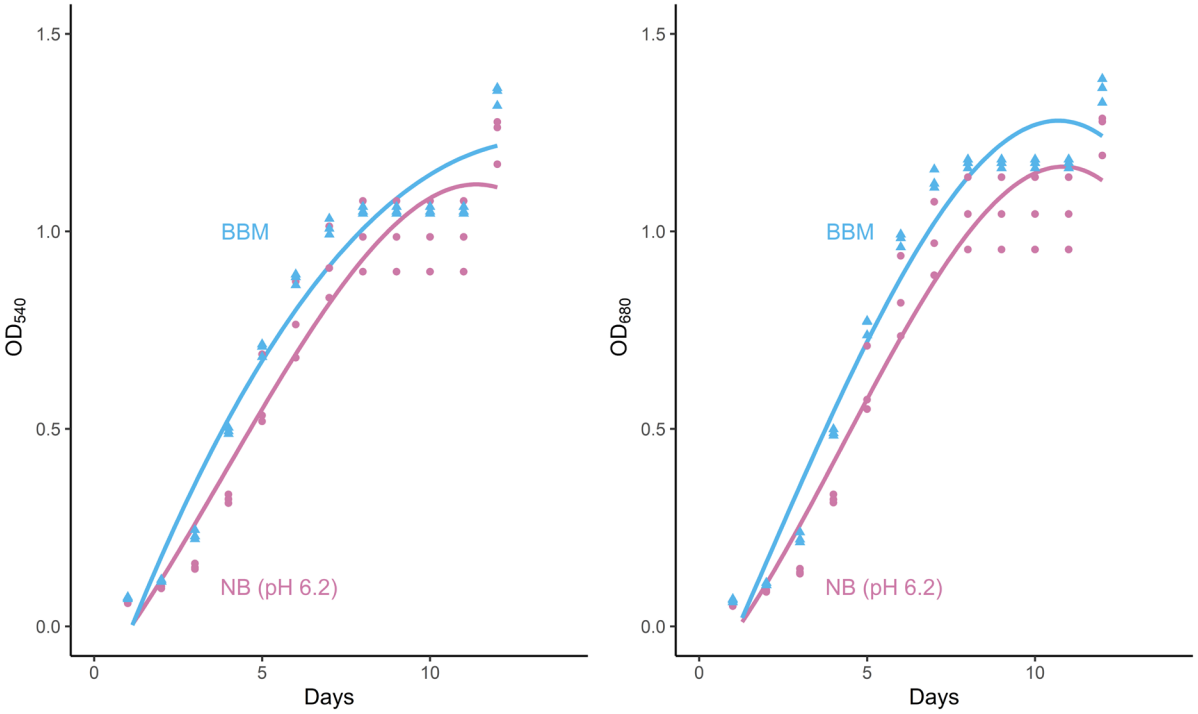


*Figure 7. Comparison between NB (pH 6.2) and BBM (pH 6.5). Both $OD_{540}$ and $OD_{680}$ did not show any statistically significant differences. The NB with adjusted pH supported rapid growth as BBM.*

### 3.2 Temperature experiment

#### 3.2.1 Cultivation conditions

Parameters in the photobioreactor including the light intensity, turbidity of the culture, air supply, $CO_2$ concentration, dry weight, and optical density were adequately constant throughout the experiment isolating the effect of temperature (Figure 8).

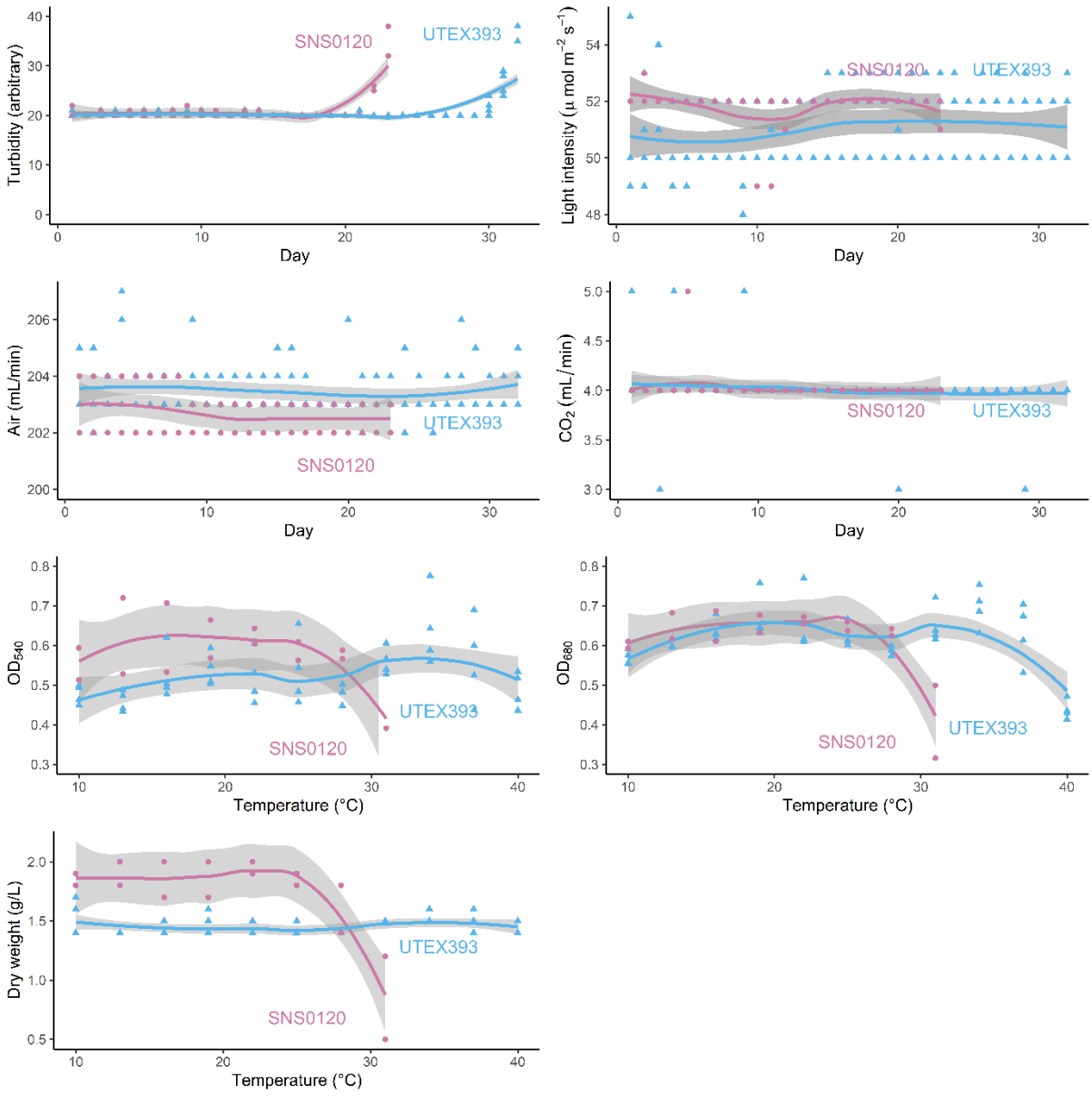


*Figure 8. Photobioreactor parameters during the temperature experiment. The light intensity, turbidity, air, and $CO_2$ supply were measured daily. The $OD_{540}$, $OD_{680}$, and dry weight were measured during the*

*sampling at each tested temperature. The SNS0120 culture collapsed at 31 °C. The shaded region represents the confidence intervals (95 % CI).*

### 3.2.2 Growth rate variation with temperature

The growth rate of both UTEX393 and the SNS0120 increased significantly up to 25 °C (Table 2). The UTEX393 strain reached to 0.99 ± 0.05 $d^{-1}$ at 25 °C ($p < 0.01$), whilst the SNS0120 reached only 0.75 ± 0.01 $d^{-1}$ ($p < 0.05$). When the temperature reached 28 °C, both strains showed a similar growth rate of 25 °C. Interestingly, after this point, the culture of the SNS0120 started to become pale yellow and flocculated within 24 hours after the temperature was set to 31°C, and then the culture collapsed shortly after (Figure 9). Out-flow was not generated from the SNS0120 culture at 31 °C. On the other hand, the UTEX393 showed strong growth until 37 °C indicating much higher growth performance and thermal tolerance than the SNS0120.

*Table 2. The specific growth rate at each tested temperature for both UTEX393 and the SNS0120. GR: specific growth rate, SD: standard deviation.*

| Strain | Temperature (°C) | GR ($d^{-1}$) | SD |
|---|---|---|---|
| UTEX393 | 10 | 0.52 | 0.02 |
| | 13 | 0.69 | 0.03 |
| | 16 | 0.75 | 0.03 |
| | 19 | 0.83 | 0.04 |
| | 22 | 0.96 | 0.02 |
| | 25 | 0.99 | 0.05 |
| | 28 | 0.99 | 0.02 |
| | 31 | 0.93 | 0.03 |
| | 34 | 0.87 | 0.04 |
| | 37 | 0.64 | 0.03 |
| | 40 | 0.04 | 0.01 |

| Strain | Temperature (°C) | GR ($d^{-1}$) | SD |
|---|---|---|---|
| SNS0120 | 10 | 0.46 | 0.01 |
| | 13 | 0.52 | 0.09 |
| | 16 | 0.53 | 0.01 |
| | 19 | 0.57 | 0.00 |
| | 22 | 0.65 | 0.06 |
| | 25 | 0.75 | 0.00 |
| | 28 | 0.71 | 0.00 |
| | 31 | 0.05 | 0.01 |

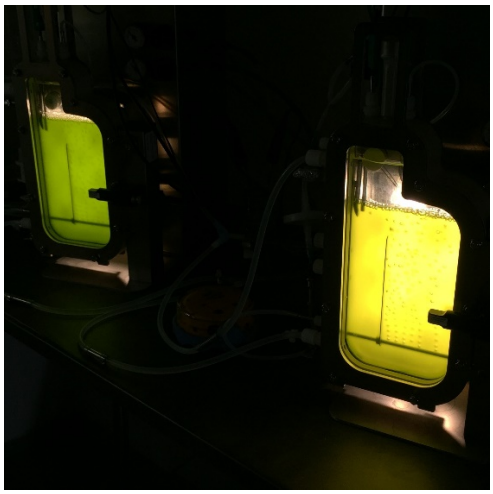

*Figure 9. Color of the cultures at 31 °C. UTEX 393 on the left and SNS0120 on the right photobioreactor. The SNS0120 showed reduced $OD_{680}$ at this temperature and displayed pale yellow culture color indicating that chlorophyll was reduced.*

### 3.3 Comparing thermal response curves

A total of 22 thermal performance curve models were fitted to the growth rate data, and the best-fitting models were determined for both UTEX393 and SNS0120. The lowest corrected AIC (AICc) value of -158 was obtained by using the Boatman model for the UTEX 393 (Figure 10) among other tested models (Appendix 2). The optimum growth temperature for the UTEX 393 was determined as 27.2 °C from the model (Figure 11).

For the SNS0120, the lowest AICc value was obtained by the Rezende model (AICc = -48) (Figure 10). The optimum growth temperature for the SNS0120 was determined as 26.8 °C by the Rezende model (Figure 11).

The area under the curves was calculated as 23.9 for the UTEX393 and 12.3 for the SNS0120, capturing striking differences in growth rate performance between the two strains. While there was a similar optimum temperature, the SNS0120 had much weaker growth performance across the full temperature range and was more susceptible to thermal inactivation above the optimum temperature.

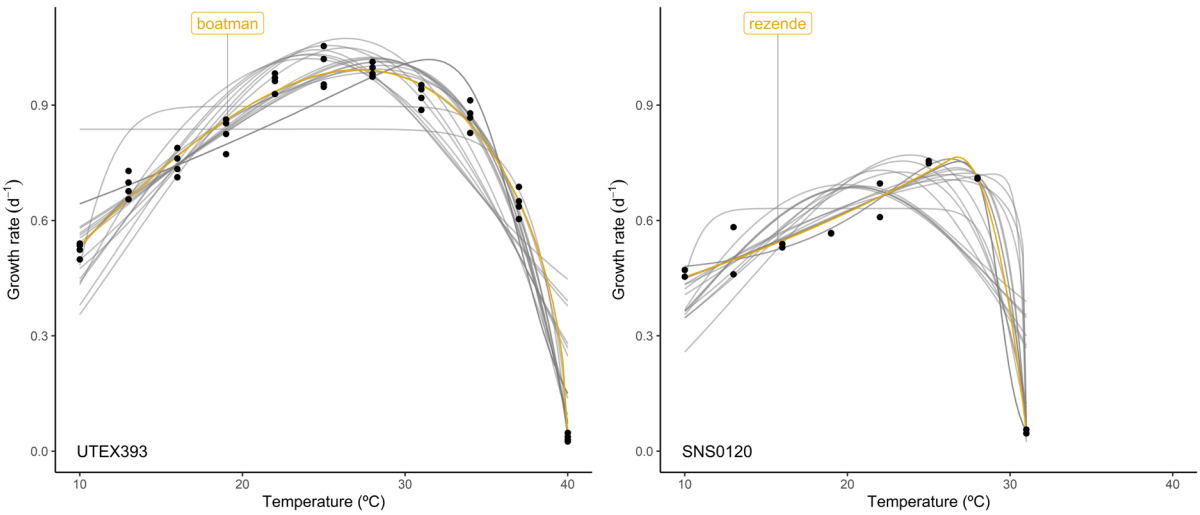


*Figure 10. The best models for each strain. Boatman model (yellow) was chosen as the best-fitted model among other models (grey) for the UTEX 393 strain (left). Rezende model was the best-fitted model for the SNS0120 (right). Growth rates measured at each temperature were shown as black dots.*

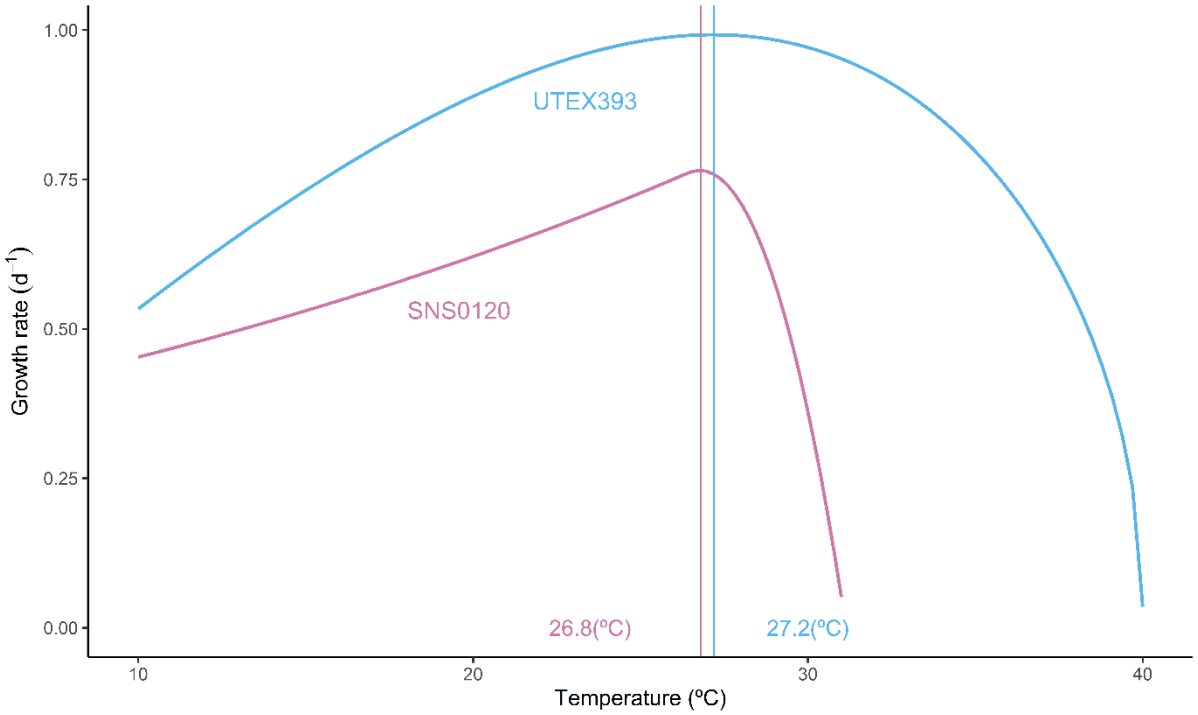


*Figure 11. The thermal performance curves fitted by the best models for each strain and an estimated optimal growth temperature. Vertical lines indicted the optimal growth temperature for each strain.*

### 3.4 Effect of temperature on photosynthesis

The maximum quantum yield of photosystem II ($F_v/F_m$) of the UTEX 393 strain showed an average $F_v/F_m$ of 0.72 at temperatures between 10 °C to 37 °C. The $F_v/F_m$ was significantly increased from 0.68 at 10 °C to 0.75 at 25 °C ($p < 0.01$). Statistically significant differences in $F_v/F_m$ were not found between 25 °C to 37 °C (Figure 12).

The $ETR_{max}$ for UTEX 393 strain at 10, 25, and 34 °C was 49.4, 36.7, and 30.3 µmol $e^- m^{-2}s^{-1}$ respectively (Table 3). There was not any statistical significance found between the tested temperatures. The $ETR_{max}$ was significantly reduced to 13.3 µmol $e^-/m^2s$ at 37 °C compared to at 34 °C ($p < 0.05$) (Figure 12).

For the SNS0120, a similar trend as the UTEX393 was observed for the $F_v/F_m$ with an average of 0.74 at the temperature between 10 to 31 °C. No statistical significance in $F_v/F_m$ was found between tested temperatures. Unlike the UTEX 393, at 31 °C where the culture of the SNS0120 started to turn yellow in color and collapse, there was no statistical significance found on $F_v/F_m$ between 28 °C and 31 °C.

The SNS0120 indicated the $ETR_{max}$ of 48.8, 21.5, and 20.7 µmol $e^- m^{-2}s^{-1}$ at 10, 25, and 31°C respectively (Table 3). The highest $ETR_{max}$ was measured at 10 °C, then reduced to 27.2 µmol $e^- m^{-2}s^{-1}$ at 13 °C and became approximately constant between 13 °C to 31 °C (Figure 12).

*Table 3. $F_v/F_m$ and ETRmax for the UTEX393 and SNS0120 at each temperature. Units for the $ETR_{max}$ were µmol $e^- m^{-2}s^{-1}$. SD: standard deviation.*

| | Temperature (°C) | 10 | 13 | 16 | 19 | 22 | 25 | 28 | 31 | 34 | 37 |
|---|---|---|---|---|---|---|---|---|---|---|---|
| $F_V/F_m$ | UTEX393 | 0.68 | 0.69 | 0.65 | 0.73 | 0.75 | 0.75 | 0.76 | 0.75 | 0.75 | 0.71 |
| | SD | 0 | 0.01 | 0.12 | 0.03 | 0.01 | 0.01 | 0.02 | 0.01 | 0.01 | 0.02 |
| | SNS0120 | 0.71 | 0.7 | 0.72 | 0.73 | 0.76 | 0.75 | 0.77 | 0.76 | | |
| | SD | 0 | 0.03 | 0.03 | 0.02 | 0.01 | 0 | 0 | 0.01 | | |
| $ETR_{max}$ | UTEX393 | 49.38 | 38.68 | 37.33 | 40.88 | 41.10 | 36.65 | 34.70 | 31.68 | 30.25 | 13.30 |
| | SD | 7.84 | 14.33 | 15.60 | 21.13 | 15.27 | 9.51 | 13.05 | 8.15 | 9.98 | 5.64 |
| | SNS0120 | 48.90 | 27.20 | 26.60 | 30.60 | 36.90 | 21.50 | 28.80 | 20.70 | | |
| | SD | 15.60 | 12.90 | 4.90 | 5.20 | 10.30 | 9.20 | 12.50 | 12.50 | | |

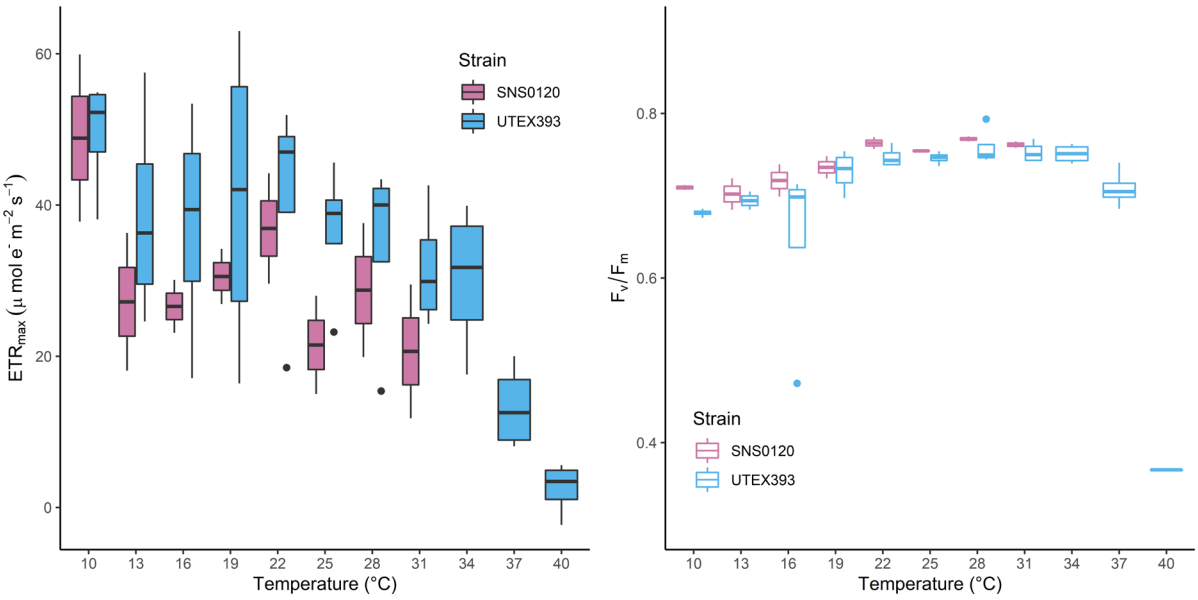


*Figure 12. The $ETR_{max}$ (left) and $F_v/F_m$ (right) at each tested temperature for each strain.*

### 3.5 Effect of temperature on fatty acids

The UTEX393 showed that the total fatty acids (TFA) contents were largely consistent from 10 °C to 37 °C (Figure 13). The TFA contents were 15.3 %, 16.5 %, and 14.5 % of the cell dry weight at 10 °C, 25 °C, and 34 °C respectively (Table 4). A paired t-test did not indicate any statistically significant differences between 10 °C and 25 °C ($p > 0.05$), 25 °C and 34 °C ($p > 0.05$), or 10 °C and 34 °C ($p > 0.05$).

For the SNS0120, the TFA contents were 12.8, 11.6, and 11.0 % of the cell dry weight at 10, 25, and 31 °C respectively, and there were no significant differences found between the tested temperatures. The TFA contents of the SNS0120 were lower than the UTEX393 throughout the experiment.

*Table 4. Total fatty acid contents of UTEX 393 and SNS0120 (n = 4 for UTEX393 and n = 2 for SNS0120) at each tested temperature. SE: standard error.*

| Temperature (°C) | 10 | 13 | 16 | 19 | 22 | 25 | 28 | 31 | 34 | 37 | 40 |
|---|---|---|---|---|---|---|---|---|---|---|---|
| UTEX393 (%) | 15.3 | 16.4 | 15.3 | 16.4 | 17.1 | 16.5 | 16.9 | 16.1 | 14.5 | 16 | 10.6 |
| SE | 1.6 | 0.3 | 0.5 | 0.9 | 0.3 | 0.6 | 0.6 | 0.8 | 0.3 | 0.8 | 1.2 |
| SNS0120 (%) | 12.3 | 12.8 | 12.1 | 14.8 | 13.4 | 11.6 | 12.3 | 11 | | | |
| SE | 0.4 | 0.1 | 0.9 | 0.3 | 0.03 | 1.7 | 0.4 | 1.3 | | | |

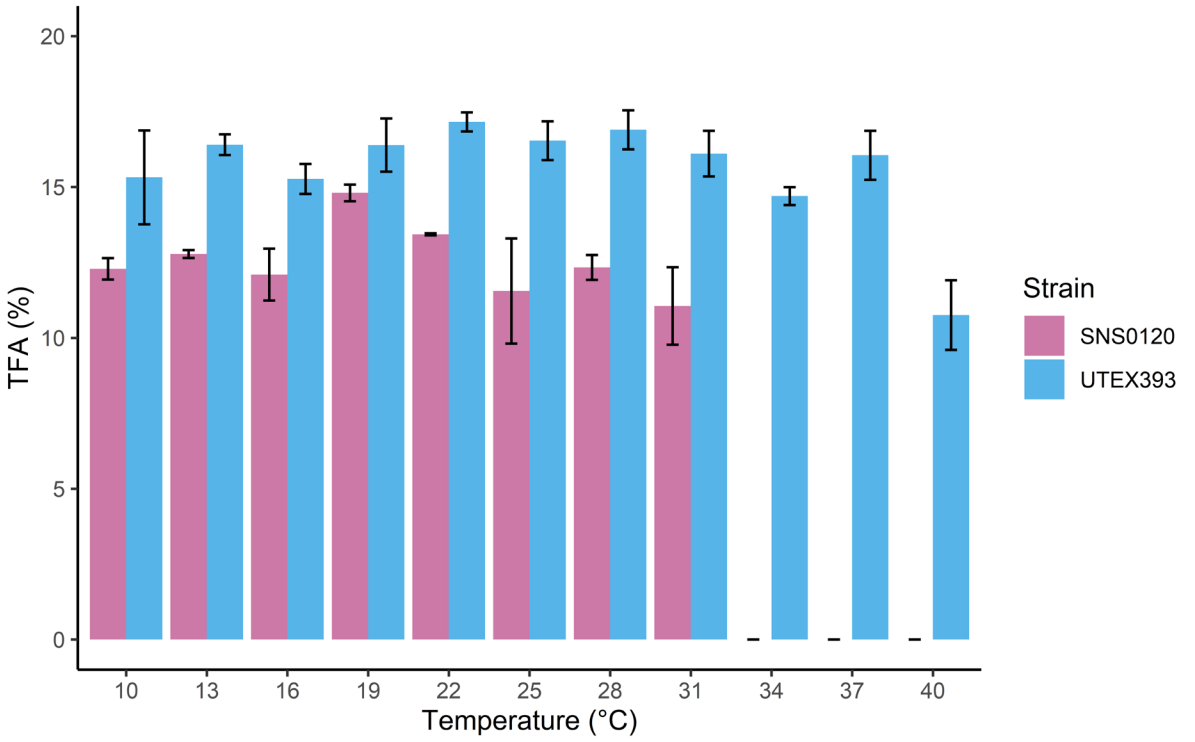


*Figure 13. The total fatty acids (TFA) contents at each tested temperature for both UTEX393 and SNS0120. The error bar indicates standard error.*

Fatty acids were comprised primarily of C18:3*n*-3 (α-linolenic acid) and C16:0 (palmitic acid) in UTEX 393. Omega-3 polyunsaturated fatty acids (PUFA) including C16:4*n*-3, C18:3*n*-3, and C18:4*n*-3 (stearidonic acid), showed decreasing trends while the omega-6 PUFA including C16:2*n*-6 (hexadecadienoic acid), C18:2*n*-6cis (linoleic acid), and C18:3*n*-6 (γ-linolenic acid), showed increasing trends as the temperature increased (Figure 14). Significant effects of temperature were found on C16:2*n*-6, C16:4*n*-3, C18:0 (stearic acid), C18:2*n*-6cis, C18:3*n*-6, C18:3*n*-3, C18:4*n*-3, and C20:1*n*-9 (Eicosenoic acid) fatty acids. The paired T-test between 10-25, 10-34, and 25-34 °C indicated that a decrease in omega-3 PUFA and an increase in omega-6 was statistically significant ($p < 0.05$) (Table 5).

For the SNS0120, significant differences were found only for the C16:4*n*-3 and the C18:3*n*-6 when compared to 10 and 31 °C. The omega-3 PUFA, C16:4*n*-3 showed a significant decrease from 8.95 mg/g at 10 °C to 4.16 mg/g at 31 °C. The omega-6 PUFA, C18:3*n*-6 indicated a significant increase from 0.11 mg/g at 10 °C to 3.37 mg/g at 31 °C (Figure 15, Table 6).

*Table 5. Quantities of each fatty acid detected in the UTEX 393 strain at 10, 25, and 34 °C. Non-significances were indicated with "-".*

| | C14:0 (mg/g) | C16:0 (mg/g) | C16:1n-9 (mg/g) | C16:2n-6 (mg/g) | C16:3n-3 (mg/g) | C16:4n-3 (mg/g) | C18:0 (mg/g) | C18:1n-9 (mg/g) | C18:2n-6cis (mg/g) | C18:3n-6 (mg/g) | C18:3n-3 (mg/g) | C18:4n-3 (mg/g) | C20:1n-9 (mg/g) |
|---|---|---|---|---|---|---|---|---|---|---|---|---|---|
| 10 °C | 1.95 | 25.61 | 0.43 | 0.56 | 3.63 | 14.33 | 7.74 | 13.57 | 6.71 | 0.23 | 73.36 | 4.34 | 0.75 |
| 25 °C | 1.81 | 31.96 | 2.43 | 3.26 | 3.38 | 16 | 1.15 | 15.16 | 31.18 | 0.69 | 53.9 | 4.22 | 0.24 |
| 34 °C | 1.67 | 32.23 | 1.43 | 5.93 | 6.67 | 7.22 | 1.52 | 14.91 | 39.05 | 2.39 | 30.94 | 2.74 | 0.32 |
| | SD | SD | SD | SD | SD | SD | SD | SD | SD | SD | SD | SD | SD |
| 10 °C | 0.63 | 6.32 | 0.44 | 0.19 | 3.55 | 1.47 | 11.5 | 3.71 | 0.76 | 0.1 | 7.11 | 0.37 | 0.59 |
| 25 °C | 0.74 | 3 | 1.58 | 0.26 | 5.03 | 1.97 | 0.99 | 0.79 | 2.26 | 0.1 | 3.08 | 0.26 | 0.12 |
| 34 °C | 0.3 | 1.58 | 0.91 | 0.14 | 7 | 0.89 | 0.91 | 0.29 | 1.84 | 0.14 | 1.05 | 0.18 | 0.13 |
| | P-value | P-value | P-value | P-value | P-value | P-value | P-value | P-value | P-value | P-value | P-value | P-value | P-value |
| 10 °C vs 25 °C | - | - | - | < 0.01 | - | - | - | - | < 0.01 | < 0.01 | 0.03 | - | - |
| 25 °C vs 34 °C | - | - | - | < 0.01 | - | < 0.01 | 0.02 | - | < 0.01 | < 0.01 | < 0.01 | < 0.01 | 0.01 |
| 10 °C vs 31 °C | - | - | - | < 0.01 | - | < 0.01 | - | - | < 0.01 | < 0.01 | < 0.01 | 0.01 | - |

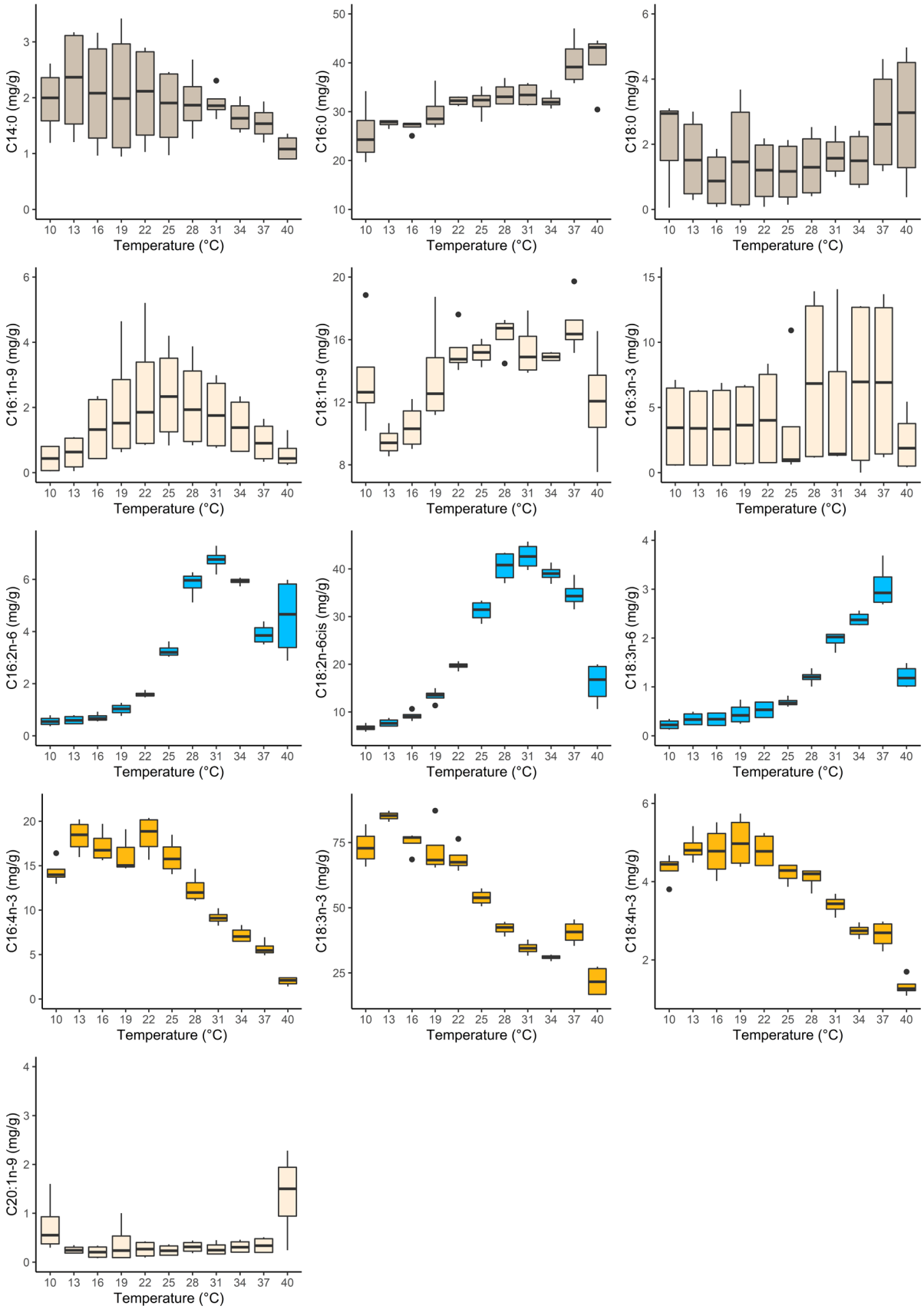


*Figure 14. Contents of each fatty acid in UTEX 393 at temperatures between 10 °C to 40 °C.*

*Table 6. Quantities of each fatty acid detected in the SNS0120 at 10, 25, and 34 °C. Non-significances were indicated with "-".*

| | C14:0 (mg/g) | C16:0 (mg/g) | C16:1n-9 (mg/g) | C16:2n-6 (mg/g) | C16:3n-3 (mg/g) | C16:4n-3 (mg/g) | C18:0 (mg/g) | C18:1n-9 (mg/g) | C18:2n-6cis (mg/g) | C18:3n-6 (mg/g) | C18:3n-3 (mg/g) | C18:4n-3 (mg/g) | C20:1n-9 (mg/g) |
|---|---|---|---|---|---|---|---|---|---|---|---|---|---|
| 10 °C | 1.65 | 24.77 | 1.80 | 0.78 | 7.03 | 8.95 | 0.30 | 12.78 | 5.24 | 0.11 | 54.64 | 4.84 | 0.54 |
| 25 °C | 1.49 | 25.20 | 3.07 | 2.40 | 11.57 | 4.82 | 0.32 | 13.94 | 17.97 | 1.41 | 28.07 | 5.28 | 0.41 |
| 34 °C | 1.49 | 25.28 | 3.97 | 2.81 | 10.79 | 4.16 | 0.82 | 16.02 | 14.39 | 3.37 | 22.62 | 4.86 | 0.66 |
| | SD | SD | SD | SD | SD | SD | SD | SD | SD | SD | SD | SD | SD |
| 10 °C | 0.32 | 1.59 | 0.10 | 0.05 | 0.23 | 0.17 | 0.42 | 2.04 | 0.08 | 0.00 | 0.52 | 0.50 | 0.06 |
| 25 °C | 0.55 | 4.57 | 0.85 | 0.39 | 2.83 | 1.25 | 0.07 | 3.18 | 3.06 | 0.21 | 7.21 | 0.89 | 0.02 |
| 34 °C | 0.30 | 7.39 | 0.02 | 0.17 | 0.70 | 0.25 | 0.25 | 2.99 | 3.06 | 0.02 | 3.21 | 0.74 | 0.43 |
| | P-value | P-value | P-value | P-value | P-value | P-value | P-value | P-value | P-value | P-value | P-value | P-value | P-value |
| 10 °C vs 25 °C | - | - | - | - | - | - | - | - | - | - | - | - | - |
| 25 °C vs 34 °C | - | - | - | - | - | - | - | - | - | - | - | - | - |
| 10 °C vs 31 °C | - | - | - | - | - | 0.02 | - | - | - | < 0.01 | - | - | - |

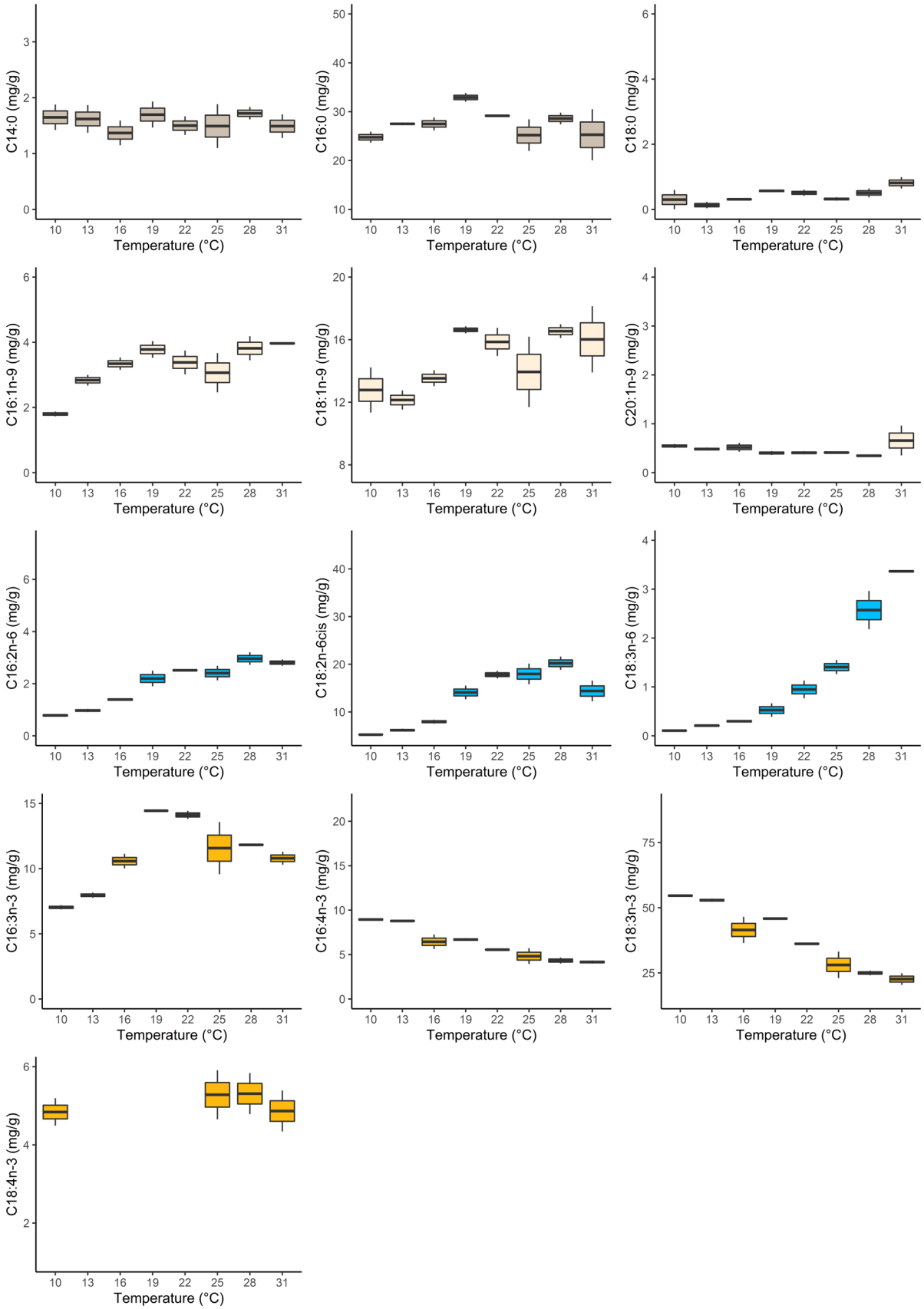


*Figure 15. Contents of each fatty acid in the SNS0120 at temperatures between 10 °C to 31 °C.*

### 3.6 Transcriptomics

#### 3.6.1 RNA quantity and RNA integrity numbers (RIN)

Samples collected at 10 °C and 25 °C indicated sufficient RNA quantities (Table 7) and RINs sufficient for the Illumina sequencing (Figure 16). Samples collected at 34 °C and 37 °C also indicated sufficient quantities of the RNA. The 37 °C samples showed lower RINs (degradation of RNA) than the minimum required for the Illumina sequencing (minimum RIN > 6.3), thus the samples taken at 34 °C were selected for sequencing (Figure 16).

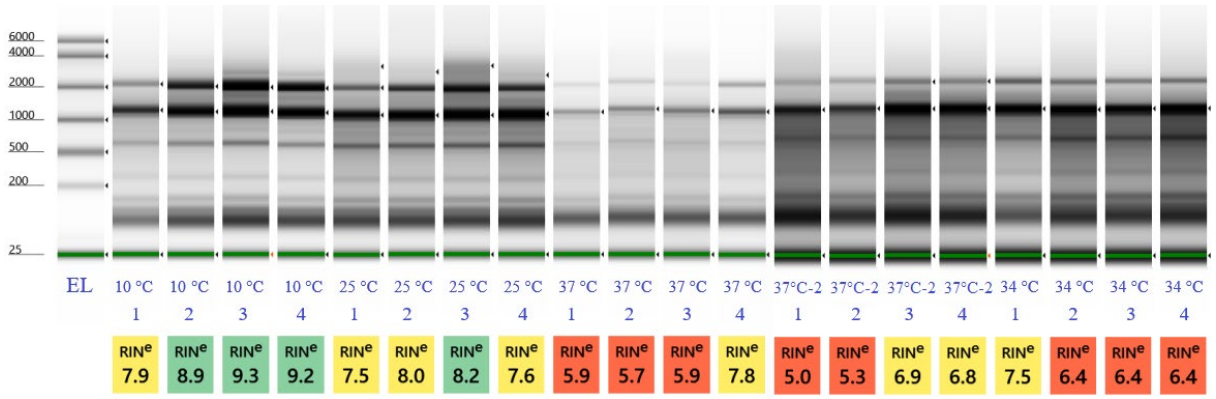


*Figure 16. RINs for RNA extracted from samples cultivated at 10 °C, 25 °C, and 37 °C. the RIN values were lower at 34 °C and 37 °C compared to the 10 °C and 25 °C. EL: electric ladder.*

*Table 7. The quantities of RNA (ng/µl) in the samples harvested at 10 °C, 25 °C, 34 °C, and 37 °C measured by the NanoDrop®.*

| Temperature | Replicate 1 | Replicate 2 | Replicate 3 | Replicate 4 |
|---|---|---|---|---|
| 10 °C | 193 | 297 | 400 | 305 |
| 25 °C | 288 | 317 | 367 | 356 |
| 37 °C | 117 | 127 | 134 | 122 |
| 37 °C - 2 | 137 | 92.4 | 140 | 125 |
| 34 °C | 93.9 | 131 | 117 | 144 |

#### 3.6.2 Mapping rates

Hisat2 was able to perform genome mapping with around 71.7 % to 80.5 % of the mapping rate across all the samples. The featureCounts results showed less than 50 % of transcripts were successfully assigned to the protein-coding genes (CDS) in the genome annotation (Appendix 3).

### 3.6.3 Differentially expressed genes (DEG)

Transcriptomics analysis showed that a total of 4,971 significantly differentially expressed genes ($p < 0.01$) were identified after the temperature was increased from 10 °C to 25 °C (41.5 % of total genes). $Log_2$ Fold-Changes ($Log_2FC$) indicated that 2,516 of 4,971 DEGs were upregulated ($Log_2FC > 0$) while 2,455 DEGs were downregulated ($Log_2FC < 0$) (Figure 17). After increasing the temperature from 25 °C to 34 °C, a total of 3,683 significant DEGs ($p < 0.01$) were identified (30.0 % of total genes). 1,915 of 3,683 DEGs were upregulated ($Log_2FC > 0$) while 1,768 DEGs were downregulated ($Log_2FC < 0$) (Figure 17).

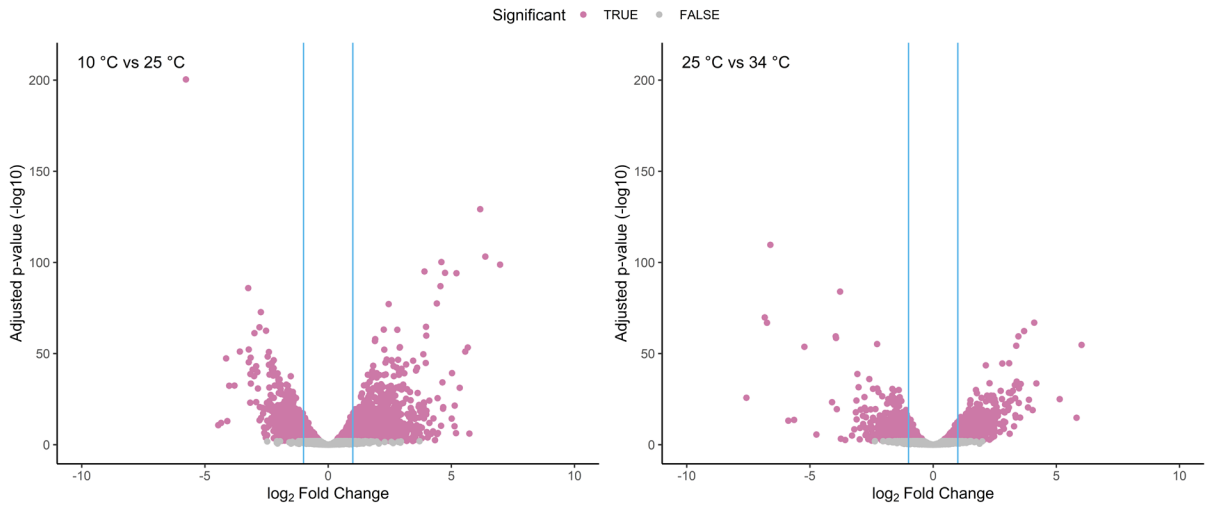


*Figure 17. Significantly differentially expressed genes after the temperature was increased from 10 °C to 25 °C (left) as well as from 25 °C to 34 °C (right). Blue vertical lines: indicating the $log_2FC$ values at -1 and 1.*

### 3.6.4 Functional annotation of the DEGs

Differential expression analysis showed that genes related to photosynthesis, lipid metabolism, and growth were significantly differently expressed when the temperature increased from 10 °C to 25 °C. (Figure 18). The most upregulated genes among the DEGs were revealed to be related to photosynthesis, chlorophyll a-b binding protein (CBP), and the CBP of LHC2 (Figure 18). In addition to the list of the top DEGs, upregulation of genes mentioned in the previous studies including the digalactosyldiacylglycerol synthase 1 (DGD1), glyceraldehyde-3-P dehydrogenase (GAPCP1), phosphatidylglycerol/phosphatidylinositol transfer protein (PG/PI-TP), omega-6 fatty acid desaturase (FAD6), plasma membrane ATPase, phosphatidylcholine-

sterol acyltransferase (LCAT), phosphoenolpyruvate carboxykinase (PCK), ribulose bisphosphate carboxylase (RuBisCo), plastocyanin (PETE), heat shock 70 kDa protein (HSP70), and subunits of both PSII and PSI reaction centers were also detected at 25 °C.

One of the most significantly downregulated genes at 25 °C was revealed to be the 5-methyltetrahydropteroyltriglutamate--homocysteine methyltransferase (MS1), histone H2A-IV, and purple acid phosphatase 15 (PAP15) (Figure 18). Furthermore, downregulations of chaperone protein DnaJ, 60S ribosome subunit biogenesis protein, and 54S ribosomal protein L51 were also detected and revealed to be responsible for the significantly downregulated biological processes at this temperature.

Some genes upregulated at 25 °C (i.e., DGD1, GAPCP1, HSP70, and CBPs) were found to be downregulated at 34 °C (Figure 19). Downregulations of genes associated with the subunits of cytochrome b6-f and b-c1 as well as further downregulation of FAD7 were detected at 34 °C. Furthermore, various heat shock proteins including the Heat shock 22 kDa protein (HSP22) and heat shock protein HSP 90-beta (HSP90AB1), and the activator of 90 kDa heat shock protein ATPase homolog 2 (Ahsa2), as well as other genes associated with stress response including auxin transporter protein 1 (AUX1), indole-3-glycerol phosphate synthase (IGPS), and ornithine decarboxylase (ODC1) were found to be upregulated at the higher temperature.

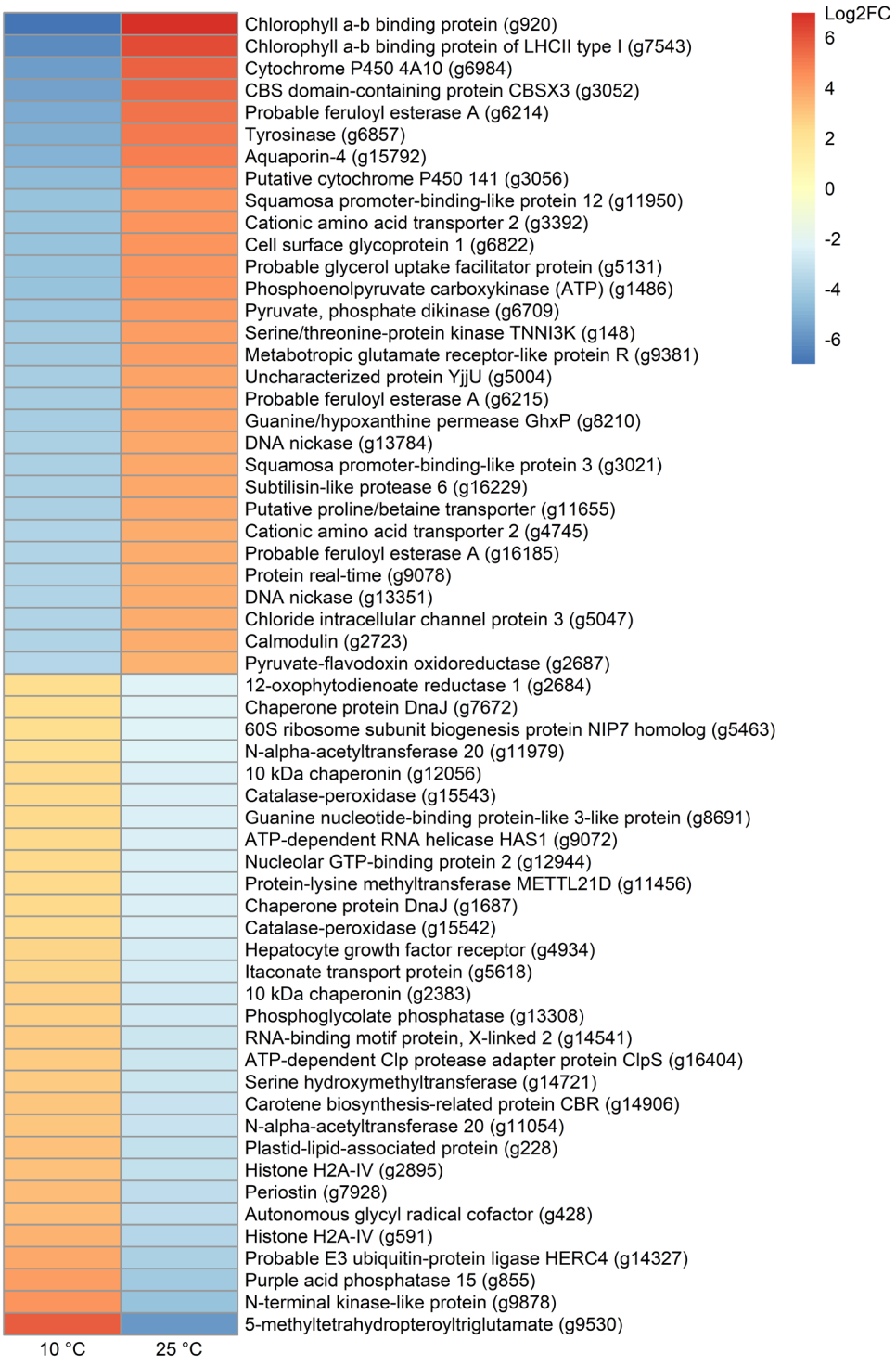


*Figure 18. The top 30 annotated DEGs with the largest fold increase and decrease at 25 °C (n = 4) relative to 10 °C (n = 4). Genes annotated as "uncharacterized" were omitted.*

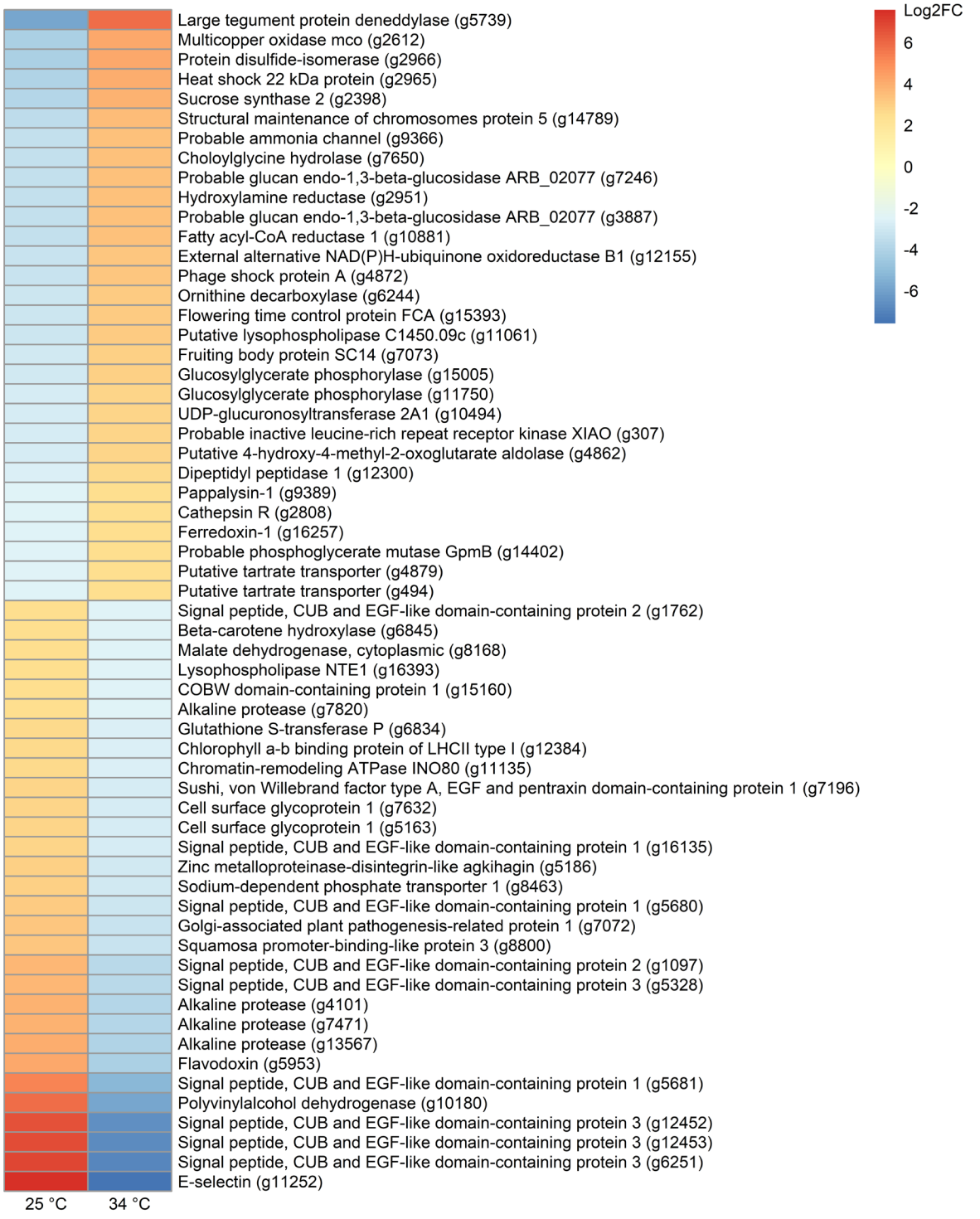


*Figure 19. The top 30 annotated DEGs with the largest fold increase and decrease at 34 °C (n = 4) relative to 25 °C (n = 4). Genes annotated as "uncharacterized" were omitted.*

### 3.6.5. Gene ontology enrichment analysis

DEGs upregulated at 25 °C were associated with biological processes of lipid metabolic process (GO:0006629), transmembrane transport (GO:0055085), negative regulation of transcription by RNA polymerase III (GO:0016480), acetyl-CoA biosynthetic process from acetate (GO:0019427), glycerophospholipid catabolic process (GO:0046475), phospholipid catabolic process (GO:0009395), tetrahydrobiopterin biosynthetic process (GO:0006729), cobalamin metabolic process (GO:0009235), and proton export across plasma membrane (GO:0120029) together with downregulation of *de novo* cotranslational protein folding (GO:0051083), regulation of translational fidelity (GO:0006450), ribosome assembly (GO:0042255), mitochondrial translation (GO:0032543), tetrahydrofolate biosynthetic process (GO:0046654), and response to oxidative stress (GO:0006979) (Figure 20). Upregulation of the genes including the probable feruloyl esterase A, phosphatidylcholine-sterol acyltransferase, and omega-6 fatty acid desaturase were related to the lipid metabolic process which is the most significantly affected metabolic pathway at 25 °C (Appendix 4). Interestingly, processes such as cotranslational protein folding (GO:0051083), regulation of translational fidelity (GO:0006450), and ribosome assembly (GO:0042255) were found to be downregulated (Figure 21). Genes related to these metabolic pathways were identified as chaperone protein DnaJ, 60S ribosome subunit biogenesis protein NIP7 homolog, and 54S ribosomal protein L51 (Appendix 4).

When the temperature was increased to 34 °C, the reduced growth rate was concordant with the upregulation of the polyamine biosynthetic process (GO:0006596), sucrose metabolic process (GO:0005985), phospholipid catabolic process (GO:0009395), transmembrane transport (GO:0055085) together with downregulation of photosynthesis light-harvesting (GO:0009765), proteolysis (GO:0006508), and lipid metabolic process (GO:0006629) (Figure 20). Genes related to these biological processes were identified as chlorophyll a-b binding protein of LHCII type I, alkaline protease, acyl-lipid (7-3)-desaturase, and lysophospholipase NTE1 (Appendix 4).

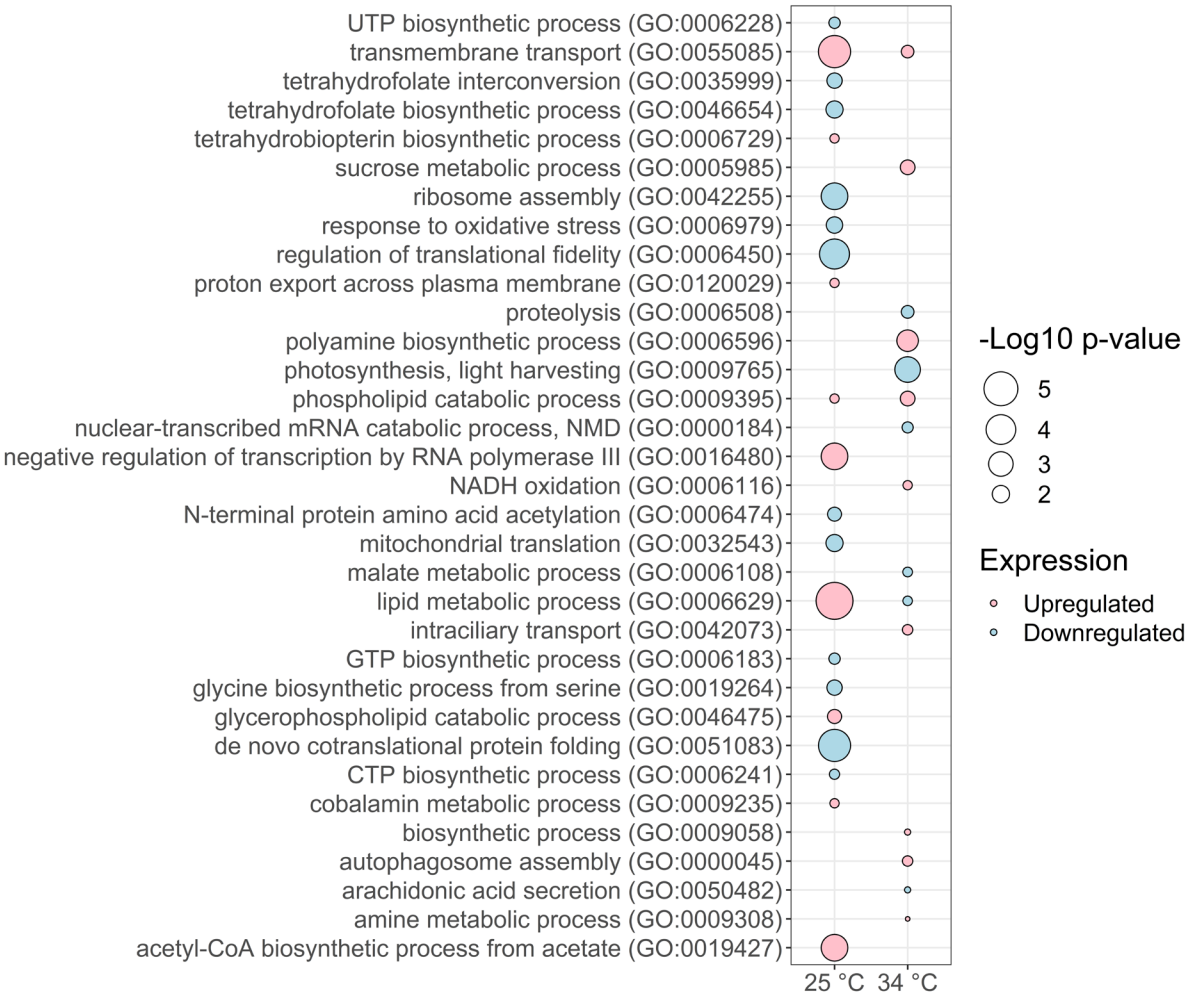


*Figure 20. Summary of the biological processing GO terms at 25 °C and 34 °C which showed statistical significance ($p < 0.05$). -Log10 p-value: -log10 of adjusted p-values calculated by using the Benjamini-Hochberg method. More detailed summary of the significant biological processes, molecular functions, and cell component GO terms and related genes are shown in the appendix (Appendix 4).*

# 4 Discussion

## 4.1 Effect of temperature on growth

Temperature is a key variable driving the growth rate and metabolism of microorganisms (Huete-Stauffer et al., 2015). Here we showed that the temperature increment until the thermal optima had significantly positive effects on the growth rate of both UTEX393 and SNS0120. Although the thermal optima for those strains were very similar, they presented substantial differences in growth rate and resistance to thermal inactivation of growth at high temperatures.

After the temperature increased beyond the thermal optima, differences in thermal tolerance between the strains became more clearly visible. Immediate growth inhibition of the SNS0120 after the temperature was increased to 31 °C, suggests that the SNS0120 requires more careful monitoring and controlling temperature fluctuation than UTEX393.

Overall, the results show that UTEX393 has a wider thermal tolerance range and better growth performance than the SNS0120, making it more practicable to cultivate throughout the year in outdoor cultivation systems that can experience major shifts in temperature during the day. Moreover, the difference in thermal tolerance perhaps can be used for selecting strains that are more suitable for the climate of the geographic locations where the culture will be established. This initial temperature screening will increase the efficiency of wastewater treatment, reduce the failure rate of cultivation, and managing costs at large scale.

In this study, the use of turbidostat cultivation coupled with fine-scale temperature resolution allowed the accurate modeling of thermal response curves. For the UTEX3939, the optimal growth temperature supports the results from Breuer et al. (2013). Although the SNS0120 showed a similar thermal optimum to UTEX393, the area under the curve was approximately 49 % smaller compared to the UTEX393. The difference in thermal response between strains should be understood prior to the cultivation for maximizing the efficiency of the cultures, especially for large-scale outdoor cultures (Béchet et al., 2010; Khan et al., 2018; Mata et al., 2010). Less precise determination of the temperature response may result in high biomass losses in such outdoor culture systems (Alabi et al., 2009).

**Effect of temperature on photosynthesis**

The results showed that the effect of a temperature increase from 10 °C to 25 °C (low temperature to optimal temperature) was associated with increased photosynthetic performance in *T. obliquus*, and also induced the expression of genes associated with various subunits of the PSII reaction center and ribulose-1,5-bisphosphate (Rubisco) which drive and regulate photosynthetic rate (Shin et al., 2016). The key effect of temperature on photosynthesis is due to an increase in the activity of the proteins in the thylakoid membrane and the affinity of Rubisco for $CO_2$ (Atkinson et al., 2003; Khan et al., 2018; Salvucci & Crafts-Brandner, 2004b). The $CO_2$ fixation activity (carboxylase activity) of the Rubisco enzyme increases with rising temperature up to a certain level and then declines which subsequently affects photosynthesis (Carvalho et al., 2011; Jacob-Lopes et al., 2009). Therefore, the temperature outside of the optimal range can cause photoinhibition which reduces photosynthesis, resulting in a decreased growth rate and biomass productivity (K. Maxwell & Johnson, 2000).

UTEX393 showed a significant reduction in $ETR_{max}$ at 37 °C (approximately 56 % reduction compared to the 34 °C) despite that $F_v/F_m$ at 37 °C was still similar to 34 °C. Further study will be needed to understand the exact cause for the discrepancy between the growth rate, $F_v/F_m$, and $ETR_{max}$. However, differential expression showed downregulation of genes related to the various subunits of cytochrome b6-f and b-c1 which are one of the key machinery for electron transport (Berger et al., 2014; Chalifour & Juneau, 2011; Malone et al., 2021). Perhaps, the reduction of the cytochrome-related genes caused by temperature may be linked to the reduction of the $ETR_{max}$ while maintaining the constant $F_v/F_m$.

**Effect of temperature on lipid contents**

Results of total fatty acids (TFA) showed that the temperature increase from 10 to 37 °C did not directly affect the TFA in the cells of *T. obliquus*. This contradicts the study done by Breuer et al. (2013b) which reported that the highest TFA content of the UTEX 393 was measured at 27.5°C among 20, 27.5, and 35 °C with different pH combinations (pH 5, 7, and 9) in nitrogen starved condition. In their study, it was pointed out that the TFA contents at 20 and 35 °C were also enhanced with increasing pH. This result regarding the effects of pH or nitrogen starvation enhancing the TFA contents was in accordance with several other studies on various microalgal species including *Chlorella, Nannochloropsis,* and *Neochloris* besides *Scenedesmus* (Gardner

et al., 2011; Hulatt et al., 2020; Santos et al., 2012). Furthermore, in our work, turbidostat cultivation mode was used to control optical density, light, and nutrient supply so that the temperature effect may be deduced more reliably from the other variables affecting the amount of TFA in the cells. The TFA contents may be more directly influenced by other factors such as pH and nutrient starvation other than the thermal stress. In the existing literature, pH, N-starvation, P-starvation, and $CO_2$ concentration were reported to significantly affect the amounts of TFA in *Scenedesmus* and other green microalgal species (Abd El Baky et al., 2012; J. Liu et al., 2012; Pal et al., 2011; Xin et al., 2010).

The temperature may also have secondary, indirect effects on microalgae growth by e.g. influencing dissolved gas solubility that may indirectly affect the amounts of the TFA. The solubility of $CO_2$ in water varies depending on the temperature while the culture was supplied with a constant amount of $CO_2$ (Bahadori et al., 2009; Mao et al., 2013; Servio & Englezos, 2001). Therefore, the temperature may be considered to have a minor indirect influence on gas exchange and solubility. In conclusion, the results imply that the optimal conditions for lipid accumulation may not be the optimal for growth of *T. obliquus* (Stengel et al., 2011).

Despite the similarity in the amount of TFA in the cells throughout the experiment, both strains showed changes in the amount of polyunsaturated fatty acids (PUFA). The proportions of omega-3 and omega-6 PUFAs displayed an inverse trend. The amount of the omega-3 PUFA significantly decreased with increasing temperature while the omega-6 PUFAs significantly increased until the proximate optimal temperature. One of the omega-3 PUFA, α-linolenic acid was especially affected by the temperature and drastically reduced while the linoleic acid, omega-6 PUFA, was substantially increased. Similar behaviour of the C18 omega-3 and the omega-6 PUFAs was observed in *Scenedesmus obliquus CPCC5* and *Ostreococcus tauri* (Degraeve-Guilbault et al., 2021; Fuschino et al., 2011). These results suggest that the level of fatty acid unsaturation in membrane lipids decreases as growth temperature is increased (Badea & Basu, 2009; Fuschino et al., 2011). In addition to the PUFA, the amount of saturated fatty acid C16:0 for both strains also showed an increasing trend as the temperature increased. Therefore, the temperature may not directly influence the total fatty acid contents in the cells of *T. obliquus*, yet it influences the fatty acid composition allowing the cells to acclimate to the surrounding temperature.

## 4.5 Transcriptomics

### Genes related to the growth, photosynthesis, and lipid contents near thermal optima

The results showed that the expression of genes associated with the proteins in the photosynthetic membrane was associated with the high growth performance near the thermal optima. Those genes include various types of chlorophyll a b binding protein (LHCB). The LHCB are normally associated with chlorophyll and xanthophylls serving as the antenna complex supporting the absorption of sunlight and transferring the excitation energy to the core complexes of PSII in order to drive photosynthetic electron transport (R. Liu et al., 2013) and thermal energy dissipation (Bonente et al., 2011; Elrad et al., 2002; Peers et al., 2009). However, more research is needed to understand the mechanisms of these genes for LHCB proteins and why they were significantly expressed near the thermal optima.

Genes associated with the lipid accumulation include digalactosyldiacylglycerol synthase 1 (DGD1), phosphatidylglycerol/phosphatidylinositol transfer protein (PG/PI-TP), and glyceraldehyde-3-P dehydrogenase (GAPCP1) were also upregulated besides the LHCB protein-coding genes at 25 °C. The DGD1 is related to the synthesis and assembly of galactolipids such as digalactosyldiacylglycerol (DGDG) in photosynthetic membranes which provides the stability to the photosystem I (PSI) (Guo et al., 2005). Along with mono-galactosyldiacylglycerol (MGDG) and sulfoquinovosyldiacylglycerol (SQDG), these glycolipids are important factors for maintaining optimal photosynthetic efficiency (Kalisch et al., 2016). Upregulation of the DGDG under the heat stress condition is in agreement with the study conducted by Calhoun et al 2021. In the study, *Scenedesmus sp.* cultivated at 25 °C was exposed to 35 °C and 15 °C, and the expression of MGDG and DGDG were increased in both temperature conditions (Calhoun et al., 2021). These results may illustrate the cell's response to the temperature fluctuations which influence the composition of the photosynthetic membranes ultimately linking to the cell's growth. In addition, the upregulation of the GAPCP1 is essential for the breakdown of starch to form sucrose for exporting to non-photosynthetic tissues, and to generate primary metabolites for anabolic pathways such as fatty acid and amino acid synthesis, linking to the higher growth rate (Muñoz-Bertomeu et al., 2009).

Gene enrichment analysis showed the lipid metabolic process (GO:0006629) as one of the most affected biological pathways at 25 °C. One of the genes associated with the metabolic pathway

was identified as the probable feruloyl esterase A (faeA). The faeA was also related to the cell wall polysaccharide catabolic process (GO:0044347) (Souza, 2013). The plant cells change their cell wall architecture during growth and development through the synthesis and degradation of wall polysaccharides (de Vries et al., 1997; Oliveira et al., 2020). The expression of this gene is associated with the synthesis of the enzyme ferulic Acid esterase which is involved in the degradation of complex cell wall polysaccharides (Oliveira et al., 2020). The feruloyl esterase A was previously reported to enhance the degradation of hemicellulose (de Vries et al., 2000). Further study on the application of the feruloyl esterase A for cell wall degradation may be interesting for enhancing the availability of biochemicals in the microalgae.

Another lipid metabolic process-related gene, omega-6 fatty acid desaturase (FAD6) also increased its expression at 25 °C, and then the expression became non-significant at 34 °C. The upregulation of the FAD6 increases the concentration of the omega-6 PUFA such as linoleic acids (C18:2*n*-6) (Choi, 2012). The results showed that the concentration of the omega-6 and omega-3 PUFAs correspond with the upregulation of the FAD6 together with the downregulation of the omega-3 fatty acid desaturase (FAD7) at the proximal thermal optimal and beyond. In the literature, the FAD7 gene is expressed under both heat and cold stress conditions whereas more strongly expressed in the cold (Lyukevich et al., 2003; Pereira et al., 2004). This suggests that the biosynthesis of the omega-3 fatty acids is possibly associated with the cell's adaptability to temperatures lower than the thermal optima (Domínguez et al., 2010; X.-Y. Liu et al., 2006; Román et al., 2015; Xing et al., 2018; Xue et al., 2018). The overall pattern of reduction in omega-3 and increment in omega-6 fatty acids as the temperature increase is in concordance with the expression of the FAD6 and FAD7 genes in *Chlamydomonas reinhardtii* (Nguyen et al., 2013). Further downregulation of the FAD7 was observed at the temperature beyond thermal optima while the proportion of the omega-3 PUFAs showed a significant reduction. The exact mechanism for the reduction of the omega-3/omega-6 ratio needs further study, yet we have found that the increasing temperature is associated with higher production of the omega-6 PUFAs in UTEX393. This indicates that the omega-6 PUFAs are more suitable for cells to acclimate to the environment with increasing temperature.

The significantly expressed Acetyl-coenzyme A synthetase (acs) gene was associated with the upregulation of the acetyl-CoA biosynthetic process from acetate (GO:0019427). One of the various functions of Acetyl-CoA is related to triglycerides (TAG) accumulation, especially under nitrogen starvation in the cells (Avidan et al., 2015). However, acs gene was found to be

expressed in algae at temperature shifts without a significant increase in the amount of total fatty acids in the UTEX 393. This may be related to the other significantly upregulated lipid catabolic processes including the glycerophospholipid catabolic process (GO:0046475) and phospholipid catabolic process (GO:0009395), yet more research is required.

Overall gene expression profile at 25 °C vs 10 °C represents the cells adapting to the higher temperature by enhancing lipid metabolism, modifying the lipid compositions, and increasing the proteins in the thylakoid membrane. It appears the temperature affected the metabolic pathways associated with a higher growth rate at 25 °C. In conclusion, the main effect of temperature near proximal thermal optima is the increased growth rate in *T. obliquus*.

**Gene expression beyond thermal optima**

Results showed that the key metabolic pathways linked to the growth, photosynthesis and lipid metabolism, were the most significantly downregulated by the effect of temperature beyond the thermal optima. Furthermore, temperature also caused RNA degradation indicated by lower RIN values obtained at 34 °C and 37 °C.

At 34 °C, interesting expressions of genes that indicate the cell's stress response against the temperature were detected. Examples of those genes include ornithine decarboxylase, auxin, and heat shock proteins.

**Polyamine biosynthesis**

The ornithine decarboxylase (ODC1) was associated with the upregulation of the polyamine biosynthetic process which was one of the most significantly affected biological pathways by temperature. In bacteria and plants, polyamine anabolism is related to the ability of these organisms to tolerate different types of environmental stress (Alcázar et al., 2010; Bouchereau et al., 1999; Groppa & Benavides, 2008; Incharoensakdi et al., 2010; Jantaro & Kanwal, 2017). Besides the stress response, intracellular polyamine levels are also associated with high growth rates and active cell division in plant systems, and it may have auxin-like or cytokinin-like bioactivity to promote growth (Du et al., 2017; B. Lin et al., 2018; H.-Y. Lin & Lin, 2018, p. 201; Mógor et al., 2018; T. Thomas & Thomas, 2001; Wallace & Fraser, 2003; Xie et al., 2014).

The results showed that the *T. obliquus* increased the biosynthesis of the polyamines as one of the strategies to countermeasure thermal stress and proliferate under such stress conditions.

**Auxin transporter protein 1**

Another interesting gene up-regulated during exposure to the high temperature (34°C) treatment was the auxin transporter protein 1 (AUX1). The AUX1 facilitates the uptake of the indole-3-acetic acid (IAA) which is the major form of auxin in higher plants (Goldsmith, 1977; Marchant et al., 1999). Auxin is a phytohormone which regulates plant growth and development (S. Zhang & Van Duijn, 2014). Also, auxin exhibits increased stress tolerance, in this case, against heat (Bielach et al., 2017; Mühlenbock et al., 2008). Multiple pathways for the biosynthesis of IAA have been described previously. The IAA can be synthesized from indole through tryptophan-dependent and independent pathways (Kiseleva et al., 2012). The tryptophan-dependent pathways have been well described, yet the tryptophan-independent pathway is still not well known (Tan et al., 2021). However, the precursor for the biosynthesis of IAA by the tryptophan-independent pathway is known to be the indole-3-glycerolphosphate (Di et al., 2016). Interestingly, temperature also induced the upregulation of indole-3-glycerolphosphate synthase (IGPS) in this thesis. Therefore, this upregulation of the AUX1 together with IGPS may indicate the enhanced activities of auxin biosynthesis in the cells at temperatures beyond the thermal optima. However, accumulation of the auxin under thermal stress was not measured in the study and further analysis is still required further analysis is needed for utilization as biostimulants.

**Heat shock protein gene expression**

The upregulation of heat shock protein 22kDa (Hsp22), heat shock protein HSP 90-beta (HSP90AB1), and activator of 90 kDa heat shock protein ATPase homolog 2 (Ahsa2) genes were also detected at 34 °C, which may indicate the cell's countermeasure to adapt to the high-temperature environment. In contrast, the heat shock 70 kDa protein (Hsp70) gene which was upregulated at 25 °C, became downregulated at 34 °C.

The heat shock proteins (Hsps) are considered one of the important subgroups of chaperones whom expression will be induced by heat stress, starvation, inflammation, water deprivation, or nitrogen deficiency which can cause proteins to become partially unfolded (Sharma &

Masison, 2009). Hsps are classified according to their molecular mass and include Hsp100, Hsp90, Hsp70, Hsp60, Hsp40, and the small Hsp families (Saibil, 2013).

Due to the very high structural homology and conserved functional properties across species, the Hsp70 is considered the predominant group of Hsps which can act on a broad range of substrates (J. Y. Kim et al., 2018; Schroda et al., 2000; Sharma & Masison, 2009). The molecular mechanism for regulation of Hsp70 induction depends on the activity of a heat shock factor 1 (HSF1) which binds to the 5'promoter regions of all Hsp genes and triggers transcription (N. Kim et al., 2012).

Another highly conserved molecular chaperone, heat shock protein 90 kDa (Hsp90) can also influence the induction of Hsp70 since the Hsp90 is bound to HSF1 (Deng et al., 2021; Zhao et al., 2012). This is in agreement with the expression result at 34 °C where the Hsp70 was downregulated while the Hsp90 together with the Ahsa2 gene which codes for the co-chaperone that stimulates HSP90 ATPase activity, was upregulated.

Besides the Hsp70 and 90, the most upregulated Hsp group was the small heat shock protein 22kDa (Hsp22). The Hsp22 had been reported to protect oxygen evolution and electron transport of Photosystem II during heat stress (Downs et al., 1999). This upregulation of the Hsp22 may explain why the electron transport rate at 34 °C was similar to the lower temperatures despite being exposed to the high heat stress condition where the SNS0120 was unable to survive. Diversity of the Hsp correlates with acquired tolerance and increases the ability of the exposed organisms to survive a subsequent more severe stress that would have otherwise been lethal (Deng et al., 2020; Kobayashi et al., 2014). In this thesis, we were unable to further study Hsp at 37 °C due to the higher degree of RNA degradation in the samples and limited resources available for high throughput sequencing. Therefore, it is still unknown if there will be expressions of different groups of Hsp or other means of adaptation mechanisms to withstand the heat stress beyond 34 °C.

# 5 Conclusion

Thermal response curves were generated for a reference strain (UTEX393) and a novel isolate from Portugal (SNS0120). The thermal optima for the UTEX393 and SNS0120 were comparable at 27.2 °C and 26.8 °C respectively, although UTEX393 showed much higher growth performance and thermal tolerance compared to the SNS0120 throughout the temperature range 10-37°C. The thermal performance curves show that UTEX393 is a much more efficient strain for cultivation in large-scale outdoor PBRs or wastewater treatment throughout the year in many parts of the world compared to the SNS0120.

Using turbidity-controlled cultures we showed that temperature did not significantly influence the total lipid accumulation in the cells, but the compositions of omega-3 and omega-6 PUFAs. The ratio of the omega-3 to omega-6 PUFAs was reduced as the temperature increased. Genes related to the most significantly upregulated metabolic pathway near thermal optima were also linked to the cell wall degradation process which may be an indication of the growth and development of the cells. Significant downregulation of the genes and GO terms associated with lipid metabolism and photosynthesis at high temperature ( 34°C ) was associated with reduced growth rate, implying that the thermal stress started to inactivate the cell's metabolic fluxes.

Our work highlights the importance of temperature screening for the selection of robust strains to maximize yields and nutrient uptake whilst reducing operating costs. Protocols for rapid temperature screening should be established at the algae wastewater treatment facilities or production companies.

# References/Bibliography


Abd El Baky, H. H., El-Baroty, G. S., Bouaid, A., Martinez, M., & Aracil, J. (2012). Enhancement of lipid accumulation in Scenedesmus obliquus by Optimizing CO2 and Fe3+ levels for biodiesel production. *Bioresource Technology*, *119*, 429–432. https://doi.org/10.1016/j.biortech.2012.05.104

Acién Fernández, F. G., Gómez-Serrano, C., & Fernández-Sevilla, J. M. (2018). Recovery of Nutrients From Wastewaters Using Microalgae. *Frontiers in Sustainable Food Systems*, *2*. https://www.frontiersin.org/article/10.3389/fsufs.2018.00059

Akaike, H. (1974). A new look at the statistical model identification. *IEEE Transactions on Automatic Control*, *19*(6), 716–723. https://doi.org/10.1109/TAC.1974.1100705

Akimov, A. I., & Solomonova, E. S. (2019). Characteristics of Growth and Fluorescence of Certain Types of Algae during Acclimation to Different Temperatures under Culture Conditions. *Oceanology*, *59*(3), 316–326. https://doi.org/10.1134/S0001437019030019

Alabi, A. O., Tampier, M., & Bibeau, E. (2009). *Microalgae technologies and processes for biofuels/bioenergy production in British Columbia: Current technology, suitability and barriers to implementation : executive summary*. https://www.osti.gov/etdeweb/biblio/21379262

Alcázar, R., Altabella, T., Marco, F., Bortolotti, C., Reymond, M., Koncz, C., Carrasco, P., & Tiburcio, A. F. (2010). Polyamines: Molecules with regulatory functions in plant abiotic stress tolerance. *Planta*, *231*(6), 1237–1249. https://doi.org/10.1007/s00425-010-1130-0

Alexa, A., & Rahnenfuhrer, J. (2021). *topGO: Enrichment Analysis for Gene Ontology. R package version 2.46.0*. https://doi.org/10.18129/B9.bioc.topGO

Algacycle. (2021). *Valorisation of greenhouse effluents with microalgae*. Algacycle. https://www.algacycle.com/en/

AlgaePARC. (2022). *About algae and cyanobacteria*. https://www.algaeparc.com/about-algea

Alsenani, F., Tupally, K. R., Chua, E. T., Eltanahy, E., Alsufyani, H., Parekh, H. S., & Schenk, P. M. (2020). Evaluation of microalgae and cyanobacteria as potential sources of antimicrobial compounds. *Saudi Pharmaceutical Journal*, *28*(12), 1834–1841. https://doi.org/10.1016/j.jsps.2020.11.010

Andersen, R. A., & America, P. S. of. (2005). *Algal Culturing Techniques*. Elsevier Science. https://books.google.no/books?id=9NADUHyFZaEC

Angilletta, M. J. (2006). Estimating and comparing thermal performance curves. *Journal of Thermal Biology*, *31*(7), 541–545. https://doi.org/10.1016/j.jtherbio.2006.06.002

Anisha, G. S., & John, R. P. (2014). 9—Bio-engineering algae as a source of hydrogen. In A. Basile & A. Iulianelli (Eds.), *Advances in Hydrogen Production, Storage and Distribution* (pp. 248–262). Woodhead Publishing. https://doi.org/10.1533/9780857097736.2.248

Anjum, M., Al-Makishah, N. H., & Barakat, M. (2016). Wastewater sludge stabilization using pre-treatment methods. *Process Safety and Environmental Protection*, *102*, 615–632.

Atkinson, D., Ciotti, B. J., & Montagnes, D. J. S. (2003). Protists decrease in size linearly with temperature: Ca. 2.5% °C−1. *Proceedings of the Royal Society of London. Series B: Biological Sciences*, *270*(1533), 2605–2611. https://doi.org/10.1098/rspb.2003.2538

Aussant, J., Guihéneuf, F., & Stengel, D. B. (2018). Impact of temperature on fatty acid composition and nutritional value in eight species of microalgae. *Applied Microbiology and Biotechnology*, *102*(12), 5279–5297. https://doi.org/10.1007/s00253-018-9001-x

Avidan, O., Brandis, A., Rogachev, I., & Pick, U. (2015). Enhanced acetyl-CoA production is associated with increased triglyceride accumulation in the green alga Chlorella desiccata. *Journal of Experimental Botany*, *66*(13), 3725–3735. https://doi.org/10.1093/jxb/erv166

Badea, C., & Basu, S. (2009). The effect of low temperature on metabolism of membrane lipids in plants and associated gene expression. *Plant Omics*, *2*.

Bahadori, A., Vuthaluru, H. B., & Mokhatab, S. (2009). New correlations predict aqueous solubility and density of carbon dioxide. *International Journal of Greenhouse Gas Control*, *4*(3), 474–480. https://doi.org/10.1016/j.ijggc.2009.01.003

Barbosa, M. J., & Wijffels, R. H. (2013). Biofuels from Microalgae. In *Handbook of Microalgal Culture* (pp. 566–577). John Wiley & Sons, Ltd. https://doi.org/10.1002/9781118567166.ch29

Bassi, N., Rodolfi, L., Zittelli, G. C., Sampietro, G., & Tredici, M. (2011). *The "Green Wall Panel": Potential and limitations of a low cost disposable photobioreactor*. https://www.semanticscholar.org/paper/The-%E2%80%9CGreen-Wall-Panel%E2%80%9D%3A-potential-and-limitations-a-Bassi-Rodolfi/1953f0fea649ce16d0224137aefd060eecccb13f

Béchet, Q., Shilton, A., Fringer, O. B., Muñoz, R., & Guieysse, B. (2010). Mechanistic modeling of broth temperature in outdoor photobioreactors. *Environmental Science & Technology*, *44*(6), 2197–2203. https://doi.org/10.1021/es903214u

Berger, H., Blifernez-Klassen, O., Ballottari, M., Bassi, R., Wobbe, L., & Kruse, O. (2014). Integration of Carbon Assimilation Modes with Photosynthetic Light Capture in the Green Alga Chlamydomonas reinhardtii. *Molecular Plant*, *7*(10), 1545–1559. https://doi.org/10.1093/mp/ssu083

Bielach, A., Hrtyan, M., & Tognetti, V. B. (2017). Plants under Stress: Involvement of Auxin and Cytokinin. *International Journal of Molecular Sciences*, *18*(7), 1427. https://doi.org/10.3390/ijms18071427

Boatman, T. G., Lawson, T., & Geider, R. J. (2017). A Key Marine Diazotroph in a Changing Ocean: The Interacting Effects of Temperature, CO2 and Light on the Growth of Trichodesmium erythraeum IMS101. *PLOS ONE*, *12*(1), e0168796. https://doi.org/10.1371/journal.pone.0168796

Bonente, G., Ballottari, M., Truong, T. B., Morosinotto, T., Ahn, T. K., Fleming, G. R., Niyogi, K. K., & Bassi, R. (2011). Analysis of LhcSR3, a Protein Essential for Feedback De-Excitation in the Green Alga Chlamydomonas reinhardtii. *PLOS Biology*, *9*(1), e1000577. https://doi.org/10.1371/journal.pbio.1000577

Bouchereau, A., Aziz, A., Larher, F., & Martin-Tanguy, J. (1999). Polyamines and environmental challenges: Recent development. *Plant Science*, *140*(2), 103–125. https://doi.org/10.1016/S0168-9452(98)00218-0

Bozkurt, H., & Erkmen, O. (2001). 17) Predictive modeling of Yersinia enterocolitica inactivation in Turkish Feta cheese during storage. *Journal of Food Engineering*, *47*, 81–87. https://doi.org/10.1016/S0260-8774(00)00102-3

Brenner, A., & Abeliovich, A. (2013). Water Purification: Algae in Wastewater Oxidation Ponds. In *Handbook of Microalgal Culture* (pp. 595–601). John Wiley & Sons, Ltd. https://doi.org/10.1002/9781118567166.ch31

Breuer, G., Evers, W. A. C., de Vree, J. H., Kleinegris, D. M. M., Martens, D. E., Wijffels, R. H., & Lamers, P. P. (2013). Analysis of fatty acid content and composition in microalgae. *Journal of Visualized Experiments: JoVE*, *80*. https://doi.org/10.3791/50628

Breuer, G., Lamers, P. P., Martens, D. E., Draaisma, R. B., & Wijffels, R. H. (2012). The impact of nitrogen starvation on the dynamics of triacylglycerol accumulation in nine microalgae strains. *Bioresource Technology*, *124*, 217–226. https://doi.org/10.1016/j.biortech.2012.08.003

Briere, J.-F., Pracros, P., Le Roux, A.-Y., & Pierre, J.-S. (1999). A Novel Rate Model of Temperature-Dependent Development for Arthropods. *Environmental Entomology*, *28*(1), 22–29. https://doi.org/10.1093/ee/28.1.22

Butterwick, C., Heaney, S. I., & Talling, J. F. (2005). Diversity in the influence of temperature on the growth rates of freshwater algae, and its ecological relevance. *Freshwater Biology*, *50*(2), 291–300. https://doi.org/10.1111/j.1365-2427.2004.01317.x

C. N. Hinshelwood. (1947). The Chemical Kinetics of the Bacterial Cell. *Science*, *106*(2754), 354–354. https://doi.org/10.1126/science.106.2754.354-b

Calhoun, S., Bell, T. A. S., Dahlin, L. R., Kunde, Y., LaButti, K., Louie, K. B., Kuftin, A., Treen, D., Dilworth, D., Mihaltcheva, S., Daum, C., Bowen, B. P., Northen, T. R., Guarnieri, M. T., Starkenburg, S. R., & Grigoriev, I. V. (2021). A multi-omic characterization of temperature stress in a halotolerant Scenedesmus strain for algal biotechnology. *Communications Biology*, *4*(1), 1–15. https://doi.org/10.1038/s42003-021-01859-y

Campbell, P. K., Beer, T., & Batten, D. (2011). Life cycle assessment of biodiesel production from microalgae in ponds. *Bioresource Technology*, *102*(1), 50–56. https://doi.org/10.1016/j.biortech.2010.06.048

Carvalho, A. P., Silva, S. O., Baptista, J. M., & Malcata, F. X. (2011). Light requirements in microalgal photobioreactors: An overview of biophotonic aspects. *Applied Microbiology and Biotechnology*, *89*(5), 1275–1288. https://doi.org/10.1007/s00253-010-3047-8

Chalifour, A., & Juneau, P. (2011). Temperature-dependent sensitivity of growth and photosynthesis of Scenedesmus obliquus, Navicula pelliculosa and two strains of Microcystis aeruginosa to the herbicide atrazine. *Aquatic Toxicology*, *103*(1), 9–17. https://doi.org/10.1016/j.aquatox.2011.01.016

Cheregi, O., Engelbrektsson, J., Andersson, M. X., Strömberg, N., Ekendahl, S., Godhe, A., & Spetea, C. (2021). Marine microalgae for outdoor biomass production—A laboratory study simulating seasonal light and temperature for the west coast of Sweden. *Physiologia Plantarum*, *173*(2), 543–554. https://doi.org/10.1111/ppl.13412

Chisti, Y. (2007). Biodiesel from microalgae. *Biotechnology Advances*, *25*(3), 294–306. https://doi.org/10.1016/j.biotechadv.2007.02.001

Choi, J.-R. (2012). Down-regulation of fatty acid desaturase-6 (FAD6) in green alga Chlamydomonas reinhardtii. *Korean Society of Biological Engineering*, 53–53.

Coelho, L. M., Rezende, H. C., Coelho, L. M., Sousa, P. A. R. de, Melo, D. F. O., & Coelho, N. M. M. (2015). Bioremediation of Polluted Waters Using Microorganisms. In *Advances in Bioremediation of Wastewater and Polluted Soil*. IntechOpen. https://doi.org/10.5772/60770

Colla, G., & Rouphael, Y. (2020). Microalgae: New Source of Plant Biostimulants. *Agronomy*, *10*(9), 1240. https://doi.org/10.3390/agronomy10091240

Craggs, R. J., Heubeck, S., Lundquist, T. J., & Benemann, J. R. (2011). Algal biofuels from wastewater treatment high rate algal ponds. *Water Science and Technology: A Journal of the International Association on Water Pollution Research*, *63*(4), 660–665. https://doi.org/10.2166/wst.2011.100

Craggs, R., Park, J., Heubeck, S., & Sutherland, D. (2014). High rate algal pond systems for low-energy wastewater treatment, nutrient recovery and energy production. *New Zealand Journal of Botany*, *52*(1), 60–73. https://doi.org/10.1080/0028825X.2013.861855

Craggs RJ.,. (2005). Advanced integrated wastewater ponds. In *Shilton A ed. Pond treatment technology* (p. p 282-310).

Culture Collection of Cryophilic Algae. (2020). *BBM Medium (Bold's Basal Medium + soil extract + vitamins)*. http://cccryo.fraunhofer.de/sources/files/medien/BBM.pdf

de Marchin, T., Erpicum, M., & Franck, F. (2015). Photosynthesis of Scenedesmus obliquus in outdoor open thin-layer cascade system in high and low CO2 in Belgium. *Journal of Biotechnology*, *215*, 2–12. https://doi.org/10.1016/j.jbiotec.2015.06.429

de Vries, R. P., Kester, H. C. M., Poulsen, C. H., Benen, J. A. E., & Visser, J. (2000). Synergy between enzymes from Aspergillus involved in the degradation of plant cell wall polysaccharides. *Carbohydrate Research*, *327*(4), 401–410. https://doi.org/10.1016/S0008-6215(00)00066-5

de Vries, R. P., Michelsen, B., Poulsen, C. H., Kroon, P. A., van den Heuvel, R. H., Faulds, C. B., Williamson, G., van den Hombergh, J. P., & Visser, J. (1997). The faeA genes from Aspergillus niger and Aspergillus tubingensis encode ferulic acid esterases involved in degradation of complex cell wall polysaccharides. *Applied and Environmental Microbiology*, *63*(12), 4638–4644. https://doi.org/10.1128/aem.63.12.4638-4644.1997

Degraeve-Guilbault, C., Pankasem, N., Gueirrero, M., Lemoigne, C., Domergue, F., Kotajima, T., Suzuki, I., Joubès, J., & Corellou, F. (2021). Temperature Acclimation of the Picoalga Ostreococcus tauri Triggers Early Fatty-Acid Variations and Involves a

Plastidial ω3-Desaturase. *Frontiers in Plant Science*, *12*, 639330. https://doi.org/10.3389/fpls.2021.639330

DellaGreca, M., Zarrelli, A., Fergola, P., Cerasuolo, M., Pollio, A., & Pinto, G. (2010). Fatty acids released by Chlorella vulgaris and their role in interference with Pseudokirchneriella subcapitata: Experiments and modelling. *Journal of Chemical Ecology*, *36*(3), 339–349. https://doi.org/10.1007/s10886-010-9753-y

DeLong, J. P., Gibert, J. P., Luhring, T. M., Bachman, G., Reed, B., Neyer, A., & Montooth, K. L. (2017). The combined effects of reactant kinetics and enzyme stability explain the temperature dependence of metabolic rates. *Ecology and Evolution*, *7*(11), 3940–3950. https://doi.org/10.1002/ece3.2955

Deng, Y., Hu, Z., Shang, L., Chai, Z., & Tang, Y. Z. (2020). Transcriptional Responses of the Heat Shock Protein 20 (Hsp20) and 40 (Hsp40) Genes to Temperature Stress and Alteration of Life Cycle Stages in the Harmful Alga Scrippsiella trochoidea (Dinophyceae). *Biology*, *9*(11), 408. https://doi.org/10.3390/biology9110408

Deng, Y., Li, F., Hu, Z., Yue, C., & Tang, Y. Z. (2021). Expression Patterns of the Heat Shock Protein 90 (Hsp90) Gene Suggest Its Possible Involvement in Maintaining the Dormancy of Dinoflagellate Resting Cysts. *International Journal of Molecular Sciences*, *22*(20), 11054. https://doi.org/10.3390/ijms222011054

Di, D.-W., Zhang, C., Luo, P., An, C.-W., & Guo, G.-Q. (2016). The biosynthesis of auxin: How many paths truly lead to IAA? *Plant Growth Regulation*, *78*(3), 275–285. https://doi.org/10.1007/s10725-015-0103-5

Domínguez, T., HernÁndez, M. L., Pennycooke, J. C., Jiménez, P., Martínez-Rivas, J. M., Sanz, C., Stockinger, E. J., SÁnchez-Serrano, J. J., & Sanmartín, M. (2010). Increasing ω-3 Desaturase Expression in Tomato Results in Altered Aroma Profile and Enhanced Resistance to Cold Stress. *Plant Physiology*, *153*(2), 655–665. https://doi.org/10.1104/pp.110.154815

Downs, C. A., Ryan, S. L., & Heckathorn, S. A. (1999). The Chloroplast Small Heat-shock Protein: Evidence for a General Role in Protecting Photosystem II against Oxidative Stress and Photoinhibition. *Journal of Plant Physiology*, *155*(4), 488–496. https://doi.org/10.1016/S0176-1617(99)80043-1

Du, H., Ahmed, F., Lin, B., Li, Z., Huang, Y., Sun, G., Ding, H., Wang, C., Meng, C., & Gao, Z. (2017). The Effects of Plant Growth Regulators on Cell Growth, Protein, Carotenoid, PUFAs and Lipid Production of Chlorella pyrenoidosa ZF Strain. *Energies*, *10*(11), 1696. https://doi.org/10.3390/en10111696

Elrad, D., Niyogi, K. K., & Grossman, A. R. (2002). A Major Light-Harvesting Polypeptide of Photosystem II Functions in Thermal Dissipation[W]. *The Plant Cell*, *14*(8), 1801–1816. https://doi.org/10.1105/tpc.002154

Falkowski, P. G. (1980). Light-Shade Adaptation in Marine Phytoplankton. In P. G. Falkowski (Ed.), *Primary Productivity in the Sea* (pp. 99–119). Springer US. https://doi.org/10.1007/978-1-4684-3890-1_6

Fawley, M. W. (1984). Effects of Light Intensity and Temperature Interactions on Growth Characteristics of Phaeodactylum Tricornutum (bacillariophyceae)1. *Journal of Phycology*, *20*(1), 67–72. https://doi.org/10.1111/j.0022-3646.1984.00067.x

Flinn, P. W. (1991). Temperature-Dependent Functional Response of the Parasitoid Cephalonomia waterstoni (Gahan) (Hymenoptera: Bethylidae) Attacking Rusty Grain Beetle Larvae (Coleoptera: Cucujidae). *Environmental Entomology*, *20*(3), 872–876. https://doi.org/10.1093/ee/20.3.872

Fuschino, J. R., Guschina, I. A., Dobson, G., Yan, N. D., Harwood, J. L., & Arts, M. T. (2011). Rising Water Temperatures Alter Lipid Dynamics and Reduce N-3 Essential Fatty Acid Concentrations in Scenedesmus Obliquus (chlorophyta)1. *Journal of Phycology*, *47*(4), 763–774. https://doi.org/10.1111/j.1529-8817.2011.01024.x

Gabriel Hoffman. (2020). *Theory and Practiceof random effects and REML invariancePartitionanddream*.

Gardner, R., Peters, P., Peyton, B., & Cooksey, K. (2011). Medium pH and nitrate concentration effects on accumulation of triacylglycerol in two members of the Chlorophyta. *Journal of Applied Phycology*, *23*, 1005–1016. https://doi.org/10.1007/s10811-010-9633-4

Genty, B., Briantais, J.-M., & Baker, N. R. (1989). The relationship between the quantum yield of photosynthetic electron transport and quenching of chlorophyll fluorescence. *Biochimica et Biophysica Acta (BBA) - General Subjects*, *990*(1), 87–92. https://doi.org/10.1016/S0304-4165(89)80016-9

Ghasemi, Y., Moradian, A., Mohagheghzadeh, A., Shokravi, S., & Morowvat, M. H. (2007). *Antifungal and Antibacterial Activity of the Microalgae Collected from Paddy Fields of Iran: Characterization of Antimicrobial Activity of Chroococcus dispersus*. Asian Network for Scientific Information, Pakistan. http://www.scialert.net/pdfs/jbs/2007/904-910.pdf

Goldsmith, M. H. M. (1977). The Polar Transport of Auxin. *Annual Review of Plant Physiology*, *28*(1), 439–478. https://doi.org/10.1146/annurev.pp.28.060177.002255

Grobbelaar, J. U. (2013). Inorganic Algal Nutrition. In *Handbook of Microalgal Culture* (pp. 123–133). John Wiley & Sons, Ltd. https://doi.org/10.1002/9781118567166.ch8

Groppa, M. D., & Benavides, M. P. (2008). Polyamines and abiotic stress: Recent advances. *Amino Acids*, *34*(1), 35–45. https://doi.org/10.1007/s00726-007-0501-8

Guedes, A. C., Amaro, H. M., Pereira, R. D., & Malcata, F. X. (2011). Effects of temperature and pH on growth and antioxidant content of the microalga Scenedesmus obliquus. *Biotechnology Progress*, *27*(5), 1218–1224. https://doi.org/10.1002/btpr.649

Guo, J., Zhang, Z., Bi, Y., Yang, W., Xu, Y., & Zhang, L. (2005). Decreased stability of photosystem I in dgd1 mutant of Arabidopsis thaliana. *FEBS Letters*, *579*(17), 3619–3624. https://doi.org/10.1016/j.febslet.2005.05.049

H. W. Bischoff, & H. C. Bold. (1963). *Phycological Studies IV. Some Soil Algae from Enchanted Rock and Related Algal Species*. University of Texas.

Heinz Walz GmbH. (2013). *MULTI-COLOR-PAM Manual*. https://www.walz.com/files/downloads/manuals/multi-color-pam/MC_PAM06.pdf

Hodaifa, G., Martínez, M., & Sánchez, S. (2009). Influence of pH on the Culture of Scenedesmus obliquus in Olive-mill Wastewater. *Biotechnology and Bioprocess Engineering*, *14*, 854–860. https://doi.org/10.1007/s12257-009-0119-7

Hodaifa, G., Martínez, M., & Sánchez, S. (2010). Influence of temperature on growth of Scenedesmus obliquus in diluted olive mill wastewater as culture medium. *Engineering in Life Sciences*, *10*, 257–264. https://doi.org/10.1002/elsc.201000005

Hoffman, G. E., & Roussos, P. (2021). Dream: Powerful differential expression analysis for repeated measures designs. *Bioinformatics*, *37*(2), 192–201. https://doi.org/10.1093/bioinformatics/btaa687

Hoffman, G. E., & Schadt, E. E. (2016). variancePartition: Interpreting drivers of variation in complex gene expression studies. *BMC Bioinformatics*, *17*(1), 483. https://doi.org/10.1186/s12859-016-1323-z

Hu, Q. (2013). Environmental Effects on Cell Composition. In *Handbook of Microalgal Culture* (pp. 114–122). John Wiley & Sons, Ltd. https://doi.org/10.1002/9781118567166.ch7

Huertas, I. E., Rouco, M., López-Rodas, V., & Costas, E. (2011). Warming will affect phytoplankton differently: Evidence through a mechanistic approach. *Proceedings of the Royal Society B: Biological Sciences*, *278*(1724), 3534–3543. https://doi.org/10.1098/rspb.2011.0160

Huete-Stauffer, T. M., Arandia-Gorostidi, N., Díaz-Pérez, L., & Morán, X. A. G. (2015). Temperature dependences of growth rates and carrying capacities of marine bacteria depart from metabolic theoretical predictions. *FEMS Microbiology Ecology*, *91*(10), fiv111. https://doi.org/10.1093/femsec/fiv111

Hulatt, C. J., Smolina, I., Dowle, A., Kopp, M., Vasanth, G. K., Hoarau, G. G., Wijffels, R. H., & Kiron, V. (2020). Proteomic and Transcriptomic Patterns during Lipid Remodeling in Nannochloropsis gaditana. *International Journal of Molecular Sciences*, *21*(18), 6946. https://doi.org/10.3390/ijms21186946

Hulatt, C. J., Wijffels, R. H., & Posewitz, M. C. (2021). The Genome of the Haptophyte Diacronema lutheri (Pavlova lutheri, Pavlovales): A Model for Lipid Biosynthesis in Eukaryotic Algae. *Genome Biology and Evolution*, *13*(8), evab178. https://doi.org/10.1093/gbe/evab178

Huner, N. P. A., Öquist, G., & Melis, A. (2003). Photostasis in Plants, Green Algae and Cyanobacteria: The Role of Light Harvesting Antenna Complexes. In B. R. Green & W. W. Parson (Eds.), *Light-Harvesting Antennas in Photosynthesis* (pp. 401–421). Springer Netherlands. https://doi.org/10.1007/978-94-017-2087-8_14

Hurvich, C. M., Simonoff, J. S., & Tsai, C.-L. (1998). Smoothing Parameter Selection in Nonparametric Regression Using an Improved Akaike Information Criterion. *Journal of the Royal Statistical Society. Series B (Statistical Methodology)*, *60*(2), 271–293.

Incharoensakdi, A., Jantaro, S., Raksajit, W., & Mäenpää, P. (2010). Polyamines in cyanobacteria: Biosynthesis, transport and abiotic stress response. *Undefined*. https://www.semanticscholar.org/paper/Polyamines-in-cyanobacteria%3A-biosynthesis%2C-and-Incharoensakdi-Jantaro/577e36418f0ea6cacd3d62e7f87f7fee7cdcccb6

Jackson, R. (2021). *The Effects of Climate Change*. Climate Change: Vital Signs of the Planet. https://climate.nasa.gov/effects

Jacob-Lopes, E., Scoparo, C. H. G., Lacerda, L. M. C. F., & Franco, T. T. (2009). Effect of light cycles (night/day) on CO2 fixation and biomass production by microalgae in photobioreactors. *Chemical Engineering and Processing: Process Intensification*, *48*(1), 306–310. https://doi.org/10.1016/j.cep.2008.04.007

Jantaro, S., & Kanwal, S. (2017). Chapter 8—Low-Molecular-Weight Nitrogenous Compounds (GABA and Polyamines) in Blue–Green Algae. In R. P. Rastogi, D. Madamwar, & A. Pandey (Eds.), *Algal Green Chemistry* (pp. 149–169). Elsevier. https://doi.org/10.1016/B978-0-444-63784-0.00008-4

Jöhnk, K. D., Huisman, J., Sharples, J., Sommeijer, B., Visser, P. M., & Stroom, J. M. (2008). Summer heatwaves promote blooms of harmful cyanobacteria. *Global Change Biology*, *14*(3), 495–512. https://doi.org/10.1111/j.1365-2486.2007.01510.x

Johnson, F. H., & Lewin, I. (1946). The growth rate of E. coli in relation to temperature, quinine and coenzyme. *Journal of Cellular and Comparative Physiology*, *28*(1), 47–75. https://doi.org/10.1002/jcp.1030280104

Johnson, G. N., Young, A. J., Scholes, J. D., & Horton, P. (1993). The dissipation of excess excitation energy in British plant species. *Plant, Cell & Environment*, *16*(6), 673–679. https://doi.org/10.1111/j.1365-3040.1993.tb00485.x

Kalisch, B., Dörmann, P., & Hölzl, G. (2016). DGDG and Glycolipids in Plants and Algae. *Sub-Cellular Biochemistry*, *86*, 51–83. https://doi.org/10.1007/978-3-319-25979-6_3

Kamali, M., Persson, K. M., Costa, M. E., & Capela, I. (2019). Sustainability criteria for assessing nanotechnology applicability in industrial wastewater treatment: Current status and future outlook. *Environment International*, *125*, 261–276. https://doi.org/10.1016/j.envint.2019.01.055

Kamykowski, D. (1985). A survey of protozoan laboratory temperature studies applied to marine dinoflagellate behavior from a field perspective. *Contributions in Marine Science. 1985.*

Karia, G. L., & Christian, R. A. (2006). *Wastewater treatment: Concepts and design approach*. Prentice-Hall of India; /z-wcorg/.

Kessler, E. (2006). Upper limits of temperature for growth inChlorella (Chlorophyceae). *Plant Systematics and Evolution*. https://doi.org/10.1007/BF02418020

Khan, M. I., Shin, J. H., & Kim, J. D. (2018). The promising future of microalgae: Current status, challenges, and optimization of a sustainable and renewable industry for biofuels, feed, and other products. *Microbial Cell Factories*, *17*(1), 36. https://doi.org/10.1186/s12934-018-0879-x

Khiewwijit, R., Temmink, H., Rijnaarts, H., & Keesman, K. J. (2015). Energy and nutrient recovery for municipal wastewater treatment: How to design a feasible plant layout? *Environmental Modelling & Software*, *68*, 156–165.

Kim, J. Y., Han, Y., Lee, J. E., & Yenari, M. A. (2018). The 70-kDa heat shock protein (Hsp70) as a therapeutic target for stroke. *Expert Opinion on Therapeutic Targets*, *22*(3), 191–199. https://doi.org/10.1080/14728222.2018.1439477

Kim, N., Kim, J. Y., & Yenari, M. A. (2012). Anti-inflammatory properties and pharmacological induction of Hsp70 after brain injury. *Inflammopharmacology*, *20*(3), 177–185. https://doi.org/10.1007/s10787-011-0115-3

Kiseleva, A. A., Tarachovskaya, E. R., & Shishova, M. F. (2012). Biosynthesis of phytohormones in algae. *Russian Journal of Plant Physiology*, *59*(5), 595–610. https://doi.org/10.1134/S1021443712050081

Kitajima, M., & Butler, W. L. (1975). Quenching of chlorophyll fluorescence and primary photochemistry in chloroplasts by dibromothymoquinone. *Biochimica Et Biophysica Acta*, *376*(1), 105–115. https://doi.org/10.1016/0005-2728(75)90209-1

Kobayashi, Y., Harada, N., Nishimura, Y., Saito, T., Nakamura, M., Fujiwara, T., Kuroiwa, T., & Misumi, O. (2014). Algae Sense Exact Temperatures: Small Heat Shock Proteins Are Expressed at the Survival Threshold Temperature in Cyanidioschyzon merolae and Chlamydomonas reinhardtii. *Genome Biology and Evolution*, *6*(10), 2731–2740. https://doi.org/10.1093/gbe/evu216

Kontopoulos, D.-G., García-Carreras, B., Sal, S., Smith, T. P., & Pawar, S. (2018). Use and misuse of temperature normalisation in meta-analyses of thermal responses of biological traits. *PeerJ*, *6*, e4363. https://doi.org/10.7717/peerj.4363

Kremp, A., Godhe, A., Egardt, J., Dupont, S., Suikkanen, S., Casabianca, S., & Penna, A. (2012). Intraspecific variability in the response of bloom-forming marine microalgae to changed climate conditions. *Ecology and Evolution*, *2*(6), 1195–1207. https://doi.org/10.1002/ece3.245

Kudo, I., Miyamoto, M., Noiri, Y., & Maita, Y. (2000). Combined Effects of Temperature and Iron on the Growth and Physiology of the Marine Diatom Phaeodactylum Tricornutum (bacillariophyceae). *Journal of Phycology*, *36*(6), 1096–1102. https://doi.org/10.1046/j.1529-8817.2000.99042.x

Lactin, D. J., Holliday, N. J., Johnson, D. L., & Craigen, R. (1995). Improved rate model of temperature-dependent development by arthropods.<em></em> *Environmental Entomology 24: 68-75.*

Lage, S., Toffolo, A., & Gentili, F. G. (2021). Microalgal growth, nitrogen uptake and storage, and dissolved oxygen production in a polyculture based-open pond fed with municipal wastewater in northern Sweden. *Chemosphere*, *276*, 130122. https://doi.org/10.1016/j.chemosphere.2021.130122

Law, C. W., Chen, Y., Shi, W., & Smyth, G. K. (2014). voom: Precision weights unlock linear model analysis tools for RNA-seq read counts. *Genome Biology*, *15*(2), R29. https://doi.org/10.1186/gb-2014-15-2-r29

Lee, J.-B., Hayashi, K., Hirata, M., Kuroda, E., Suzuki, E., Kubo, Y., & Hayashi, T. (2006). Antiviral Sulfated Polysaccharide from *Navicula directa*, a Diatom Collected from Deep-Sea Water in Toyama Bay. *Biological and Pharmaceutical Bulletin*, *29*(10), 2135–2139. https://doi.org/10.1248/bpb.29.2135

Li, W. K. W. (1980). Temperature Adaptation in Phytoplankton: Cellular and Photosynthetic Characteristics. In P. G. Falkowski (Ed.), *Primary Productivity in the Sea* (pp. 259–279). Springer US. https://doi.org/10.1007/978-1-4684-3890-1_15

Lin, B., Ahmed, F., Du, H., Li, Z., Yan, Y., Huang, Y., Cui, M., Yin, Y., Li, B., Wang, M., Meng, C., & Gao, Z. (2018). Plant growth regulators promote lipid and carotenoid accumulation in Chlorella vulgaris. *Journal of Applied Phycology*, *30*(3), 1549–1561. https://doi.org/10.1007/s10811-017-1350-9

Lin, H.-Y., & Lin, H.-J. (2018). Polyamines in Microalgae: Something Borrowed, Something New. *Marine Drugs*, *17*(1), E1. https://doi.org/10.3390/md17010001

Liu, J., Yuan, C., Hu, G., & Li, F. (2012). Effects of light intensity on the growth and lipid accumulation of microalga Scenedesmus sp. 11-1 under nitrogen limitation. *Applied Biochemistry and Biotechnology*, *166*(8), 2127–2137. https://doi.org/10.1007/s12010-012-9639-2

Liu, R., Xu, Y.-H., Jiang, S.-C., Lu, K., Lu, Y.-F., Feng, X.-J., Wu, Z., Liang, S., Yu, Y.-T., Wang, X.-F., & Zhang, D.-P. (2013). Light-harvesting chlorophyll a/b-binding proteins, positively involved in abscisic acid signalling, require a transcription repressor, WRKY40, to balance their function. *Journal of Experimental Botany*, *64*(18), 5443–5456. https://doi.org/10.1093/jxb/ert307

Liu, X.-Y., Yang, J.-H., Li, B., Yang, X.-M., & Meng, Q.-W. (2006). Antisense-Mediated Depletion of Tomato Chloroplast Omega-3 Fatty Acid Desaturase Enhances Thermal Tolerance. *Journal of Integrative Plant Biology*, *48*(9), 1096–1107. https://doi.org/10.1111/j.1744-7909.2006.00335.x

Lynch, M., & Gabriel, W. (1987). Environmental Tolerance. *The American Naturalist*, *129*(2), 283–303. https://doi.org/10.1086/284635

Lyukevich, A. A., Mouradyan, E. A., & Los, D. A. (2003). Molecular Cloning and Stress-Dependent Expression of a Gene Encoding ω3-Fatty Acid Desaturase in the Microalga

Dunaliella salina. *Russian Journal of Plant Physiology*, *50*(4), 481–486. https://doi.org/10.1023/A:1024764522062

Malone, L. A., Proctor, M. S., Hitchcock, A., Hunter, C. N., & Johnson, M. P. (2021). Cytochrome b6f – Orchestrator of photosynthetic electron transfer. *Biochimica et Biophysica Acta (BBA) - Bioenergetics*, *1862*(5), 148380. https://doi.org/10.1016/j.bbabio.2021.148380

Mao, S., Zhang, D., Li, Y., & Liu, N. (2013). An improved model for calculating CO2 solubility in aqueous NaCl solutions and the application to CO2–H2O–NaCl fluid inclusions. *Chemical Geology*, *347*, 43–58. https://doi.org/10.1016/j.chemgeo.2013.03.010

Marchant, A., Kargul, J., May, S. T., Muller, P., Delbarre, A., Perrot-Rechenmann, C., & Bennett, M. J. (1999). AUX1 regulates root gravitropism in Arabidopsis by facilitating auxin uptake within root apical tissues. *The EMBO Journal*, *18*(8), 2066–2073. https://doi.org/10.1093/emboj/18.8.2066

Marinova, G., Ivanova, J., Pilarski, P., Chernev, G., & Chaneva, G. (2018). Effect of heavy metals on the green alga scenedesmus incrassatulus. *Oxidation Communications*, *41*, 318–328.

Masojídek, J., Grobbelaar, J. U., Pechar, L., & KoblíŽek, M. (2001). Photosystem II Electron Transport Rates and Oxygen Production in Natural Waterblooms of Freshwater Cyanobacteria During a Diel Cycle. *Journal of Plankton Research*, *23*(1), 57–66. https://doi.org/10.1093/plankt/23.1.57

Mata, T. M., Martins, A. A., & Caetano, Nidia. S. (2010). Microalgae for biodiesel production and other applications: A review. *Renewable and Sustainable Energy Reviews*, *14*(1), 217–232. https://doi.org/10.1016/j.rser.2009.07.020

Maxwell, D. P., Falk, S., Trick, C. G., & Huner, N. P. A. (1994). Growth at Low Temperature Mimics High-Light Acclimation in Chlorella vulgaris. *Plant Physiology*, *105*(2), 535–543. https://doi.org/10.1104/pp.105.2.535

Maxwell, K., & Johnson, G. N. (2000). Chlorophyll fluorescence—A practical guide. *Journal of Experimental Botany*, *51*(345), 659–668. https://doi.org/10.1093/jexbot/51.345.659

McGrath, R. J., & Mason, I. G. (2004). An Observational Method for the Assessment of Biogas Production from an Anaerobic Waste Stabilisation Pond treating Farm Dairy Wastewater. *Biosystems Engineering*, *87*, 471–478. https://doi.org/10.1016/j.biosystemseng.2003.12.011

Michalak, I., Chojnacka, K., & Witek-Krowiak, A. (2013). State of the Art for the Biosorption Process—A Review. *Applied Biochemistry and Biotechnology*, *170*(6), 1389–1416. https://doi.org/10.1007/s12010-013-0269-0

Milward, E. A., Shahandeh, A., Heidari, M., Johnstone, D. M., Daneshi, N., & Hondermarck, H. (2016). Transcriptomics. In R. A. Bradshaw & P. D. Stahl (Eds.), *Encyclopedia of Cell Biology* (pp. 160–165). Academic Press. https://doi.org/10.1016/B978-0-12-394447-4.40029-5

Mógor, Á. F., Ördög, V., Lima, G. P. P., Molnár, Z., & Mógor, G. (2018). Biostimulant properties of cyanobacterial hydrolysate related to polyamines. *Journal of Applied Phycology*, *30*(1), 453–460. https://doi.org/10.1007/s10811-017-1242-z

Mohammed, M. H., & Markert, B. (2006). Toxicity of heavy metals on Scenedesmus quadricauda (Turp.) de Brébisson in batch cultures. *Environmental Science and Pollution Research International*, *13*(2), 98–104. https://doi.org/10.1065/espr2005.07.274

Montagnes, D. J. S., Morgan, G., Bissinger, J. E., Atkinson, D., & Weisse, T. (2008). Short-term temperature change may impact freshwater carbon flux: A microbial perspective. *Global Change Biology*, *14*(12), 2823–2838. https://doi.org/10.1111/j.1365-2486.2008.01700.x

Monteiro, C. M., Castro, P. M. L., & Malcata, F. X. (2009). Use of the microalga Scenedesmus obliquus to remove cadmium cations from aqueous solutions. *World Journal of Microbiology and Biotechnology*, *25*(9), 1573–1578. https://doi.org/10.1007/s11274-009-0046-y

Msanne, J., Polle, J., & Starkenburg, S. (2020). An assessment of heterotrophy and mixotrophy in Scenedesmus and its utilization in wastewater treatment. *Algal Research*, *48*, 101911. https://doi.org/10.1016/j.algal.2020.101911

Mühlenbock, P., Szechynska-Hebda, M., Plaszczyca, M., Baudo, M., Mateo, A., Mullineaux, P. M., Parker, J. E., Karpinska, B., & Karpinski, S. (2008). Chloroplast signaling and LESION SIMULATING DISEASE1 regulate crosstalk between light acclimation and immunity in Arabidopsis. *The Plant Cell*, *20*(9), 2339–2356. https://doi.org/10.1105/tpc.108.059618

Muñoz, R., & Guieysse, B. (2006). Algal–bacterial processes for the treatment of hazardous contaminants: A review. *Water Research*, *40*(15), 2799–2815. https://doi.org/10.1016/j.watres.2006.06.011

Muñoz-Bertomeu, J., Cascales-Miñana, B., Mulet, J. M., Baroja-Fernández, E., Pozueta-Romero, J., Kuhn, J. M., Segura, J., & Ros, R. (2009). Plastidial glyceraldehyde-3-phosphate dehydrogenase deficiency leads to altered root development and affects the sugar and amino acid balance in Arabidopsis. *Plant Physiology*, *151*(2), 541–558. https://doi.org/10.1104/pp.109.143701

Najdenski, H. M., Gigova, L. G., Iliev, I. I., Pilarski, P. S., Lukavský, J., Tsvetkova, I. V., Ninova, M. S., & Kussovski, V. K. (2013). Antibacterial and antifungal activities of selected microalgae and cyanobacteria. *International Journal of Food Science & Technology*, *48*(7), 1533–1540. https://doi.org/10.1111/ijfs.12122

National Ocean Service. (2022). *How much oxygen comes from the ocean?* https://oceanservice.noaa.gov/facts/ocean-oxygen.html

Navarro-López, E., Ruíz-Nieto, A., Ferreira, A., Acién, F. G., & Gouveia, L. (2020). Biostimulant Potential of Scenedesmus obliquus Grown in Brewery Wastewater. *Molecules*, *25*(3), 664. https://doi.org/10.3390/molecules25030664

Necchi Jnr, O. (2004). Photosynthetic responses to temperature in tropical lotic macroalgae. *Phycological Research*, *52*(2), 140–148. https://doi.org/10.1111/j.1440-183.2004.00334.x

Nguyen, H. M., Cuiné, S., Beyly-Adriano, A., Légeret, B., Billon, E., Auroy, P., Beisson, F., Peltier, G., & Li-Beisson, Y. (2013). The Green Microalga Chlamydomonas reinhardtii Has a Single ω-3 Fatty Acid Desaturase That Localizes to the Chloroplast and Impacts Both Plastidic and Extraplastidic Membrane Lipids. *Plant Physiology*, *163*(2), 914–928. https://doi.org/10.1104/pp.113.223941

Niehaus, A. C., Angilletta, M. J., Jr, Sears, M. W., Franklin, C. E., & Wilson, R. S. (2012). Predicting the physiological performance of ectotherms in fluctuating thermal environments. *Journal of Experimental Biology*, *215*(4), 694–701. https://doi.org/10.1242/jeb.058032

Niveshika, Verma, E., Mishra, A. K., Singh, A. K., & Singh, V. K. (2016). Structural Elucidation and Molecular Docking of a Novel Antibiotic Compound from Cyanobacterium Nostoc sp. MGL001. *Frontiers in Microbiology*, *7*. https://www.frontiersin.org/article/10.3389/fmicb.2016.01899

Oliveira, D. M., Mota, T. R., Salatta, F. V., de Almeida, G. H. G., Olher, V. G. A., Oliveira, M. A. S., Marchiosi, R., Ferrarese-Filho, O., & dos Santos, W. D. (2020). Feruloyl esterase activity and its role in regulating the feruloylation of maize cell walls. *Plant Physiology and Biochemistry*, *156*, 49–54. https://doi.org/10.1016/j.plaphy.2020.08.046

Olvera, R. C., Silva, S. L., Robles-Belmont, E., & Lau, E. Z. (2017). Review of nanotechnology value chain for water treatment applications in Mexico. *Resource-Efficient Technologies*, *3*(1), 1–11. https://doi.org/10.1016/j.reffit.2017.01.008

O'Neill, R.V., Goldstein, R.A., Shugart, H.H., & Mankin, J.B. (1972). Terrestrial Ecosystem Energy Model. *Eastern Deciduous Forest Biome Memo Report Oak Ridge. The Environmental Sciences Division of the Oak Ridge National Laboratory.*

Oruganti, R. K., Katam, K., Show, P. L., Gadhamshetty, V., Upadhyayula, V. K. K., & Bhattacharyya, D. (2022). A comprehensive review on the use of algal-bacterial systems for wastewater treatment with emphasis on nutrient and micropollutant removal. *Bioengineered*, *13*(4), 10412–10453. https://doi.org/10.1080/21655979.2022.2056823

Padfield, D., O'Sullivan, H., & Pawar, S. (2021). rTPC and nls.multstart: A new pipeline to fit thermal performance curves in r. *Methods in Ecology and Evolution*, *12*(6), 1138–1143. https://doi.org/10.1111/2041-210X.13585

Pal, D., Khozin-Goldberg, I., Cohen, Z., & Boussiba, S. (2011). The effect of light, salinity, and nitrogen availability on lipid production by Nannochloropsis sp. *Applied Microbiology and Biotechnology*, *90*(4), 1429–1441. https://doi.org/10.1007/s00253-011-3170-1

Patnaik, R., Singh, N. K., Bagchi, S. K., Rao, P. S., & Mallick, N. (2019). Utilization of Scenedesmus obliquus Protein as a Replacement of the Commercially Available Fish Meal Under an Algal Refinery Approach. *Frontiers in Microbiology*, *10*, 2114. https://doi.org/10.3389/fmicb.2019.02114

Peers, G., Truong, T. B., Ostendorf, E., Busch, A., Elrad, D., Grossman, A. R., Hippler, M., & Niyogi, K. K. (2009). An ancient light-harvesting protein is critical for the regulation of algal photosynthesis. *Nature*, *462*(7272), 518–521. https://doi.org/10.1038/nature08587

Pereira, S. L., Huang, Y.-S., Bobik, E. G., Kinney, A. J., Stecca, K. L., Packer, J. C. L., & Mukerji, P. (2004). A novel omega3-fatty acid desaturase involved in the biosynthesis of eicosapentaenoic acid. *Biochemical Journal*, *378*(Pt 2), 665–671. https://doi.org/10.1042/BJ20031319

Platt, T., Gallegos, C., & Harrison, W. G. (1980). Photoinhibition of photosynthesis in natural assemblages of marine phytoplankton. *Undefined*. https://www.semanticscholar.org/paper/Photoinhibition-of-photosynthesis-in-natural-of-Platt-Gallegos/9cc6f2193c1740004a8be875b805d0258a3ad1da

Plöhn, M., Spain, O., Sirin, S., Silva, M., Escudero-Oñate, C., Ferrando-Climent, L., Allahverdiyeva, Y., & Funk, C. (2021). Wastewater treatment by microalgae. *Physiologia Plantarum*, *173*(2), 568–578. https://doi.org/10.1111/ppl.13427

Polycarpou, P. (2019). Temperature Control of Flat-panel Airlift Photobioreactors for Microalgae Prduction – A Numerical Investigation. *International Journal of Energy and Power Engineering*, *8*, 79. https://doi.org/10.11648/j.ijepe.20190806.12

Ramanan, R., Kim, B.-H., Cho, D.-H., Oh, H.-M., & Kim, H.-S. (2016). Algae–bacteria interactions: Evolution, ecology and emerging applications. *Biotechnology Advances*, *34*(1), 14–29. https://doi.org/10.1016/j.biotechadv.2015.12.003

Ras, M., Steyer, J.-P., & Bernard, O. (2013). Temperature effect on microalgae: A crucial factor for outdoor production. *Reviews in Environmental Science and Bio/Technology*, *12*(2), 153–164. https://doi.org/10.1007/s11157-013-9310-6

Ratkowsky, D. A., Lowry, R. K., McMeekin, T. A., Stokes, A. N., & Chandler, R. E. (1983a). Model for bacterial culture growth rate throughout the entire biokinetic temperature range. *Journal of Bacteriology*, *154*(3), 1222–1226.

Ratkowsky, D. A., Lowry, R. K., McMeekin, T. A., Stokes, A. N., & Chandler, R. E. (1983b). Model for bacterial culture growth rate throughout the entire biokinetic temperature range. *Journal of Bacteriology*, *154*(3), 1222–1226.

Raven, J. A., & Geider, R. J. (1988). Temperature and algal growth. *New Phytologist*, *110*(4), 441–461. https://doi.org/10.1111/j.1469-8137.1988.tb00282.x

Rezende, E. L., & Bozinovic, F. (2019). Thermal performance across levels of biological organization. *Philosophical Transactions of the Royal Society B: Biological Sciences*, *374*(1778), 20180549. https://doi.org/10.1098/rstb.2018.0549

Richmond, A. (2013). Biological Principles of Mass Cultivation of Photoautotrophic Microalgae. In *Handbook of Microalgal Culture* (pp. 169–204). John Wiley & Sons, Ltd. https://doi.org/10.1002/9781118567166.ch11

Robertson, R., Guihéneuf, F., Schmid, M., Stengel, D., Fitzgerald, G., Ross, P., & Stanton, C. (2013). *Algae-Derived Polyunsaturated Fatty Acids: Implications for Human Health.*

Robinson, M. D., McCarthy, D. J., & Smyth, G. K. (2010). edgeR: A Bioconductor package for differential expression analysis of digital gene expression data. *Bioinformatics*, *26*(1), 139–140. https://doi.org/10.1093/bioinformatics/btp616

Rodolfi, L., Tredici, M. R., & Chini Zittelli, G. (2010). Photobioreactors. In *Encyclopedia of Industrial Biotechnology* (pp. 1–15). John Wiley & Sons, Ltd. https://doi.org/10.1002/9780470054581.eib479

Román, Á., Hernández, M. L., Soria-García, Á., López-Gomollón, S., Lagunas, B., Picorel, R., Martínez-Rivas, J. M., & Alfonso, M. (2015). Non-redundant Contribution of the Plastidial FAD8 ω-3 Desaturase to Glycerolipid Unsaturation at Different Temperatures in Arabidopsis. *Molecular Plant*, *8*(11), 1599–1611. https://doi.org/10.1016/j.molp.2015.06.004

Saibil, H. (2013). Chaperone machines for protein folding, unfolding and disaggregation. *Nature Reviews Molecular Cell Biology*, *14*(10), 630–642. https://doi.org/10.1038/nrm3658

Salah El Din, R., Gharib, F. A., Ghazy, S. M., & Johny, E. Y. R. (2009). EFFECT OF SOME HEAVY METALS ON GROWTH OF SCENEDESMUS OBLIQUUS (TURPIN) KÜTZING. *Egyptian Journal of Phycology*, *10*(1), 23–37. https://doi.org/10.21608/egyjs.2009.114839

Salvucci, M. E., & Crafts-Brandner, S. J. (2004a). Inhibition of photosynthesis by heat stress: The activation state of Rubisco as a limiting factor in photosynthesis. *Physiologia Plantarum*, *120*(2), 179–186. https://doi.org/10.1111/j.0031-9317.2004.0173.x

Salvucci, M. E., & Crafts-Brandner, S. J. (2004b). Relationship between the Heat Tolerance of Photosynthesis and the Thermal Stability of Rubisco Activase in Plants from Contrasting Thermal Environments. *Plant Physiology*, *134*(4), 1460–1470. https://doi.org/10.1104/pp.103.038323

Santos, A. M., Janssen, M., Lamers, P. P., Evers, W. a. C., & Wijffels, R. H. (2012). Growth of oil accumulating microalga Neochloris oleoabundans under alkaline-saline conditions. *Bioresource Technology*, *104*, 593–599. https://doi.org/10.1016/j.biortech.2011.10.084

Schoolfield, R. M., Sharpe, P. J., & Magnuson, C. E. (1981). Non-linear regression of biological temperature-dependent rate models based on absolute reaction-rate theory. *Journal of Theoretical Biology*, *88*(4), 719–731. https://doi.org/10.1016/0022-5193(81)90246-0

Schroda, M., Blöcker, D., & Beck, C. F. (2000). The HSP70A promoter as a tool for the improved expression of transgenes in Chlamydomonas. *The Plant Journal: For Cell and Molecular Biology*, *21*(2), 121–131. https://doi.org/10.1046/j.1365-313x.2000.00652.x

Schulze, P. S. C., Carvalho, C. F. M., Pereira, H., Gangadhar, K. N., Schüler, L. M., Santos, T. F., Varela, J. C. S., & Barreira, L. (2017). Urban wastewater treatment by Tetraselmis sp. CTP4 (Chlorophyta). *Bioresource Technology*, *223*, 175–183. https://doi.org/10.1016/j.biortech.2016.10.027

Servio, P., & Englezos, P. (2001). Effect of temperature and pressure on the solubility of carbon dioxide in water in the presence of gas hydrate. *Fluid Phase Equilibria*, *190*(1), 127–134. https://doi.org/10.1016/S0378-3812(01)00598-2

Shao, Y., Fang, H., Zhou, H., Wang, Q., Zhu, Y., & He, Y. (2017). Detection and imaging of lipids of Scenedesmus obliquus based on confocal Raman microspectroscopy. *Biotechnology for Biofuels*, *10*(1), 300. https://doi.org/10.1186/s13068-017-0977-8

Sharma, D., & Masison, D. C. (2009). Hsp70 Structure, Function, Regulation and Influence on Yeast Prions. *Protein and Peptide Letters*, *16*(6), 571–581.

Shin, H., Hong, S.-J., Yoo, C., Han, M.-A., Lee, H., Choi, H.-K., Cho, S., Lee, C.-G., & Cho, B.-K. (2016). Genome-wide transcriptome analysis revealed organelle specific responses to temperature variations in algae. *Scientific Reports*, *6*(1), 37770. https://doi.org/10.1038/srep37770

Skjånes, K., Andersen, U., Heidorn, T., & Borgvang, S. A. (2016). Design and construction of a photobioreactor for hydrogen production, including status in the field. *Journal of Applied Phycology*, *28*, 2205–2223. https://doi.org/10.1007/s10811-016-0789-4

Slegers, P. M., van Beveren, P. J. M., Wijffels, R. H., van Straten, G., & van Boxtel, A. J. B. (2013). Scenario analysis of large scale algae production in tubular photobioreactors. *Applied Energy*, *105*, 395–406. https://doi.org/10.1016/j.apenergy.2012.12.068

Soomaree, K. (2015). *Detail design of wastewater treatment plant*.

Souza, W. R. de. (2013). Microbial Degradation of Lignocellulosic Biomass. In *Sustainable Degradation of Lignocellulosic Biomass—Techniques, Applications and Commercialization*. IntechOpen. https://doi.org/10.5772/54325

Spain, J. D. (1982). *BASIC microcomputer models in biology*. Reading, MA (USA) Addison-Wesley. https://scholar.google.com/scholar_lookup?title=BASIC+microcomputer+models+in+biology&author=Spain%2C+J.D.&publication_year=1982

Spain, O., Plöhn, M., & Funk, C. (2021). The cell wall of green microalgae and its role in heavy metal removal. *Physiologia Plantarum*, *173*(2), 526–535. https://doi.org/10.1111/ppl.13405

Starr, R. C., & Zeikus, J. A. (1993). UTEX—THE CULTURE COLLECTION OF ALGAE AT THE UNIVERSITY OF TEXAS AT AUSTIN 1993 LIST OF CULTURES1. *Journal of Phycology*, *29*(s2), 1–106. https://doi.org/10.1111/j.0022-3646.1993.00001.x

Stengel, D. B., Connan, S., & Popper, Z. A. (2011). Algal chemodiversity and bioactivity: Sources of natural variability and implications for commercial application.

*Biotechnology Advances*, *29*(5), 483–501. https://doi.org/10.1016/j.biotechadv.2011.05.016

Suzuki, Y., & Takahashi, M. (2008). Growth of several diatom species isolated from various environments to temperature. *Journal of Phycology*, *31*, 880–888. https://doi.org/10.1111/j.0022-3646.1995.00880.x

Tan, C.-Y., Dodd, I. C., Chen, J. E., Phang, S.-M., Chin, C. F., Yow, Y.-Y., & Ratnayeke, S. (2021). Regulation of algal and cyanobacterial auxin production, physiology, and application in agriculture: An overview. *Journal of Applied Phycology*, *33*(5), 2995–3023. https://doi.org/10.1007/s10811-021-02475-3

Thomas, M. K., Aranguren-Gassis, M., Kremer, C. T., Gould, M. R., Anderson, K., Klausmeier, C. A., & Litchman, E. (2017). Temperature–nutrient interactions exacerbate sensitivity to warming in phytoplankton. *Global Change Biology*, *23*(8), 3269–3280. https://doi.org/10.1111/gcb.13641

Thomas, M. K., Kremer, C. T., Klausmeier, C. A., & Litchman, E. (2012). A global pattern of thermal adaptation in marine phytoplankton. *Science (New York, N.Y.)*, *338*(6110), 1085–1088. https://doi.org/10.1126/science.1224836

Thomas, T., & Thomas, T. J. (2001). Polyamines in cell growth and cell death: Molecular mechanisms and therapeutic applications. *Cellular and Molecular Life Sciences: CMLS*, *58*(2), 244–258. https://doi.org/10.1007/PL00000852

Tortajada, C., & Biswas, A. K. (2018). Achieving universal access to clean water and sanitation in an era of water scarcity: Strengthening contributions from academia. *Current Opinion in Environmental Sustainability*, *34*, 21–25. https://doi.org/10.1016/j.cosust.2018.08.001

Tredici, M. R. (2010). Photobiology of microalgae mass cultures: Understanding the tools for the next green revolution. *Biofuels*, *1*(1), 143–162. https://doi.org/10.4155/bfs.09.10

UN SDG. (2022). *Water and Sanitation | Department of Economic and Social Affairs*. https://sdgs.un.org/topics/water-and-sanitation

United Nations. (2019). *Human Beings Face an Existential Threat of Their Own Making*. https://www.un.org/sustainabledevelopment/blog/2019/05/why-waste-water/

Vieira Costa, J. A., Colla, L. M., Filho, P. D., Kabke, K., & Weber, A. (2002). Modelling of Spirulina platensis growth in fresh water using response surface methodology. *World Journal of Microbiology and Biotechnology*, *18*(7), 603–607. https://doi.org/10.1023/A:1016822717583

Wallace, H. M., & Fraser, A. V. (2003). Polyamine analogues as anticancer drugs. *Biochemical Society Transactions*, *31*(2), 393–396. https://doi.org/10.1042/bst0310393

Wang, M., Yang, H., Ergas, S. J., & van der Steen, P. (2015). A novel shortcut nitrogen removal process using an algal-bacterial consortium in a photo-sequencing batch reactor (PSBR). *Water Research*, *87*, 38–48. https://doi.org/10.1016/j.watres.2015.09.016

Weibull, J. W. (1995). *Evolutionary Game Theory*. MIT Press.

Wijffels, R. H., & Barbosa, M. J. (2010). An outlook on microalgal biofuels. *Science (New York, N.Y.)*, *329*(5993), 796–799. https://doi.org/10.1126/science.1189003

Xiaoming, F., Qinglong, L., Lichang, Y., Fu, B., & Yongzhe, C. (2018). Linking water research with the sustainability of the human–natural system. *Current Opinion in Environmental Sustainability*, *33*, 99–103. https://doi.org/10.1016/j.cosust.2018.05.012

Xie, S.-S., Wu, H.-J., Zang, H.-Y., Wu, L.-M., Zhu, Q.-Q., & Gao, X.-W. (2014). Plant growth promotion by spermidine-producing Bacillus subtilis OKB105. *Molecular Plant-Microbe Interactions: MPMI*, *27*(7), 655–663. https://doi.org/10.1094/MPMI-01-14-0010-R

Xin, L., Hong-ying, H., Ke, G., & Ying-xue, S. (2010). Effects of different nitrogen and phosphorus concentrations on the growth, nutrient uptake, and lipid accumulation of a freshwater microalga Scenedesmus sp. *Bioresource Technology*, *101*(14), 5494–5500. https://doi.org/10.1016/j.biortech.2010.02.016

Xing, G., Yuan, H., Yang, J., Li, J., Gao, Q., Li, W., & Wang, E. (2018). Integrated analyses of transcriptome, proteome and fatty acid profilings of the oleaginous microalga Auxenochlorella protothecoides UTEX 2341 reveal differential reprogramming of fatty acid metabolism in response to low and high temperatures. *Algal Research*, *33*, 16–27. https://doi.org/10.1016/j.algal.2018.04.028

Xue, Y., Chen, B., Win, A. N., Fu, C., Lian, J., Liu, X., Wang, R., Zhang, X., & Chai, Y. (2018). Omega-3 fatty acid desaturase gene family from two ω-3 sources, Salvia hispanica and Perilla frutescens: Cloning, characterization and expression. *PLoS ONE*, *13*(1), e0191432. https://doi.org/10.1371/journal.pone.0191432

Yadav, D., Tanveer, A., Malviya, N., & Yadav, S. (2018). Chapter 1 - Overview and Principles of Bioengineering: The Drivers of Omics Technologies. In D. Barh & V. Azevedo (Eds.), *Omics Technologies and Bio-Engineering* (pp. 3–23). Academic Press. https://doi.org/10.1016/B978-0-12-804659-3.00001-4

Yap, J. K., Sankaran, R., Chew, K. W., Halimatul Munawaroh, H. S., Ho, S.-H., Rajesh Banu, J., & Show, P. L. (2021). Advancement of green technologies: A comprehensive review

on the potential application of microalgae biomass. *Chemosphere*, *281*, 130886. https://doi.org/10.1016/j.chemosphere.2021.130886

Yong, W.-K., Sim, K.-S., Poong, S.-W., Wei, D., Phang, S.-M., & Lim, P.-E. (2019). Physiological and metabolic responses of Scenedesmus quadricauda (Chlorophyceae) to nickel toxicity and warming. *3 Biotech*, *9*(8), 315. https://doi.org/10.1007/s13205-019-1848-8

Zhang, C., Zhang, Y., Zhuang, B., & Zhou, X. (2014). Strategic enhancement of algal biomass, nutrient uptake and lipid through statistical optimization of nutrient supplementation in coupling Scenedesmus obliquus-like microalgae cultivation and municipal wastewater treatment. *Bioresource Technology*, *171*, 71–79. https://doi.org/10.1016/j.biortech.2014.07.060

Zhang, L., Cheng, L., Chiew, F., & Fu, B. (2018). Understanding the impacts of climate and landuse change on water yield. *Current Opinion in Environmental Sustainability*, *33*, 167–174. https://doi.org/10.1016/j.cosust.2018.04.017

Zhang, S., & Van Duijn, B. (2014). Cellular Auxin Transport in Algae. *Plants*, *3*(1), 58–69. https://doi.org/10.3390/plants3010058

Zhao, H., Michaelis, M. L., & Blagg, B. S. J. (2012). Hsp90 modulation for the treatment of Alzheimer's disease. *Advances in Pharmacology (San Diego, Calif.)*, *64*, 1–25. https://doi.org/10.1016/B978-0-12-394816-8.00001-5

Zittelli, G. C., Biondi, N., Rodolfi, L., & Tredici, M. R. (2013). Photobioreactors for Mass Production of Microalgae. In *Handbook of Microalgal Culture* (pp. 225–266). John Wiley & Sons, Ltd. https://doi.org/10.1002/9781118567166.ch13

# Appendix

## Appendix 1. thermal performance curve models

Descriptions of 24 thermal performance curve models used in this thesis to determine the optimum growth temperatures and thermal response for the UTEX 393 and SNS0120.

| | |
|---|---|
| Beta (Niehaus et al., 2012) | $$rate = \frac{a\left(\frac{temp - b + \frac{c(d-1)}{d+e-2}}{c}\right)^{d-1} \cdot \left(1 - \frac{temp - b + \frac{c(d-1)}{d+e-2}}{c}\right)^{e-1}}{\left(\frac{d-1}{d+e-2}\right)^{d-1} \cdot \left(\frac{e-1}{d+e-2}\right)^{e-1}}$$ **temp**: temperature in celsius; **a, b, c, d & e**: demention less parameters. |
| Boatamn (Boatman et al., 2017) | $$rate = r_{max} \cdot \left(sin\left(\pi\left(\frac{temp - t_{min}}{t_{max} - t_{min}}\right)^{a}\right)\right)^{b}$$ **temp**: temperature in degrees centigrade; **rmax**: the rate at optimum temperature; **tmin**: low temperature (ºC) at which rates become negative; **tmax**: high temperature (ºC) at which rates become negative; **a**: shape parameter to adjust the skewness of the curve; **b**: shape parameter to adjust the kurtosis of the curve. |
| Briere2 (Briere et al., 1999) | $$rate = a \cdot temp \cdot (temp - t_{min}) \cdot (t_{max} - temp)^{\frac{1}{b}}$$ **temp**: temperature in degrees centigrade; **tmin**: low temperature (ºC) at which rates become negative; **tmax**: high temperature (ºC) at which rates become negative; **a**: scale parameter to adjust maximum rate of the curve; **b**: shape parameter to adjust the asymmetry of the curve. |
| Delong (DeLong et al., 2017) | $$\text{rate} = c \cdot \exp\frac{-\left(e_b - \left(e_f\left(1 - \frac{\text{temp} + 273.15}{t_m}\right) + e_{hc} \cdot \left((\text{temp} + 273.15) - t_m - (\text{temp} + 273.15) \cdot \ln\left(\frac{\text{temp} + 273.15}{t_m}\right)\right)\right)\right)}{k \cdot (\text{temp} + 273.15)}$$ **temp**: temperature in degrees centigrade; **c**: potential reaction rate; **eb**: baseline energy needed for the reaction to occur (eV); **ef**: temperature dependence of folding the enzymes used in the metabolic reaction, relative to the melting temperature (eV); **tm**: melting temperature in degrees centigrade; **ehc**: temperature dependence of the heat capacity between the folded and unfolded state of the enzymes, relative to the melting temperature (eV). |
| Flinn (Flinn, 1991) | $$\text{rate} = \frac{1}{1 + a + b \cdot \text{temp} + c \cdot \text{temp}^2}$$ **temp**: temperature in degrees centigrade; **a**: parameter that controls the height of the curve; **b**: parameter that controls the slope of the initial increase of the curve; **c**: parameter that controls the position and steepness of the decline of the curve. |
| Gaussian (Lynch & Gabriel, 1987) | $$\text{rate} = r_{max} \cdot \exp^{\left(-0.5\left(\frac{\lvert \text{temp} - t_{opt} \rvert}{a}\right)^2\right)}$$ **temp**: temperature in degrees centigrade; **rmax**: maximum rate at optimum temperature; **topt**: optimum temperature (ºC); **a**: related to the full curve width. |
| Hinshelwood (C. N. Hinshelwood, 1947) | $$\text{rate} = a \cdot \exp^{\frac{-e}{k \cdot (\text{temp} + 273.15)}} - b \cdot \exp^{\frac{-e_h}{k \cdot (\text{temp} + 273.15)}}$$ **temp**: temperature in degrees centigrade; **a**: pre-exponential constant for the activation energy; **e**: activation energy (eV); **b**: pre-exponential constant for the deactivation energy; **eh**: de-activation energy (eV). |

| | |
|---|---|
| Joehnk (Jöhnk et al., 2008) | $$\text{rate} = r_{max}\left(1 + a\left(\left(b^{temp-t_{opt}} - 1\right) - \frac{\ln(b)}{\ln(c)}\left(c^{temp-t_{opt}} - 1\right)\right)\right)$$ **temp**: temperature in degrees centigrade; **rmax**: the rate at optimum temperature; **topt**: optimum temperatute (ºC); **a, b and c**: parameter with no biological meaning. |
| Johnson-Lewin (F. H. Johnson & Lewin, 1946) | $$\text{rate} = \frac{r_0 \cdot \exp^{\frac{-e}{k\cdot(temp+273.15)}}}{1 + \exp^{-\frac{e_h - \left(\frac{e_h}{(t_{opt}+273.15)} + k\cdot\ln\left(\frac{e}{e_h - e}\right)\right)\cdot(temp+273.15)}{k\cdot(temp+273.15)}}}$$ **temp**: temperature in degrees centigrade; **r0**: scaling parameter; **e**: activation energy (eV); **eh**: high temperature deactivation energy (eV); **topt**: optimum temperature (ºC). |
| Kamykowski (Kamykowski, 1985) | $$\text{rate} = a \cdot \left(1 - \exp^{-b\cdot(temp-t_{min})}\right) \cdot \left(1 - \exp^{-c\cdot(t_{max}-temp)}\right)$$ **temp**: temperature in degrees centigrade; **tmin**: low temperature (ºC) at which rates become negative; **tmax**: high temperature (ºC) at which rates become negative; **a, b and c**: parameter with no biological meaning. |
| Lactin2 (Lactin et al., 1995) | $$\text{rate} = \exp^{a\cdot temp} - \exp^{a\cdot t_{max} - \left(\frac{t_{max}-temp}{\delta_t}\right)} + b$$ **temp**: temperature in degrees centigrade; **a**: constant that determines the steepness of the rising portion of the curve; **b**: constant that determines the height of the overall curve; **tmax**: the temperature at which the curve begins to decelerate beyond the optimum (ºC); **delta-t**: thermal safety margin (ºC). |
| Modified gaussian (Angilletta, 2006) | $$\text{rate} = r_{max} \cdot \exp^{\left[-0.5\left(\frac{\lvert temp - t_{opt}\rvert}{a}\right)^b\right]}$$ **temp**: temperature in degrees centigrade; **rmax**: maximum rate at optimum temperature; **topt**: optimum temperature; **a**: related to full curve width; **b**: allows for asymmetry in the curve fit. |
| O'neill (O'Neill, R.V. et al., 1972) | $$\text{rate} = r_{max} \cdot \left(\frac{ct_{max} - temp}{ct_{max} - t_{opt}}\right)^x \cdot \exp^{x\cdot\frac{temp - t_{opt}}{ct_{max} - t_{opt}}}$$ $$\text{where: } x = \frac{w^2}{400} \cdot \left(1 + \sqrt{1 + \frac{40}{w}}\right)^2$$ $$\text{and: } w = (q_{10} - 1) \cdot \left(ct_{max} - t_{opt}\right)$$ **temp**: temperature in degrees centigrade; **rmax**: maximum rate at optimum temperature; **ctmax**: high temperature (ºC) at which rates become negative; **topt**: optimum temperature (ºC); **q10**: defines the fold change in performance as a result of increasing the temperature by 10 ºC. |
| Pawar (Kontopoulos et al., 2018) | $$\text{rate} = \frac{r_{tref} \cdot \exp^{\frac{-e}{k}\left(\frac{1}{temp+273.15} - \frac{1}{t_{ref}+273.15}\right)}}{1 + \left(\frac{e}{eh - e}\right) \cdot \exp^{\frac{e_h}{k}\left(\frac{1}{t_opt+273.15} - \frac{1}{temp+273.15}\right)}}$$ **temp**: temperature in degrees centigrade; **r_tref**: rate at the standardised temperature, tref; **e**: activation energy (eV); **eh**: high temperature deactivation energy (eV); **topt**: optimum temperature (ºC); **tref**: standardisation temperature in degrees centigrade. Temperature at which rates are not inactivated by high temperatures. |
| Quadratic (Montagnes et al., 2008) | $$\text{rate} = a + b \cdot temp + c \cdot temp^2$$ **temp**: temperature in degrees centigrade; **a**: parameter that defines the rate at 0 ºC; **b & c**: parameter with no biological meaning. |
| Ratkowsky (Ratkowsky et al., 1983b) | $$\text{rate} = \left(a \cdot (temp - t_{min})\right)^2 \cdot \left(1 - \exp\left(b \cdot (temp - t_{max})\right)\right)^2$$ |

| | |
|---|---|
| | **temp**: temperature in degrees centigrade; **tmin**: low temperature (ºC) at which rates become negative; **tmax**: high temperature (ºC) at which rates become negative; **a**: parameter defined as sqrt(rate)/(temp - tmin); **b**: empirical parameter needed to fit the data for temperatures beyond the optimum temperature. |
| Rezende (Rezende & Bozinovic, 2019) | $\text{if} \quad \text{temp} < \text{b}: \text{rate} = \text{a} \cdot 10^{\frac{\log_{10}(\text{q}_{10})}{\left(\frac{10}{\text{temp}}\right)}}$<br>$\text{if} \quad \text{temp} > \text{b}: \text{rate} = \text{a} \cdot 10^{\frac{\log_{10}(\text{q}_{10})}{\left(\frac{10}{\text{temp}}\right)}} \cdot (1 - \text{c} \cdot (\text{b} - \text{temp})^2)$<br>**temp**: temperature in degrees centigrade; **q10**: defines the fold change in performance as a result of increasing the temperature by 10 ºC; **a**: parameter describing shifts in rate; **b**: parameter threshold temperature (ºC) beyond which the downward curve starts; **c**: parameter controlling the rate of decline beyond the threshold temperature, b. |
| Sharpe-Schoolfield high temperature (Schoolfield et al., 1981) | $\text{rate} = \frac{\text{r}_{\text{tref}} \cdot \exp^{\frac{-\text{e}}{\text{k}}\left(\frac{1}{\text{temp}+273.15} - \frac{1}{\text{t}_{\text{ref}}+273.15}\right)}}{1 + \exp^{\frac{\text{e}_\text{h}}{\text{k}}\left(\frac{1}{\text{t}_\text{h}} - \frac{1}{\text{temp}+273.15}\right)}}$<br>**temp**: temperature in degrees centigrade; **r_tref**: rate at the standardised temperature, tref; **e**: activation energy (eV); **eh**: high temperature deactivation energy (eV); **th**: temperature (ºC) at which enzyme is 1/2 active and 1/2 suppressed due to high temperatures; **tref**: standardisation temperature in degrees centigrade. Temperature at which rates are not inactivated by high temperatures. |
| Spain (J. D. Spain, 1982) | $\text{rate} = \text{r}_0 \cdot \exp^{\text{a}\cdot\text{temp}} \cdot (1 - \text{b} \cdot \exp^{\text{c}\cdot\text{temp}})$<br>**temp**: temperature in degrees centigrade; **a**: constant that determines the steepness of the rising portion of the curve; **b**: constant that determines the position of topt; **c**: constant that determines the steepness of the decreasing part of the curve; **r0**: the apparent rate at 0 ºC. |
| Thomas1 (M. K. Thomas et al., 2012) | $\text{rate} = \text{a} \cdot \exp^{\text{b}\cdot\text{temp}} \left(1 - \left(\frac{\text{temp} - \text{t}_{\text{opt}}}{\text{c}}\right)^2\right)$<br>**temp**: temperature in degrees centigrade; **a & b**: arbitrary constant; **c**: the range of temperatures over which growth rate is positive, or the thermal niche width (ºC); **topt**: determines the location of the maximum of the quadratic portion of this function. When b = 0, tref would equal topt. |
| Thomas2 (M. K. Thomas et al., 2017) | $\text{rate} = \text{a} \cdot \exp^{\text{b}\cdot\text{temp}} - (\text{c} + \text{d} \cdot \exp^{\text{e}\cdot\text{temp}})$<br>**temp**: temperature in degrees centigrade; **a**: birth rate at 0 ºC; **b**: describes the exponential increase in birth rate with increasing temperature; **c**: temperature-independent mortality term; **d**: along with e controls the exponential increase in mortality rates with temperature; **e**: along with d controls the exponential increase in mortality rates with temperature. |
| Weibull (Weibull, 1995) | $\text{rate} = \text{a} \cdot \left(\frac{\text{c}-1}{\text{c}}\right)^{\frac{1-\text{c}}{\text{c}}} \left(\frac{\text{temp} - \text{t}_{\text{opt}}}{\text{b}} + \left(\frac{\text{c}-1}{\text{c}}\right)^{\frac{1}{\text{c}}}\right)^{\text{c}-1} \exp^{-\left(\frac{\text{temp}-\text{t}_{\text{opt}}}{\text{b}} + \left(\frac{\text{c}-1}{\text{c}}\right)^{\frac{1}{\text{c}}}\right)^{\text{c}}} + \frac{\text{c}-1}{\text{c}}$<br>**temp**: temperature in degrees centigrade; **a**: scale the height of the curve; **topt**: optimum temperature; **b**: defines the breadth of the curve; **c**: defines the curve shape. |
| Sharpe-Schoolfield full (Schoolfield et al., 1981) | $rate = \frac{r_{tref} \cdot exp^{\frac{-e}{k}\left(\frac{1}{temp+273.15} - \frac{1}{t_{ref}+273.15}\right)}}{1 + exp^{\frac{e_l}{k}\left(\frac{1}{t_l} - \frac{1}{temp+273.15}\right)} + exp^{\frac{e_h}{k}\left(\frac{1}{t_h} - \frac{1}{temp+273.15}\right)}}$<br>**temp**: temperature in degrees centigrade; **r_tref**: rate at the standardised temperature, tref; **e**: activation energy (eV); **eh**: high temperature deactivation energy (eV); **th**: temperature (ºC) at which enzyme is 1/2 active and 1/2 suppressed due to high temperatures; **tref**: standardisation temperature in degrees centigrade. Temperature at which rates are not inactivated by high temperatures; **el**: low temperature de-activation energy (eV); **tl**: temperature (ºC) at which enzyme is 1/2 active and 1/2 suppressed due to low temperatures. |

| | |
|---|---|
| Sharpe-Schoolfield low (Schoolfield et al., 1981) | $$rate = \frac{r_{tref} \cdot exp^{\frac{-e}{k}\left(\frac{1}{temp+273.15}-\frac{1}{t_{ref}+273.15}\right)}}{1+exp^{\frac{e_l}{k}\left(\frac{1}{t_l}-\frac{1}{temp+273.15}\right)}}$$ **temp**: temperature in degrees centigrade; **r_tref**: rate at the standardised temperature, tref; **e**: activation energy (eV); **el**: low temperature de-activation energy (eV); **tl**: temperature (ºC) at which enzyme is 1/2 active and 1/2 suppressed due to low temperatures.; **tref**: standardisation temperature in degrees centigrade. Temperature at which rates are not inactivated by high temperatures. |

**Appendix 2. AICc and thermal optima calculated by each model**

List of AICc and the optimal temperatures calculated by each tested model for both UTEX393 and SNS0120.

| UTEX393 | | | SNS0120 | | |
|---|---|---|---|---|---|
| Models | Thermal optima (°C) | AICc | Models | Thermal optima (°C) | AICc |
| boatman | 27.18 | -157.80 | rezende | 26.77 | -48.13 |
| beta | 27.28 | -157.69 | johnson_lewin | 26.88 | -47.54 |
| kamykowski | 28.25 | -152.07 | pawar | 26.88 | -47.54 |
| thomas2 | 28.19 | -150.36 | sharpeschoolhigh | 26.88 | -47.54 |
| oneill | 28.56 | -141.68 | spain | 26.72 | -47.22 |
| lactin2 | 28.47 | -138.90 | lactin2 | 26.83 | -46.10 |
| spain | 28.62 | -134.97 | joehnk | 26.34 | -45.95 |
| hinshelwood | 28.2 | -133.82 | thomas2 | 26.34 | -45.95 |
| rezende | 28.08 | -132.96 | oneill | 27.34 | -44.44 |
| thomas1 | 27.87 | -130.73 | beta | 26.14 | -36.53 |
| johnson_lewin | 31.47 | -81.52 | boatman | 26.23 | -34.61 |
| pawar | 31.47 | -81.52 | kamykowski | 28.94 | -33.00 |
| sharpeschoolhigh | 31.47 | -81.52 | hinshelwood | 23.26 | -17.84 |
| modifiedgaussian | 23.86 | -78.43 | modifiedgaussian | 19.6 | -15.55 |
| weibull | 26.32 | -64.95 | thomas1 | 23.38 | -14.87 |
| briere2 | 26.38 | -64.91 | briere2 | 23.87 | -10.45 |
| quadratic | 23.98 | -61.13 | quadratic | 19.8 | -4.34 |
| ratkowsky | 25.3 | -53.32 | weibull | 22.05 | -2.91 |
| gaussian | 24.3 | -43.47 | gaussian | 20.32 | -2.19 |
| delong | 24.01 | -35.02 | flinn | 20.88 | -1.12 |
| joehnk | 26.19 | -34.52 | ratkowsky | 20.44 | 0.38 |
| flinn | 24.59 | -34.17 | delong | 20.13 | 7.96 |

## Appendix 3. RNA extraction parameters

Transcriptomics samples collected at 28 °C were used for determining the optimum parameters for the RNA extraction. Cell disruption for 60 seconds twice was the optimum. after the cell disruption, 500 µl of Trizol followed by 5 minutes retention time at room temperature and then 3 minutes of retention time after the addition of chloroform increased the RNA yields. Additionally, excluding the addition of the RNA-binding buffer further increased the RNA yields (Table A1). However, all the tested transcriptomics samples indicated very low RIN (Figure A1). Thus, the RNA extraction was done by using the samples primarily prepared for the lipid analysis, were used for the transcriptomics analysis.

Table A2 indicated the genome alignment rate with Hisat2 for each sample and with featureCounts. Hisat2 was able to map around 80 %. The mapping rate of featureCounts was around 30 % to 40 % (Table A2). This is because the only protein-coding genes in the *.gft* file were used for the annotation. Thus, rRNA transcripts which are abundant in the samples, will not align to anything and shown as "No feature". The actual unmapped genes were less than 5 % across the samples (Table A3).

*Table A1. showing the combinations of each parameter affecting the RNA yields.*

| NanoDrop (ng/µl) | NanoDrop (260nm/280nm) | NanoDrop (260nm/230nm) | bead-beater duration | RT1 (min) | RT2 (min) | Trizol (µl) | RNA-binding buffer (µl) |
|---|---|---|---|---|---|---|---|
| 28.8 | 2 | 0.88 | 60sec x1 | 0 | 0 | 500 | 200 |
| 4.6 | 2.05 | 0.45 | 60sec x1 | 0 | 0 | 1000 | 200 |
| 8 | 1.81 | 0.13 | 15sec x1 | 5 | 3 | 500 | 200 |
| 11.1 | 1.67 | 0.3 | 15sec x1 | 5 | 3 | 500 | 0 |
| 38.8 | 2.09 | 0.94 | 60sec x2 | 5 | 3 | 500 | 200 |
| 51.7 | 2.17 | 2.24 | 60sec x2 | 5 | 3 | 500 | 0 |

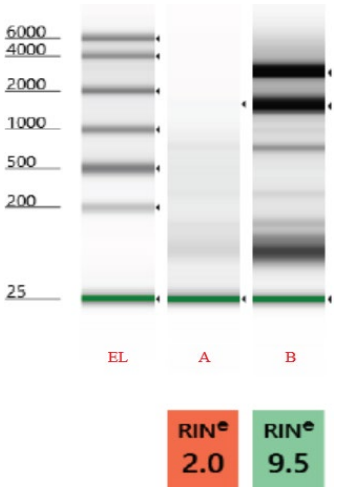

*Figure A1. showing the comparison between the samples prepared for the transcriptomics and lipid analysis. A: transcriptomics sample collected at 28 °C, B: lipid sample collected at 28 °C, EL: electronic ladder.*

*Table A2. The proportion of total reads mapped to the genome by Hisat2, and the proportion of total reads ultimately assigned to annotated gene features by featureCounts.*

| | Temperature | Replicate 1 | Replicate 2 | Replicate 3 | Replicate 4 |
|---|---|---|---|---|---|
| Hisat2 | 10 °C | 79.1% | 79.0% | 80.5% | 80.0% |
| | 25 °C | 74.3% | 71.7% | 76.2% | 76.2% |
| | 34 °C | 76.0% | 75.6% | 76.1% | 74.8% |
| featureCounts | 10 °C | 42.4% | 46.3% | 45.4% | 45.5% |
| | 25 °C | 41.1% | 37.2% | 41.2% | 47.1% |
| | 34 °C | 39.0% | 33.7% | 31.0% | 34.1% |

*Table A3. The summary of the featureCounts.*

| | 10 °C - 1 | 10 °C - 2 | 10 °C - 3 | 10 °C - 4 | 25 °C - 1 | 25 °C - 2 | 25 °C - 3 | 25 °C - 4 | 34 °C - 1 | 34 °C - 2 | 34 °C - 3 | 34 °C - 4 |
|---|---|---|---|---|---|---|---|---|---|---|---|---|
| Assigned genes | 16170092 | 17361742 | 18570987 | 18950965 | 18324388 | 17190191 | 18823582 | 21243243 | 15226644 | 14339200 | 15758209 | 16925802 |
| Unassigned genes | | | | | | | | | | | | |
| - Unmapped | 1181988 | 1121481 | 1006982 | 1102145 | 1249905 | 1108632 | 1160035 | 1266216 | 1766161 | 1365942 | 1522788 | 1758720 |
| - Read_Type | 0 | 0 | 0 | 0 | 0 | 0 | 0 | 0 | 0 | 0 | 0 | 0 |
| - Singleton | 0 | 0 | 0 | 0 | 0 | 0 | 0 | 0 | 0 | 0 | 0 | 0 |
| - MappingQuality | 0 | 0 | 0 | 0 | 0 | 0 | 0 | 0 | 0 | 0 | 0 | 0 |
| - Chimera | 0 | 0 | 0 | 0 | 0 | 0 | 0 | 0 | 0 | 0 | 0 | 0 |
| - FragmentLength | 0 | 0 | 0 | 0 | 0 | 0 | 0 | 0 | 0 | 0 | 0 | 0 |
| - Duplicate | 0 | 0 | 0 | 0 | 0 | 0 | 0 | 0 | 0 | 0 | 0 | 0 |
| - MultiMapping | 0 | 0 | 0 | 0 | 0 | 0 | 0 | 0 | 0 | 0 | 0 | 0 |
| - Secondary | 0 | 0 | 0 | 0 | 0 | 0 | 0 | 0 | 0 | 0 | 0 | 0 |
| - NonSplit | 0 | 0 | 0 | 0 | 0 | 0 | 0 | 0 | 0 | 0 | 0 | 0 |
| - NoFeatures | 20818486 | 19023358 | 21310614 | 21568467 | 24996780 | 27956928 | 25653230 | 22564348 | 22068090 | 26886334 | 28881348 | 35996459 |
| - Overlapping_Length | 0 | 0 | 0 | 0 | 0 | 0 | 0 | 0 | 0 | 0 | 0 | 0 |
| - Ambiguity | 0 | 0 | 0 | 0 | 0 | 0 | 0 | 0 | 0 | 0 | 0 | 0 |
| Total | 38170566 | 37506581 | 40888583 | 41621577 | 44571073 | 46255751 | 45636847 | 45073807 | 39060895 | 42591476 | 46162345 | 54680981 |

## Appendix 4. Detailed GO terms and related genes

| Upregulated at 25 °C | | | | | |
|---|---|---|---|---|---|
| **GO ID** | **Biological process** | **P-value** | **Gene ID** | **logFC** | **Genes** |
| GO:0006629 | lipid metabolic process | 0.0000015 | g6212.t1 | 2.95 | Probable feruloyl esterase A |
| | | | g6215.t1 | 3.98 | |
| | | | g6214.t1 | 5.19 | |
| | | | g10093.t1 | 2.79 | |
| | | | g16185.t1 | 3.73 | |
| | | | g10079.t1 | 3.30 | |
| | | | g16230.t1 | 3.35 | Lipase |
| | | | g12563.t1 | 2.52 | |
| | | | g6224.t1 | 2.52 | |
| | | | g16403.t1 | 2.65 | Glycerophosphodiester phosphodiesterase GDE1 |
| | | | g4686.t1 | 3.41 | Phosphatidylcholine-sterol acyltransferase |
| | | | g1568.t1 | 2.46 | Omega-6 fatty acid desaturase, chloroplastic |
| | | | g10782.t1 | 2.84 | Sn1-specific diacylglycerol lipase alpha |
| | | | g5004.t1 | 4.00 | Uncharacterized protein YjjU |
| GO:0055085 | transmembrane transport | 0.000027 | g16205.t1 | 2.99 | ATP-binding cassette sub-family D member 4 |
| | | | g11656.t1 | 2.21 | Putative proline/betaine transporter |
| | | | g11655.t1 | 3.83 | |
| | | | g11348.t1 | 2.81 | Probable formate transporter 1 |
| | | | g6787.t1 | 2.34 | Probable septum site-determining protein MinC |
| | | | g5131.t1 | 4.41 | Probable glycerol uptake facilitator protein |
| | | | g12525.t1 | 2.05 | Amino-acid permease BAT1 |
| | | | g10598.t1 | 2.23 | Putative tartrate transporter |
| | | | g8414.t1 | 2.35 | Small-conductance mechanosensitive channel |
| | | | g7059.t1 | 2.31 | Sugar transport protein 9 |
| | | | g15792.t1 | 5.02 | Aquaporin-4 |
| | | | g7982.t1 | 2.31 | Vesicular glutamate transporter 3 |
| | | | g11367.t1 | 2.91 | Cationic amino acid transporter 2 |
| | | | g4745.t1 | 3.73 | |
| | | | g3392.t1 | 4.44 | |
| | | | g4295.t1 | 2.21 | Solute carrier family 13 member 2 |
| | | | g7529.t1 | 2.03 | Solute carrier family 23 member 2 |
| | | | g1334.t1 | 2.72 | Solute carrier family 17 member 9 |
| | | | g3880.t1 | 3.04 | Solute carrier family 35 member F5 |
| | | | g7240.t1 | 3.03 | |
| | | | g8210.t1 | 3.91 | Guanine/hypoxanthine permease GhxP |
| | | | g10805.t1 | 3.47 | |
| GO:0016480 | negative regulation of transcription by RNA polymerase III | 0.00042 | g10532.t1 | 2.58 | Repressor of RNA polymerase III transcription MAF1 homolog |
| | | | g9097.t1 | 2.54 | |
| GO:0019427 | acetyl-CoA biosynthetic process from acetate | | g6440.t1 | 2.04 | Acetyl-coenzyme A synthetase |
| | | | g9278.t1 | 2.29 | |
| GO:0046475 | glycerophospholipid catabolic process | 0.02057 | g16403.t1 | 2.65 | Glycerophosphodiester phosphodiesterase GDE1 |
| GO:0009395 | phospholipid catabolic process | 0.04031 | g12140.t1 | 2.71 | Putative meiotic phospholipase SPO1 |
| GO:0006729 | tetrahydrobiopterin biosynthetic process | 0.04071 | g6635.t1 | 2.58 | Putative pterin-4-alpha-carbinolamine dehydratase |
| GO:0009235 | cobalamin metabolic process | | g16205.t1 | 2.99 | ATP-binding cassette sub-family D member 4 |
| GO:0120029 | proton export across plasma membrane | | g866.t1 | 2.05 | Plasma membrane ATPase |
| **GO ID** | **Molecular function** | **P-value** | **Gene ID** | **logFC** | **Genes** |
| GO:0022857 | transmembrane transporter activity | 0.00017 | g7529.t1 | 2.03 | Solute carrier family 23 member 2 |
| | | | g10805.t1 | 3.47 | Guanine/hypoxanthine permease GhxP |
| | | | g4745.t1 | 3.73 | Cationic amino acid transporter 2 |
| | | | g11348.t1 | 2.81 | Probable formate transporter 1 |
| | | | g7059.t1 | 2.31 | Sugar transport protein 9 |
| | | | g7240.t1 | 3.03 | Solute carrier family 35 member F5 |
| | | | g11655.t1 | 3.83 | Putative proline/betaine transporter |
| | | | g11367.t1 | 2.91 | Cationic amino acid transporter 2 |
| | | | g12525.t1 | 2.05 | Amino-acid permease BAT1 |
| | | | g3392.t1 | 4.44 | Cationic amino acid transporter 2 |
| | | | g10598.t1 | 2.23 | Putative tartrate transporter |
| | | | g11656.t1 | 2.21 | Putative proline/betaine transporter |
| | | | g7982.t1 | 2.31 | Vesicular glutamate transporter 3 |
| | | | g8210.t1 | 3.91 | Guanine/hypoxanthine permease GhxP |
| | | | g1334.t1 | 2.72 | Solute carrier family 17 member 9 |
| | | | g3880.t1 | 3.04 | Solute carrier family 35 member F5 |
| **Downregulated at 25 °C** | | | | | |
| **GO ID** | **Biological process** | **P-value** | **Gene ID** | **logFC** | **Genes** |
| GO:0051083 | de novo cotranslational protein folding | 0.000028 | g7672.t1 | -2.28 | Chaperone protein DnaJ |
| | | | g1687.t1 | -2.45 | |
| GO:0006450 | regulation of translational fidelity | 0.000084 | g1687.t1 | -2.45 | |
| | | | g7672.t1 | -2.28 | |
| GO:0042255 | ribosome assembly | 0.00042 | g5463.t1 | -2.29 | 60S ribosome subunit biogenesis protein NIP7 homolog |
| | | | g13758.t1 | -2.16 | |
| GO:0032543 | mitochondrial translation | 0.01077 | g4249.t1 | -2.07 | 54S ribosomal protein L51, mitochondrial |
| GO:0046654 | tetrahydrofolate biosynthetic process | | g7288.t1 | -2.04 | GTP cyclohydrolase 1 |
| GO:0006979 | response to oxidative stress | 0.0126 | g15542.t1 | -2.48 | Catalase-peroxidase |
| | | | g15543.t1 | -2.39 | |
| GO:0019264 | glycine biosynthetic process from serine | 0.01612 | g14721.t1 | -2.92 | Serine hydroxymethyltransferase, mitochondrial |
| GO:0035999 | tetrahydrofolate interconversion | | g14721.t1 | -2.92 | |
| GO:0006474 | N-terminal protein amino acid acetylation | 0.02144 | g11979.t1 | -2.32 | N-alpha-acetyltransferase 20 |
| GO:0006183 | GTP biosynthetic process | 0.03199 | g3069.t1 | -2.21 | Nucleoside diphosphate kinase 1 |
| GO:0006228 | UTP biosynthetic process | | g3069.t1 | -2.21 | |
| GO:0006241 | CTP biosynthetic process | 0.03722 | g3069.t1 | -2.21 | |
| **GO ID** | **Molecular function** | **P-value** | **Gene ID** | **logFC** | **Genes** |
| GO:0003871 | 5-methyltetrahydropteroyltriglutamate-homocysteine S-methyltransferase activity | 0.00599 | g9530.t1 | -5.77 | 5-methyltetrahydropteroyltriglutamate--homocysteine methyltransferase |
| GO:0003934 | GTP cyclohydrolase I activity | | g7288.t1 | -2.04 | GTP cyclohydrolase 1 |
| GO:0004096 | catalase activity | 0.01788 | g15543.t1 | -2.39 | Catalase-peroxidase |
| GO:0004372 | glycine hydroxymethyltransferase activity | | g14721.t1 | -2.92 | Serine hydroxymethyltransferase, mitochondrial |
| GO:0004550 | nucleoside diphosphate kinase activity | 0.03544 | g3069.t1 | -2.21 | Nucleoside diphosphate kinase 1 |
| GO:0004596 | peptide alpha-N-acetyltransferase activity | 0.02377 | g11979.t1 | -2.32 | N-alpha-acetyltransferase 20 |
| GO:0008252 | nucleotidase activity | 0.00096 | g11684.t1 | -2.18 | 5'-nucleotidase SurE |
| | | | g12935.t1 | -2.02 | 5'-nucleotidase SurE |
| GO:0008861 | formate C-acetyltransferase activity | 0.01195 | g428.t1 | -3.22 | Autonomous glycyl radical cofactor |
| GO:0030544 | Hsp70 protein binding | 0.00305 | g7672.t1 | -2.28 | Chaperone protein DnaJ |
| | | | g1687.t1 | -2.45 | Chaperone protein DnaJ |
| GO:0043022 | ribosome binding | 0.00187 | g7672.t1 | -2.28 | Chaperone protein DnaJ |
| | | | g1687.t1 | -2.45 | Chaperone protein DnaJ |
| GO:0046982 | protein heterodimerization activity | 0.0399 | g2895.t1 | -3.16 | Histone H2A-IV |
| | | | g591.t1 | -3.58 | Histone H2A-IV |
| **GO ID** | **Cellular component** | **P-value** | **Gene ID** | **logFC** | **Genes** |
| GO:0000786 | nucleosome | 0.0186 | g2895.t1 | -3.16 | Histone H2A-IV |
| | | | g591.t1 | -3.58 | Histone H2A-IV |
| GO:0031415 | NatA complex | 0.0058 | g11979.t1 | -2.32 | N-alpha-acetyltransferase 20 |

| Upregulated at 34 °C | | | | | |
|---|---|---|---|---|---|
| **GO ID** | **Biological process** | **P-value** | **Gene ID** | **logFC** | **Genes** |
| GO:0006596 | polyamine biosynthetic process | 0.003 | g8450.t1 | 2.03 | Omega-amidase NIT2 |
| | | | g6244.t1 | 3.15 | Ornithine decarboxylase |
| GO:0005985 | sucrose metabolic process | 0.018 | g2398.t1 | 3.89 | Sucrose synthase 2 |
| GO:0009395 | phospholipid catabolic process | | g11061.t1 | 3.08 | Putative lysophospholipase C1450.09c |
| GO:0055085 | transmembrane transport | 0.027 | g3487.t1 | 2.33 | Solute carrier family 23 member 2 |
| | | | g3392.t1 | 2.39 | Cationic amino acid transporter 2 |
| | | | g865.t1 | 2.14 | Itaconate transport protein |
| | | | g9366.t1 | 3.49 | Probable ammonia channel |
| | | | g5213.t1 | 2.44 | Putative tartrate transporter |
| | | | g5214.t1 | 2.46 | |
| | | | g4879.t1 | 2.48 | |
| GO:0000045 | autophagosome assembly | 0.036 | g1574.t1 | 2.21 | Katanin p80 WD40 repeat-containing subunit B1 |
| GO:0042073 | intraciliary transport | | g13163.t1 | 2.03 | Intraflagellar transport protein 46 homolog |
| GO:0006116 | NADH oxidation | 0.041 | g12155.t1 | 3.32 | External alternative NAD(P)H-ubiquinone oxidoreductase B1, mitochondrial |
| GO:0009058 | biosynthetic process | 0.049 | g3124.t1 | 2.02 | Aspartate aminotransferase, mitochondrial |
| | | | g12649.t1 | 2.07 | |
| GO:0009308 | amine metabolic process | 0.05 | g10600.t1 | 2.17 | Primary amine oxidase |
| **GO ID** | **Molecular function** | **P-value** | **Gene ID** | **logFC** | **Genes** |
| GO:0004451 | isocitrate lyase activity | 0.0183 | g15617.t1 | 2.03 | Isocitrate lyase |
| GO:0005507 | copper ion binding | 0.0172 | g10600.t1 | 2.17 | Primary amine oxidase |
| | | | g2612.t1 | 4.19 | Multicopper oxidase mco |
| GO:0008234 | cysteine-type peptidase activity | 0.006 | g2808.t1 | 2.51 | Cathepsin R |
| | | | g12300.t1 | 2.62 | Dipeptidyl peptidase 1 |
| | | | g307.t1 | 2.83 | Probable inactive leucine-rich repeat receptor kinase XIAO |
| | | | g9366.t1 | 3.49 | Probable ammonia channel |
| GO:0008428 | ribonuclease inhibitor activity | 0.0122 | g4862.t1 | 2.74 | Putative 4-hydroxy-4-methyl-2-oxoglutarate aldolase |
| GO:0008483 | transaminase activity | 0.0072 | g3124.t1 | 2.02 | Aspartate aminotransferase, mitochondrial |
| | | | g12649.t1 | 2.07 | Aspartate aminotransferase, mitochondrial |
| GO:0008901 | ferredoxin hydrogenase activity | 0.0061 | g3016.t1 | 2.40 | Cytosolic iron-sulfur assembly component 3 |
| GO:0016157 | sucrose synthase activity | 0.0122 | g2398.t1 | 3.89 | Sucrose synthase 2 |
| GO:0016661 | oxidoreductase activity, acting on other nitrogenous compounds as donors | 0.0303 | g2951.t1 | 3.39 | Hydroxylamine reductase |
| GO:0022857 | transmembrane transporter activity | 0.0084 | g3487.t1 | 2.33 | Solute carrier family 23 member 2 |
| | | | g865.t1 | 2.14 | Itaconate transport protein |
| | | | g3392.t1 | 2.39 | Cationic amino acid transporter 2 |
| | | | g5213.t1 | 2.44 | Putative tartrate transporter |
| | | | g5214.t1 | 2.46 | Putative tartrate transporter |
| | | | g4879.t1 | 2.48 | Putative tartrate transporter |
| GO:0050126 | N-carbamoylputrescine amidase activity | 0.0061 | g8450.t1 | 2.03 | Omega-amidase NIT2 |
| GO:0051536 | iron-sulfur cluster binding | 0.0053 | g16257.t1 | 2.50 | Ferredoxin-1 |
| | | | g3016.t1 | 2.40 | Cytosolic iron-sulfur assembly component 3 |
| | | | g2951.t1 | 3.39 | Hydroxylamine reductase |
| | | | g5400.t1 | 2.02 | 2-iminoacetate synthase |
| GO:0071949 | FAD binding | | g15005.t1 | 2.92 | Glucosylglycerate phosphorylase |
| | | | g4736.t1 | 2.42 | Probable L-gulonolactone oxidase 6 |
| | | | g11750.t1 | 2.86 | Glucosylglycerate phosphorylase |
| **GO ID** | **Cellular component** | **P-value** | **Gene ID** | **logFC** | **Genes** |
| GO:0005576 | extracellular region | 0.0047 | g715.t1 | 2.01 | Endoglucanase F |
| | | | g7073.t1 | 2.99 | Fruiting body protein SC14 |
| GO:0005615 | extracellular space | 0.0231 | g6899.t1 | 2.48 | Serpin A3-8 |
| **Downregulated at 34 °C** | | | | | |
| **GO ID** | **Biological process** | **P-value** | **Gene ID** | **logFC** | **Genes** |
| GO:0009765 | photosynthesis, light harvesting | 0.00064 | g7543.t1 | -2.07 | Chlorophyll a-b binding protein of LHCII type I, chloroplastic |
| | | | g12384.t1 | -2.63 | |
| | | | g920.t1 | -2.16 | Chlorophyll a-b binding protein, chloroplastic |
| GO:0006508 | proteolysis | 0.02617 | g13567.t1 | -3.96 | Alkaline protease |
| | | | g7471.t1 | -3.94 | |
| | | | g4101.t1 | -3.91 | |
| | | | g7820.t1 | -2.57 | |
| | | | g5679.t1 | -2.34 | |
| | | | g6962.t1 | -2.29 | Dipeptidyl peptidase 1 |
| GO:0000184 | nuclear-transcribed mRNA catabolic process, nonsense-mediated decay | 0.0332 | g3565.t1 | -2.22 | Serine/threonine-protein kinase smg-1 |
| GO:0006108 | malate metabolic process | 0.03863 | g8168.t1 | -2.50 | Malate dehydrogenase, cytoplasmic |
| GO:0006629 | lipid metabolic process | 0.03941 | g13617.t1 | -2.31 | Acyl-lipid (7-3)-desaturase |
| | | | g899.t1 | -2.18 | |
| | | | g16393.t1 | -2.53 | Lysophospholipase NTE1 |
| GO:0050482 | arachidonic acid secretion | 0.0494 | g5539.t1 | -2.30 | Vitelline membrane outer layer protein 1 homolog |
| **GO ID** | **Molecular function** | **P-value** | **Gene ID** | **logFC** | **Genes** |
| GO:0003690 | double-stranded DNA binding | 0.01478 | g12731.t1 | -2.24 | Periostin |
| | | | g14108.t1 | -2.22 | Uncharacterized protein sll1483 |
| GO:0004252 | serine-type endopeptidase activity | 0.00034 | g4101.t1 | -3.91 | Alkaline protease |
| | | | g7820.t1 | -2.57 | Alkaline protease |
| | | | g13567.t1 | -3.96 | Alkaline protease |
| | | | g5679.t1 | -2.34 | Alkaline protease |
| | | | g7471.t1 | -3.94 | Alkaline protease |
| GO:0004623 | phospholipase A2 activity | 0.03383 | g5539.t1 | -2.30 | Vitelline membrane outer layer protein 1 homolog |
| GO:0015112 | nitrate transmembrane transporter activity | 0.01517 | g333.t1 | -2.16 | Nitrate transporter 2.2 |
| GO:0016851 | magnesium chelatase activity | 0.01893 | g1086.t1 | -2.08 | Magnesium-chelatase subunit H |
| GO:0030060 | L-malate dehydrogenase activity | | g8168.t1 | -2.50 | Malate dehydrogenase, cytoplasmic |